DEFINITION OF A
RESISTOJET CONTROL SYSTEM FOR
THE MANNED ORBITAL RESEARCH LABORATORY
FINAL REPORT

VOLUME V

RESISTOJET DESIGN AND DEVELOPMENT

MAY 1968

GPO PRICE $ _____

CFSTI PRICE(S) $ _____

Hard copy (HC) _____

Microfiche (MF) _____

ff 653 July 65

FACILITY FORM 602

(ACCESSION NUMBER)

(PAGES)

(NASA CR OR TMX OR AD NUMBER)

(THRU)

(CODE)

(CATEGORY)

DEFINITION OF A
RESISTOJET CONTROL SYSTEM FOR
THE MANNED ORBITAL RESEARCH LABORATORY
FINAL REPORT

VOLUME V
RESISTOJET DESIGN AND DEVELOPMENT

PREFACE

This report is submitted to the National Aeronautics and Space Administration's Langley Research Center (NASA-LRC), Langley AFB, Virginia. It has been prepared under Contract No. NAS1-6702 and describes the results of a detailed assessment of the use of a resistojet control system for the MORL.

The study results are documented in five volumes:

DAC-58130	I	Summary
DAC-58131	II	Resistojet Control System Analysis
DAC-58132	III	Biowaste Utilization
DAC-58133	IV	Ground and Flight Test Plan
DAC-58134	V	Resistojet Design and Development

Volume I is a summary report in which the significant results are presented. Volume II contains a detailed definition of the selected resistojet control system, the recommended orbit injection system, the supporting system analyses and integration, and comparative evaluation data. Volume III presents the biowaste utilization analysis. Volume IV details the ground and flight test program for a resistojet control system. Volume V presents the results of the resistojet design and development program. Life test data will be provided in a separately bound addendum to Volume V at the conclusion of the life test.

Requests for further information concerning this report will be welcomed by the following Douglas representative:

Mr. T. J. Gordon, Director, Advance Space and
Launch Systems
Huntington Beach, California
Telephone: 714-897-0311, Extension 2994

FOREWORD

Units, abbreviations, and prefixes used in this report correspond to the
International System of Units (SI) as prescribed by the Eleventh General
Conference on Weights and Measures and presented in NASA Report SP-7012.
The basic units for length, mass, and time are meter, kilogram, and second,
respectively. Throughout the report, the English equivalent (foot, pound,
and second) are presented for convenience.

The SI units, abbreviations, and prefixes most frequently used in this report
are summarized below:

Basic Units

Length	meter	m
Mass	kilogram	kg
Time	sec	s
Electric current	ampere	A
Temperature	degree Kelvin	$^{\circ}K$

Supplementary Units

Plane angle	radian	rad

Derived Units

Area	square meter	m^2	
Volume	cubic meter	m^3	
Frequency	hertz	Hz	(s^{-1})
Density	kilogram per cubic meter	kg/m^3	
Velocity	meter per second	m/s	
Angular velocity	radian per second	rad/s	
Acceleration	meter per second squared	m/s^2	
Angular acceleration	radian per second squared	rad/s^2	
Force	newton	N	$(kg\text{-}m/s^2)$
Pressure	newton per sq meter	N/m^2	
Kinematic viscosity	sq meter per second	m^2/s	
Dynamic viscosity	newton-second per sq meter	$N\text{-}s/m^2$	

Work, energy, quantity of heat	joule	J	(N-m)
Power	watt	W	(J/s)
Electric charge	coulomb	C	(A-s)
Voltage, potential difference, electromotive force	volt	V	(W/A)
Electric field strength	volt per meter	V/m	
Electric resistance	ohm	Ω	(V/A)
Electric capacitance	farad	F	(A-s/V)
Magnetic flux	weber	Wb	(V-s)
Inductance	henry	H	(V-s/A)
Magnetic flux density	tesla	T	(Wb/m^2)
Magnetic field strength	ampere per meter	A/m	
Magnetomotive force	ampere	A	

Prefixes

Factor by which unit is multiplied	Prefix	Symbol
10^6	mega	M
10^3	kilo	k
10^{-2}	centi	c
10^{-3}	milli	m
10^{-6}	micro	μ

CONTENTS

FIGURES

TABLES

DEFINITION OF A RESISTOJET CONTROL SYSTEM FOR THE MANNED ORBITAL RESEARCH LABORATORY

FINAL REPORT

VOLUME V--RESISTOJET DESIGN AND DEVELOPMENT

By R. J. Page and R. A. Short

INTRODUCTION

This report describes the resistojet design, development, and tests performed by The Marquardt Corporation under subcontract to the Douglas Aircraft Company, a component of the McDonnell Douglas Corporation. Presented herein are resistojet design criteria, materials selection, heat transfer and gas dynamics analyses, fabrication methods, testing procedures, and test results.

Two thrustor models are described, both with essentially the same heat-exchanger design: Model I, which demonstrated the feasibility of using rhenium for all high-temperature elements, and Model II which incorporated improvements to enhance the ease of fabrication and assembly.

For the final configuration, at measured specific impulse values of 700 sec for hydrogen (H_2) and 320 sec for ammonia (NH_3), the overall electric efficiencies, $\eta_o{}^*$, were 0.65 and 0.45. The heater efficiencies were 0.96 and 0.86.

Model II demonstrated its ability to start and stop suddenly from the high specific-impulse condition. Its performance was stable over an operation period of 20 hours at > 680 sec for H_2 and 20 hours at > 320 sec for NH_3. The unit was cycled on and off from full power with both H_2 and NH_3 for a total of 27 hours. An additional 77 hours of testing on the design-verification-test thrustor was undertaken before preparation for life testing curtailed the further accrual of time. Life-test data will be presented in an addendum to this volume when available.

An influence of cell pressure on thrust performance (at the 0.044-N [10-mlbf] level) was discovered and evaluated. Cell pressures less than 0.1 μm Hg are required for negligible influence. All the reported thrust values (hence, specific impulse) here are conservative compared to those achievable in space.

An addendum to this volume is in the process of preparation. This will report the results of a 720-hour life test on six Model II thrustors, two operating on H_2 and four on NH_3. The results of such tests as these will more accurately define the specific impulse and temperature levels to be associated with the Model II.

MODEL I DESIGN

The design of the Model I thrustor was based on a 30-kW concentric-tube resistojet built for the Air Force about 3 years ago. The 30-kW unit produced a specific impulse of 860 sec on H_2 and an overall total power efficiency of 81%. The design of this unit has since been twice scaled downward, an order of magnitude each time. The first order-of-magnitude reduction to 3-kW produced a thrust of 0.65 N (66.5 grams force) at a specific impulse of 840 sec on H_2. This report presents the second reduction in power level, which entailed the introduction of some novel features to produce an efficient resistojet at 4.58-grams (approximately 0.01-lbf) thrust for operation either on H_2 or NH_3.

The 30- and 3-kW resistojets were laboratory units with the high-temperature elements made of tungsten, which became brittle after being heated over the recrystallization temperature. Through the introduction of rhenium parts, which are assembled by electron-beam welding, the basic design of this resistojet has a greater durability. (Rhenium remains ductile after heating.) The size of the thrustor has been significantly reduced as well.

The Model I evacuated, concentric-tube resistojet was developed for the 0.044-N (10-mlbf) thrustor. Fig. 1 shows the model, in simplified form, and the flows of electric current and propellant. Both of its basic parts, the gas heater and the nozzle, must undergo geometrical changes because of the difference in size in this thrustor and the 30-kW unit.

As the resistojet is reduced in size for a constant chamber temperature, it is necessary to support a steeper radial thermal gradient between the inner heater tube and the outer surface. This gradient could cause prohibitive radial conductive losses through an intervening gas. One solution is to introduce an evacuated jacket which, is exposed to space. Heat flowing radially by thermal conduction through the gas is essentially in the free-molecule regime. As free-molecule thermal conductivity is proportional to pressure, the radial heat flow is negligible, unlike that for continuum flow, where thermal conductivity is independent of pressure. Radiation shields in the jacket further reduce heat losses.

The objectives of the exchanger design were to achieve a gas temperature closely approaching that of the wall, a high heater efficiency, and an acceptable pressure drop. The chamber pressure was selected at 1.5 atm. The selected chamber temperature, $2420^{\circ}K$, was run for a 25-hour period on the 0.67-N (150-mlbf) or 3-kW design tested previously. It is $200^{\circ}K$ less than the 30-kW unit which was tested 3 years ago for 50 hours.
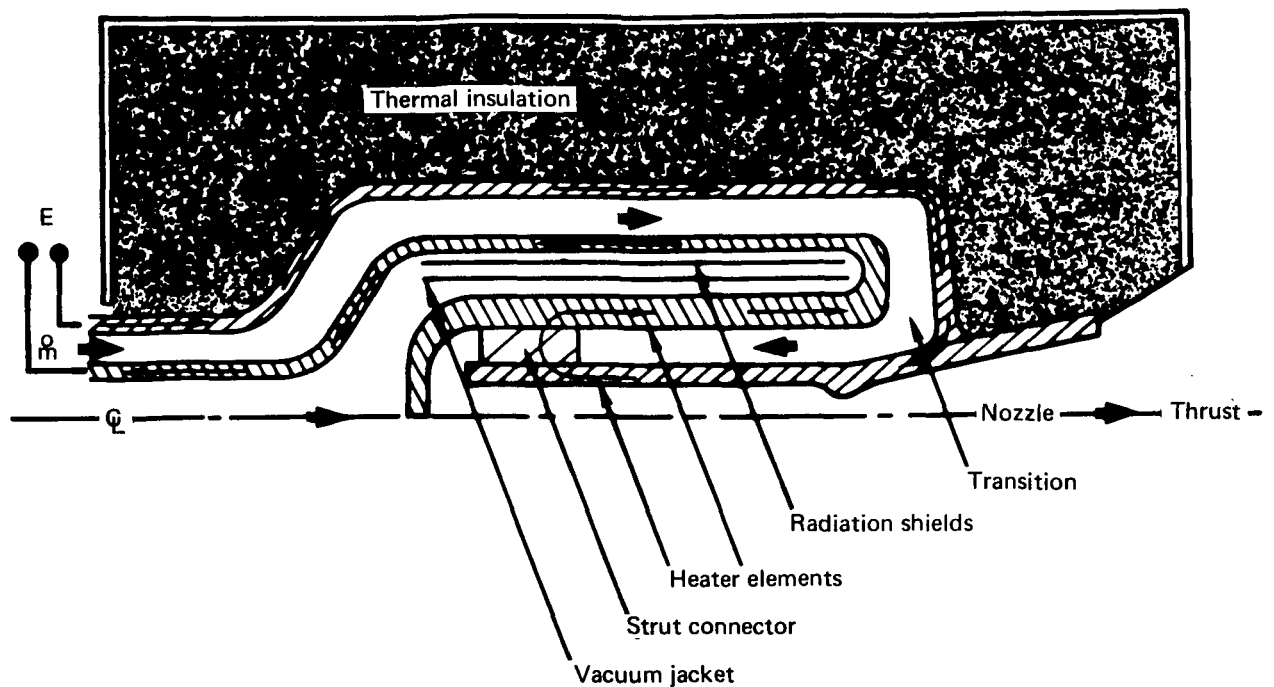
Figure 1. Model I Evacuated Resistojet Concept – Simplified

The diameters of the inner elements were based on not exceeding a Mach number of approximately 0.3. This reduced the radiative transfer losses from lowered wall area and increased the laminar flow heat-transfer coefficients to the gas. The pressure drop is increased but not prohibitively.

Because of a realistic limit on throat size (0.5 mm), the chamber pressure has been lowered to 1.5 atm over the 10 atm of the previous design. Because of the high temperature levels of the case, high-performance thermal insulation with radiation shields is used.

Within the limitations of the small size and narrow passages necessary for good heat transfer and thermal efficiency, the highest possible voltage was desired. A further requirement was 0.016-cm (0.004 in.) minimum heater-element wall thickness (for strength and operational life requirements). For example, these requirements produced a nominal operating condition of 6 volts and 40 amps for 240 watts of input electric power when operating on H_2.

The vacuum jacket innovation allows a three-gas pass concept to be used as opposed to 12 in the larger model (ref. 1). This eliminates the need for electrical insulator-spacers which also act as pressure seals within the heat exchanger itself. The only electrical insulator seal in the 0.044-N (10-mlbf) design is now located at the propellant inlet, which is in a relatively cool location. This is a brazed metal-to-ceramic seal instead of the compression type formerly used.

Since there are no sliding joints in this thrustor, a bellows has been incorporated to prevent deformation of the inner heating element by differential thermal expansion. The Model I design is shown in fig. 2.

14

TIG weld

Braze

12

Braze

16

15

TIG weld
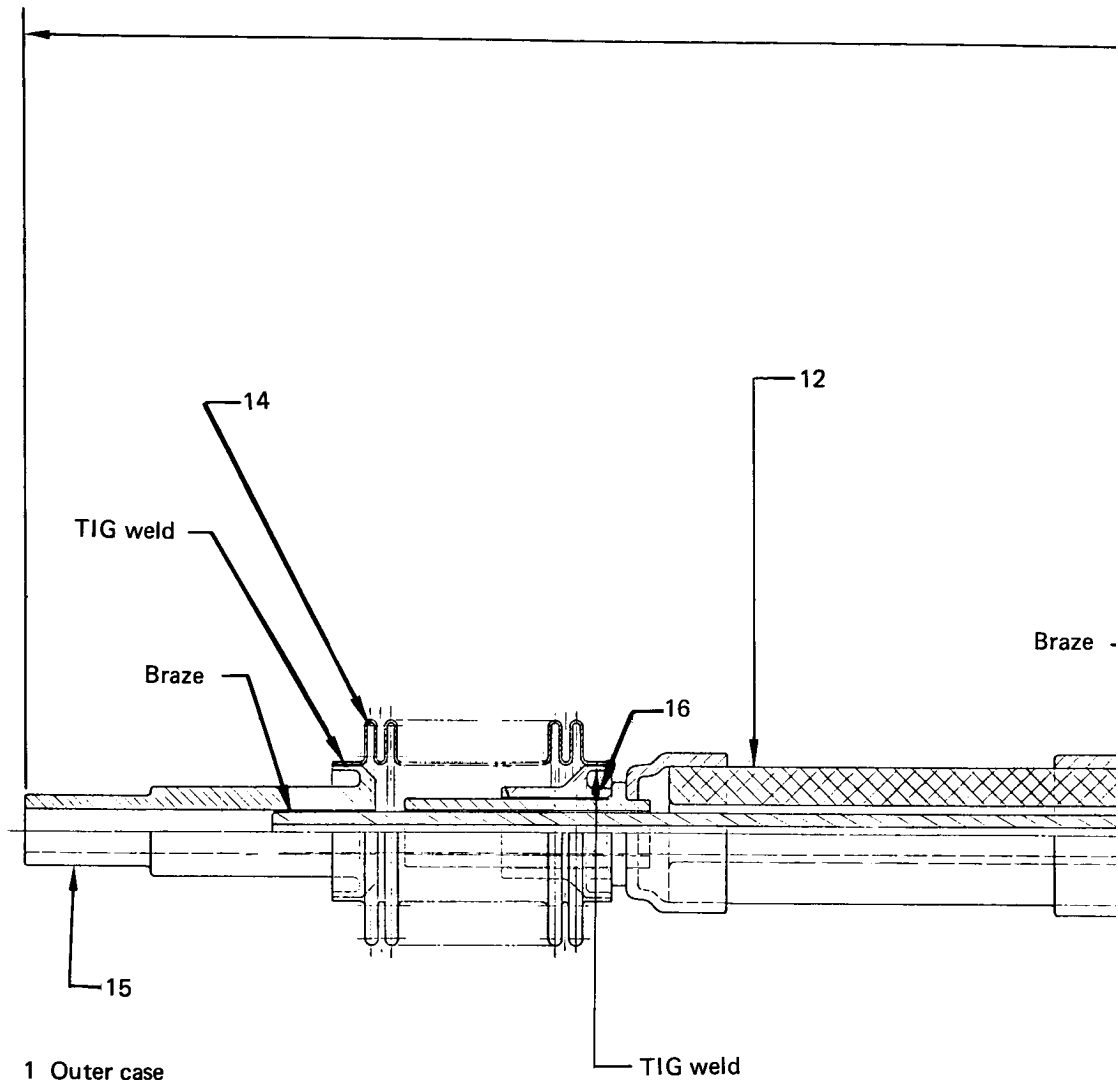
1 Outer case
2 Inner case
3 Outer heater
4 Inner heater and nozzle
5 Case cover
6 Electrical insulation
7 Radiation shield
8 Housing
9 Cover
10 Fitting, tee
11 Thermal insulation
12 Electrical insulator and
   metal to ceramic seal assembly
13 Screws
14 Bellows
15 Fitting
16 Fitting

Figure 2. Resistojet Thrustor

5.90

10

13

9

8

11

1

2

Braze

EB weld (typ)

A

Section A-A

6

7

3

4

Electron-beam
weld

5

3.5 cm diam.

0.533 cm

Throat diam., 0.053 cm

6.67 cm
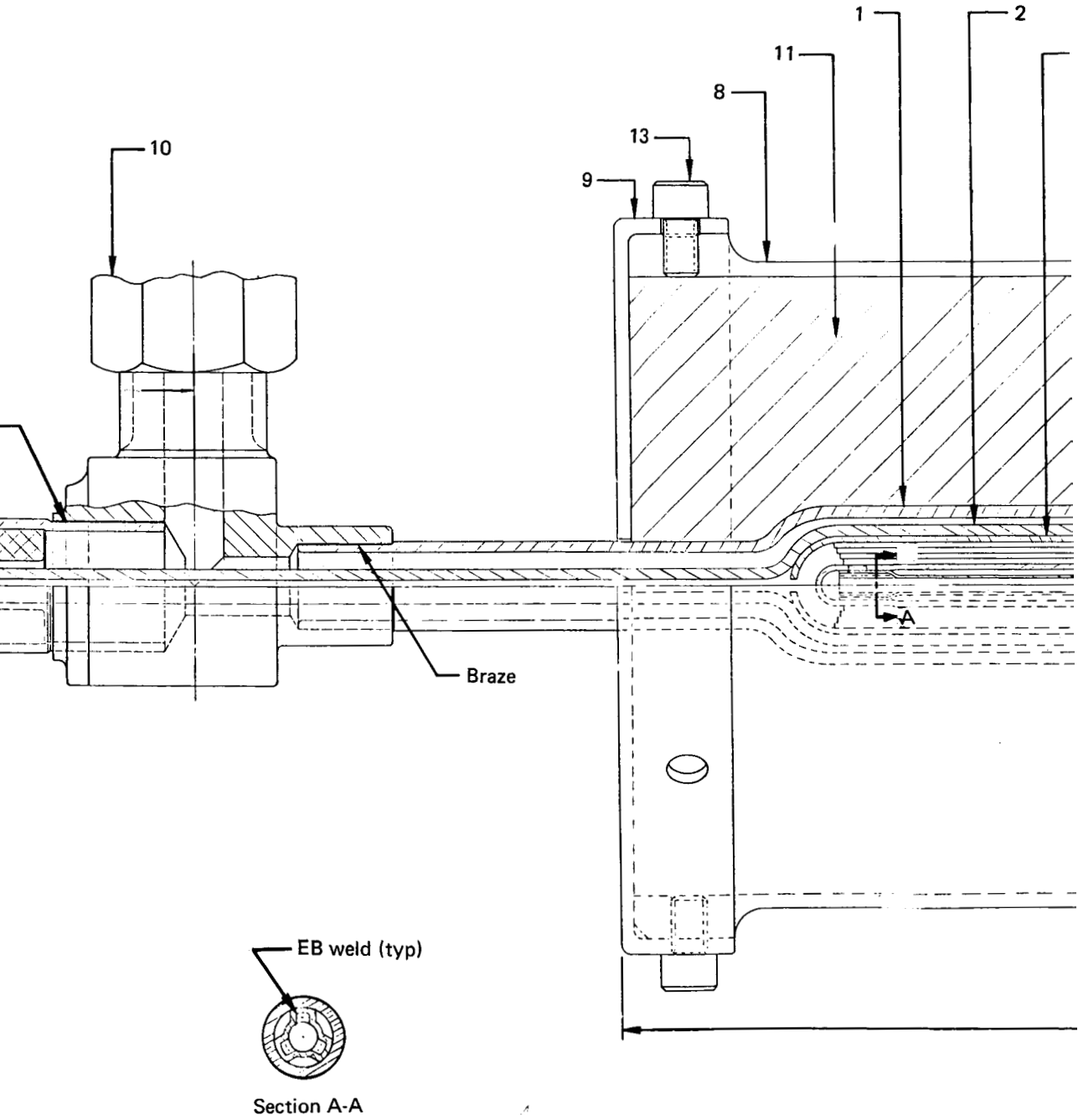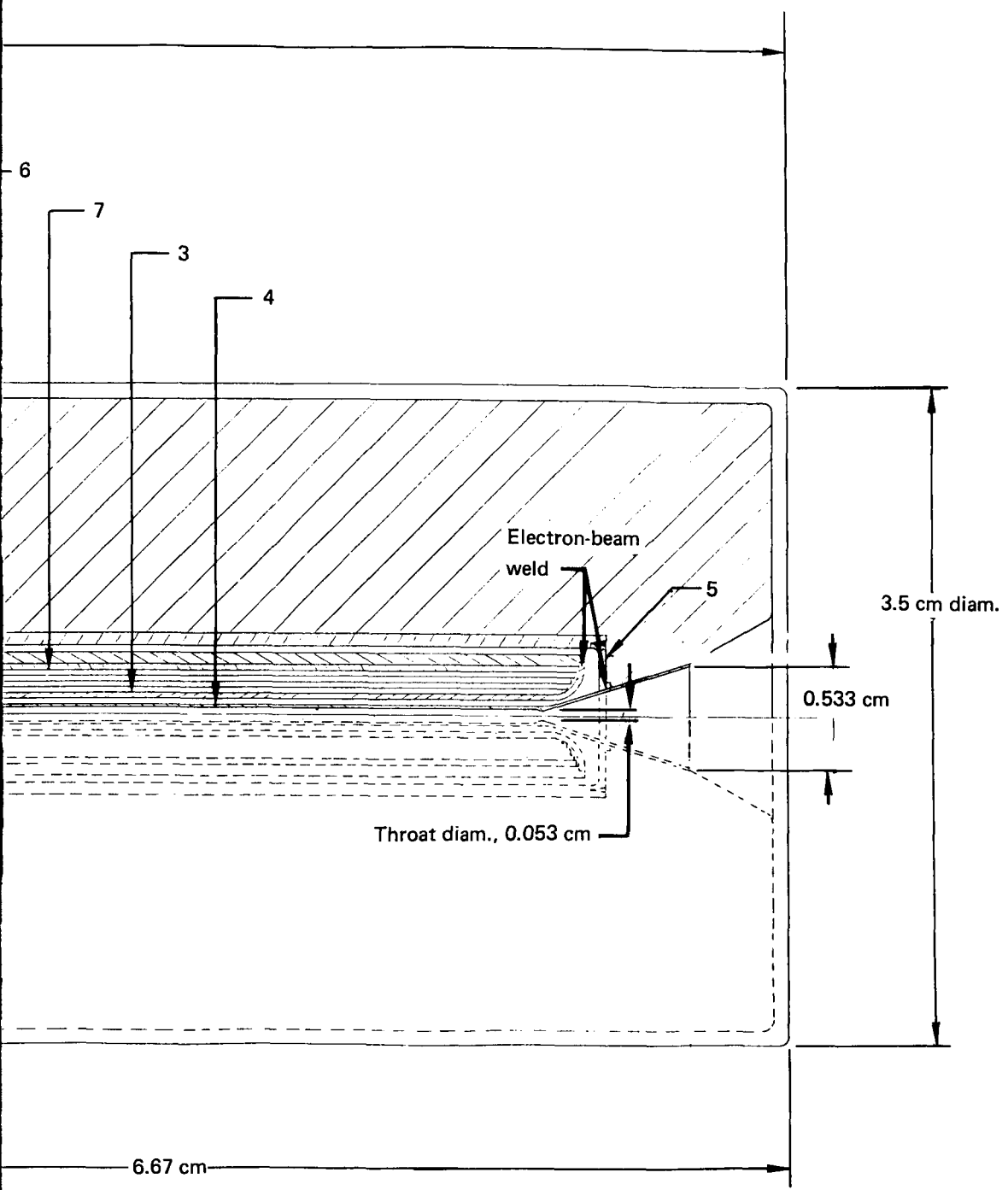
MODEL I FABRICATION

Material Selection

Rhenium was selected for the high-temperature elements. The main reason for its selection was because it does not exhibit a ductile-to-brittle transition after being heated over the recrystallization temperature. Its ductile behavior is in marked contrast to that of tungsten. It is comparable to tungsten, however, in its high-temperature endurance strength, its creep and sublimation rates, its resistivity, and its fabricability.

Rhenium was also selected for the intermediate temperature parts so that no dissimilar parts are used in the structure. This selection is based on the excellent weldability of rhenium to rhenium and the elimination of differential thermal expansion problems.

An alloy--50% molybdenum/50% rhenium--initially appeared attractive for some intermediate temperature parts because of its lower cost and availability. Its similarity to pure rhenium indicated that there would be no problem in welding it to pure rhenium parts. Although some sample welds were successful, there was electron-beam-weld cracking because of the brittle intermetallics, Mo_2Re_3 and Re_4Mo (σ and X phases, respective) at the joint. The use of molybdenum/rhenium was therefore discontinued.

Stainless steel and nickel were selected for the low-temperature auxiliary parts. They are joined by BT Lithobraze, which has a service temperature capability of $815^{\circ}K$. Boron nitride is selected for high-temperature insulation. Min-K-2000 appears to be the best thermal insulator.

Candidate materials for high-temperature parts. — The maximum specific impulse and life capability of a resistojet are governed by the heating element material. The first materials to be chosen must therefore be for the inner heating element and nozzle.

Property requirements which influence the choice of material are summarized in table 1.

The materials initially considered for the highest-temperature parts were the refractory metals: columbium, tantalum, molybdenum, tungsten, rhenium, and their alloys.

Part no.	Part	Function	Environment		
			Thrusting mode		Therma m (P_e =
			Max. temp ($^{\circ}$K)	Pressure[a] range (atm)	Max. temp ($^{\circ}$K)
1	Outer case	a. Pressure vessel b. Electric conductor c. Regenerative heat exchanger	775	4×10^{-5} -- 1.5	1300
2	Inner case		825	6×10^{-5} -- 1.5	1473
5	End case		2075	4×10^{-5} -- 1.5	1600
3	Outer heating element	a. Pressure vessel b. Ohmic heater c. Heat exchanger	1875	6×10^{-5} -- 1.5	1873
4	Inner heating element and nozzle	a. Ohmic heater b. Heat exchanger c. Gas accelerator	2525	1.5	2000
6	Electric insulator	Electric insulator	875	6×10^{-5}	1523
7	Radiation shield	Radial thermal radiation shield	1775	6×10^{-5}	1773

[a]The pressures given are those to be tested. For space operation, all vacuum num

[b]The temperatures given correspond to the desired thermal holding temperature pr with the inner element at design temperature (P_e = 16.8 W) at no propellant flow. F

[c]A common requirement is that there be no chemical reactivity with the propellants

MODEL I MATERIALS

holding bde (10.5 W)	Joints				
	Welds		Brazes[b]		
Pressure[a] (atm)	Ident no.	Max. temp (^{O}K)	Ident no.	Max. temp (^{O}K)	Primary material requirements[c]
10^{-6}	4	1300	6	600	a. Thermal expansion coefficient compatibility with mating welded parts. b. Weldable and brazable.
10^{-6}	3	1475	1	500	
10^{-6}	1	2075	---	---	c. Ductile.
	4	1300	---	---	
10^{-6}	2	1875	---	---	a. High-resistance to interatomic diffusion of propellant. b. High electrical resistivity. c. Ductile. d. Weldable.
10^{-6}	1	2075	---	---	a. Low sublimation rates. b. High electrical resistivity. c. High-temperature fatigue strength. d. High-temperature endurance strength. e. Ductile. f. Weldable.
	2	2075	---	---	
10^{-6}	---	---	---	---	High-temperature electrical insulation.
10^{-6}	---	---	---	---	a. Low thermal emissivity. b. Thin-sheet availability. c. Ductility.

:rs are replaced by those corresponding to those of the orbital attitude.
:le (P_e = 10.5 W); however, steady-state braze site temperatures could reach $975^{O}K$
ice, $975^{O}K$ braze capability is highly desirable.
r their contained contaminants.

Part no.	Part	Function	Thrusting mode		Therm r (P_e)
			Max. temp (°K)	Pressure[a] range (atm)	Max. temp (°K)
8, 9, 13	Insulation cover	Effective insulation retainer	400	6×10^{-5}	400
10	Propellant fittings	a. Gas-tight propellant connector	300	4×10^{-5} -- 1.5	600
		b. Electric terminal	---	---	---
11	Thermal insulation	Thermal insulator	1575	4×10^{-5} -- 1.5	---
12	Electrical insulator-seal	Gas-tight electric insulator	300	4×10^{-5} -- 1.5	600
14, 15	Flexible bellows, fittings	a. Thermal expansion alleviator	300	4×10^{-5} -- 1.5	600
		b. Electric terminal	---	---	---
17	Spacer pin	Concentric alignment of cases	825	1.5	1475

[a]The pressures given are those to be tested. For space operation, all vacuum numb
[b]The temperatures given correspond to the desired thermal holding temperature pro
with the inner element at design temperature (P_e = 16.8 W) at no propellant flow. I
[c]A common requirement is that there be no chemical reactivity with the propellants

TABLE 1

CE OF MODEL I MATERIALS (Concluded)

al holding mode - 10.5w)		Joints			
		Welds		Brazes[b]	
Pressure[a] (atm)	Ident. no.	Max. temp (°K)	Ident no.	Max. temp (°K)	Primary material requirements[c]
10^{-6}	---	---	---	---	Low thermal emissivity.
10^{-6}	---	---	5	600	a. Reliable brazability to refractory metal used.
---	---	---	6	600	b. Capable of a leakproof design.
10^{-6}	---	---	---	---	Low thermal conductivity at high temperature.
10^{-6}	---	---	3	600	a. Moderate dielectric strength (<10).
			4	600	b. Impervious to H_2 (leakage).
					c. Reliable metal-to-ceramic bond.
					d. Highest braze liquidus temperature compared to rest of assembly.
10^{-6}	5	600	1	600	a. Reliable brazability to refractory metal used.
---	6	600	2	600	b. Impervious to H_2 (leakage).
					c. High cyclic stress capability.
10^{-6}	---	---	---	---	High-temperature electric insulation.

ers are replaced by those corresponding to those of the orbital attitude.

file (P_e = 10.5 W); however, steady-state braze site temperatures could reach 700°C

lence, 700°C braze capability is highly desirable.

or their contained contaminants.

These parts are all exposed to H_2, even in the case of NH_3, where that gas is essentially dissociated at $2420^\circ K$ to its H_2 and N_2 constituents. Columbium and tantalum absorb very large amounts of H_2 and become quite brittle on subsequent cooling. In fact, they powder. These materials were therefore excluded from further consideration where H_2 exposure is required.

Table 2 and the figures that follow summarize the significant properties of the remaining candidates, tungsten, rhenium, molybdenum, and the alloys 74% tungsten/26% rhenium and 50% molybdenum/50% rhenium.

Table 3 summarizes the reactions of these materials to O_2 and some possible propellants and contaminants.

Table 4 summarizes the propellant requirements with regard to the permissible contaminant levels for rhenium, for example, compared to the levels found in various H_2 sources. Table 5 treats NH_3.

Ductility: Experience with resistojet development has shown that one of the most important properties is ductility. This property has the tremendous advantage of weldability and gives greater confidence that catastrophic brittle fracture will not occur.

The crystal structure of all four of the refractory metals (molybdenum and tungsten, as well as the discarded columbium and tantalum) is body centered cubic (bcc). A familiar characteristic of bcc metals that are raised above their recrystallization temperature is their transition from ductile to brittle behavior on cooling over a relatively narrow temperature range. This is illustrated in fig. 3 for the unalloyed, recrystallized metals using reduction in area in a simple tensile test as the measure of ductility. Rhenium, on the other hand, is hexagonal close-packed in structure and possess no known transition temperature, an important point in its favor.

Note that once a bcc metal is melted, as in electron-beam welding, it exhibits a ductile-to-brittle transition temperature. This temperature is not far above room temperature for molybdenum, but is well above room temperature for tungsten. Solid-solution alloying does not seem to improve this situation for tungsten, except the tungsten-rhenium alloy, whose properties are included for comparison in table 2. Rhenium similarly reduces the transition temperature for molybdenum.

Fig. 4 shows the reduction in transition temperature for tungsten and molybdenum that occurred when additions of rhenium were varied. The compositions 74% tungsten/26% rhenum and 50% molybdenum/50% rhenium are optimal, respectively, in this regard.

On the basis of ductility, rhenium and 74% tungsten/26% rhenium were preferred as candidates in that order for the highest-temperature element.

Property	Figure no.	Tungsten (ref. 2)	74% Tung
Melting point, ^{O}K	- - -	3683	
Density at $293^{O}K$, g-cm^{-3}	- - -	19.3	
Electrical resistivity, $\mu\Omega$-cm			
$293^{O}K$	7	5.5	
$2473^{O}K$	- - -	71.7	
Thermal conductivity watts, cm^{-1} ^{O}K-1	- - -		
$293^{O}K$	- - -	1.30	
$2473^{O}K$	- - -	1.00	
Sublimation rate, g-cm^{-2} sec^{-1}	5, 6	*	
Specific heat ($20^{O}K$), cal g^{-1} ^{O}K-1	- - -	0.032	
Modulus of elasticity ($293^{O}K$), lb-in.$^{-2}$ x 10^{-6}	- - -	50 x 10^{6}	
Recrystallization temp ^{O}K	- - -	1838	
Ductility	3, 4	*	
Endurance strength, psi	8, 9	*	
Creep, min^{-1}	9, 10	*	
Prices ($/lb) (depends on form and quantity)	- - -	$15 to $30	$4

*See figures given.
**See text.

sten/26% rhenium (ref. 3)	Rhenium (ref. 3)	50% Molybdenum/50% rhenium (ref. 4)	Molybdenum (ref. 2)
3393	3453	2823	2883
19.5	21.02	13.76	10.2
31	19.3	19.4	6.0
93	107.8	81 (extrap)	50.0
NA	0.38	0.355	1.365
	0.510	NA	0.730
**	*	**	*
0.032	0.033	NA	0.063
NA	68×10^6	53×10^6	47×10^6
1923	1673	1675 to 1875	1400
*	*	*	*
*	*	*	*
NA	*	NA	*
50 to $1000	$800 to $2000	$570 to $1100	$10 to $25

TABLE 3

REACTIONS WITH RHENIUM, TUNGSTEN, AND MOLYBDENUM

Item	Gas	Rhenium	Tungsten	Molybdenum
1.	Oxygen, O_2	$> 875^\circ K$, catastrophic oxidation occurs: $7O_2 + 4Re \longrightarrow 2Re_2O_7$. Re_2O_7 boils at $636^\circ K$ (white fumes).	$< 575^\circ K$, metal remains bright. $< 875^\circ K$, blueblack adherent oxide. $> 875^\circ K$, yellow or yellow-green WO_3. $> 1275^\circ K$, WO_3 volatile; $> 1746^\circ K$, , WO_3 melts. Other suboxides, WO_2, $W_{18}O_{49}$ W_4O_{11}, $W_{20}O_{58}$.	$> 925^\circ K$, molybdenum oxidizes rapidly to MO_3 $> 975^\circ K$, MO_3 sublimes. $1070^\circ K$, MO_3 melts.
2.	Nitrogen, N_2	Does not react with N_2.	$> 2775^\circ K$, WN_2 by N_2 over tungsten, but is reduced by H_2.	*
3.	Argon, Ar	No reaction.	No reaction.	No reaction.
4.	Methane, CH_4	It is debatable whether rhenium heated in presence of CH_4 and CO cause carbides. Carbon will form a eutectic at $2753^\circ K$.	Tungsten combines readily with carbon beginning at $1475^\circ K$.	*

*Review incomplete; no further work planned.

TABLE 3

REACTIONS WITH RHENIUM, TUNGSTEN, AND MOLYBDENUM - Concluded

Item	Gas	Rhenium	Tungsten	Molybdenum
5.	Water, H_2O	Has high resistance to water vapor compared to tungsten. In moist air, the metal is gradually oxidized to perrhenic acid $HReO_4$ (necessitates storage with desiccants).	$> 975^{\circ}K$ oxidation	*
6.	Carbon monoxide, CO	See item 4.	Carbon monoxide carburizes about $1975^{\circ}K$.	*
7.	Carbon dioxide, CO_2	See item 4.	$> 1475^{\circ}K$ oxidation.	*
8.	Ammonia, NH_3	No reaction.	No reaction.	*
9.	Hydrogen, H_2	No reaction.	No reaction.	No reaction.

*Review incomplete; no further work planned.

TABLE 4

RESISTOJET H_2 PROPELLANT REQUIREMENTS

Item	Requirements for resistojet life tests	Electrolytic grade H_2 (Airco)	LH_2 (MIL-P-27201A)
Purity, % by volume	>99.95	>99.95	>99.995
Oxygen, ppm	<3	<2	<1
Inert gases, ppm	- - -	- - -	<48
Nitrogen, N_2	*	<350	
Argon, Ar	*	<4	<9
Methane, CH_3	<2**	<0.2	
Carbon gases, ppm			
Carbon monoxide, CO	<2**	<2	1
Carbon dioxide, CO_2	<2**	<1	
Water vapor			
ppm	<3	<3	0
Dewpoint, $^{\circ}K$	<204	<204	- - -
Filtered to:	To be filtered on site to 10μ		
Nominal	- - -	- - -	10
Absolute	- - -	(Not available)	40

*Contaminant level limited only by purity requirement.
**Preliminary limit set by controversially possible carbon reactions with rhenium.

TABLE 5

RESISTOJET NH$_3$ PROPELLANT REQUIREMENTS

Item	Requirements for resistojet life tests	Laboratory grade anhydrous NH$_3$ (Armour)	(Unacceptable) NH$_3$ MIL-P-27406
Purity, % by weight	99.99	99.99	99.5
Oxygen, ppm	<3	0	not specified
Nonbasic gases	---	---	not specified
Vapor phase	*	<25	---
Liquid phase	*	<10	---
Water vapor, ppm	<3	<33	<5000
Oil, ppm	<2 **	<2	<5
Filtered to, μ			
Nominal	10	10	10
Absolute	40	40	40

*Contaminant level limited only by purity requirement.
**Preliminary limit set by controversially possible carbon reactions with rhenium.
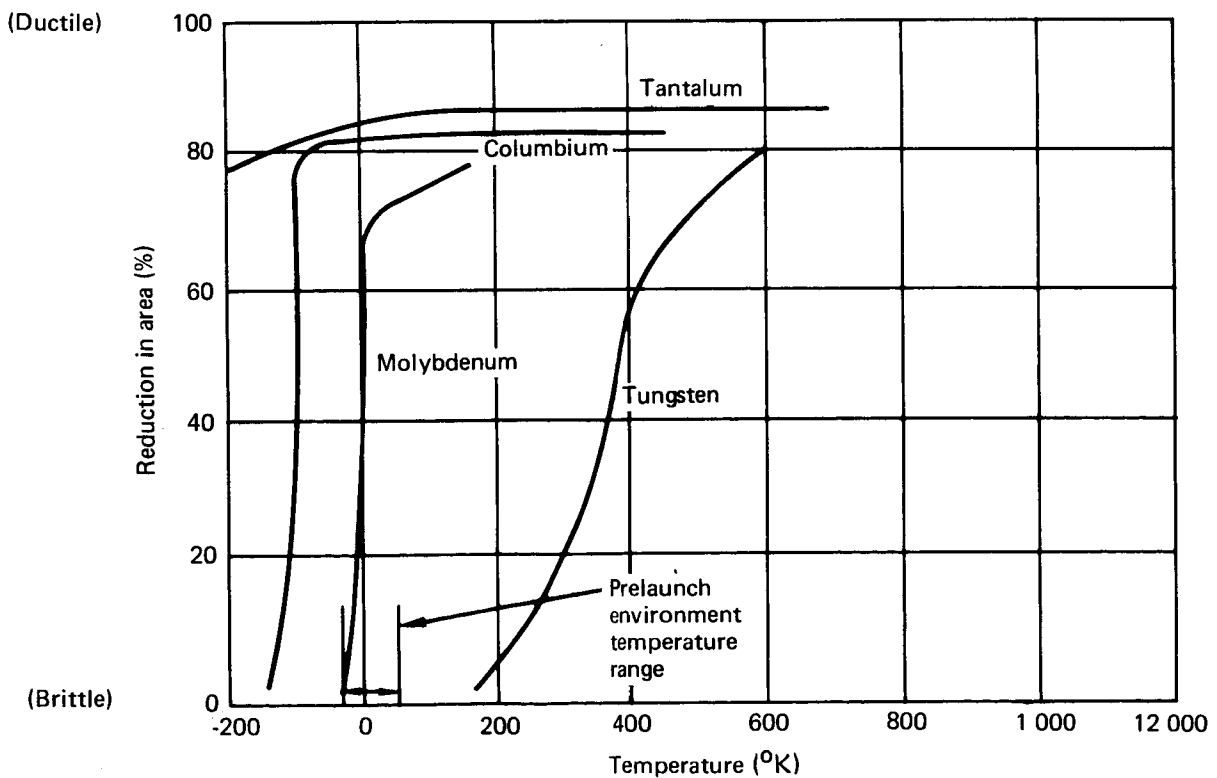
Figure 3. Ductile-Brittle Transition Behavior of Unalloyed Recrystallized Refractory Metals
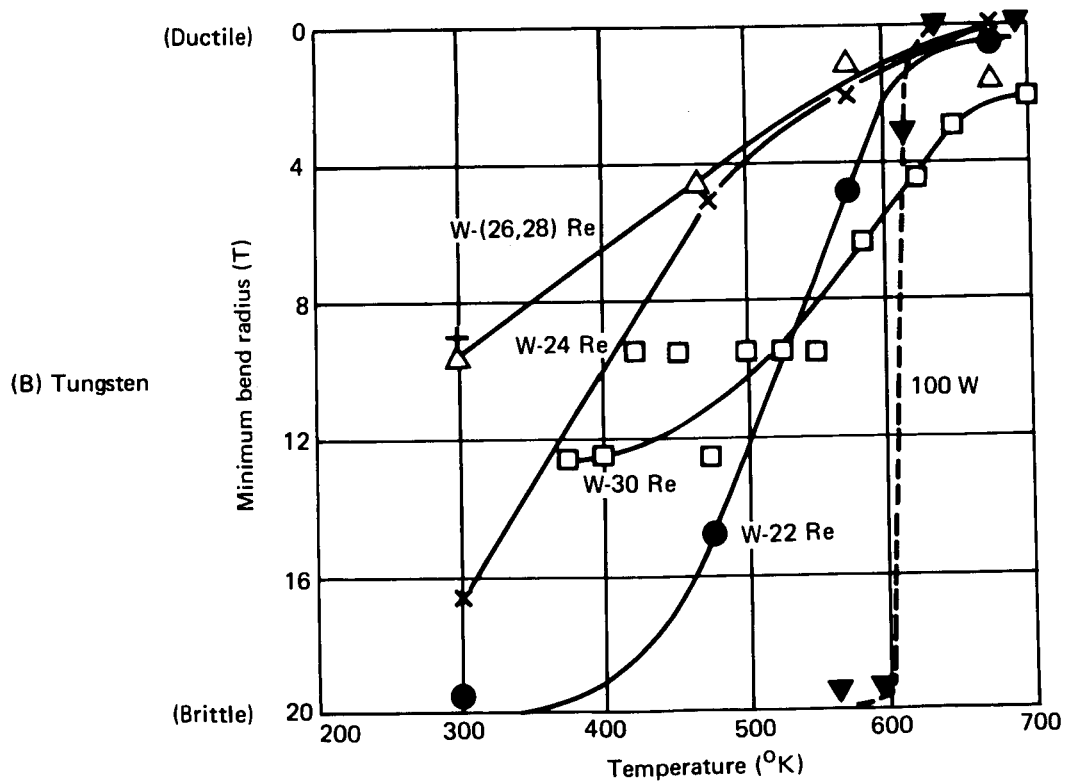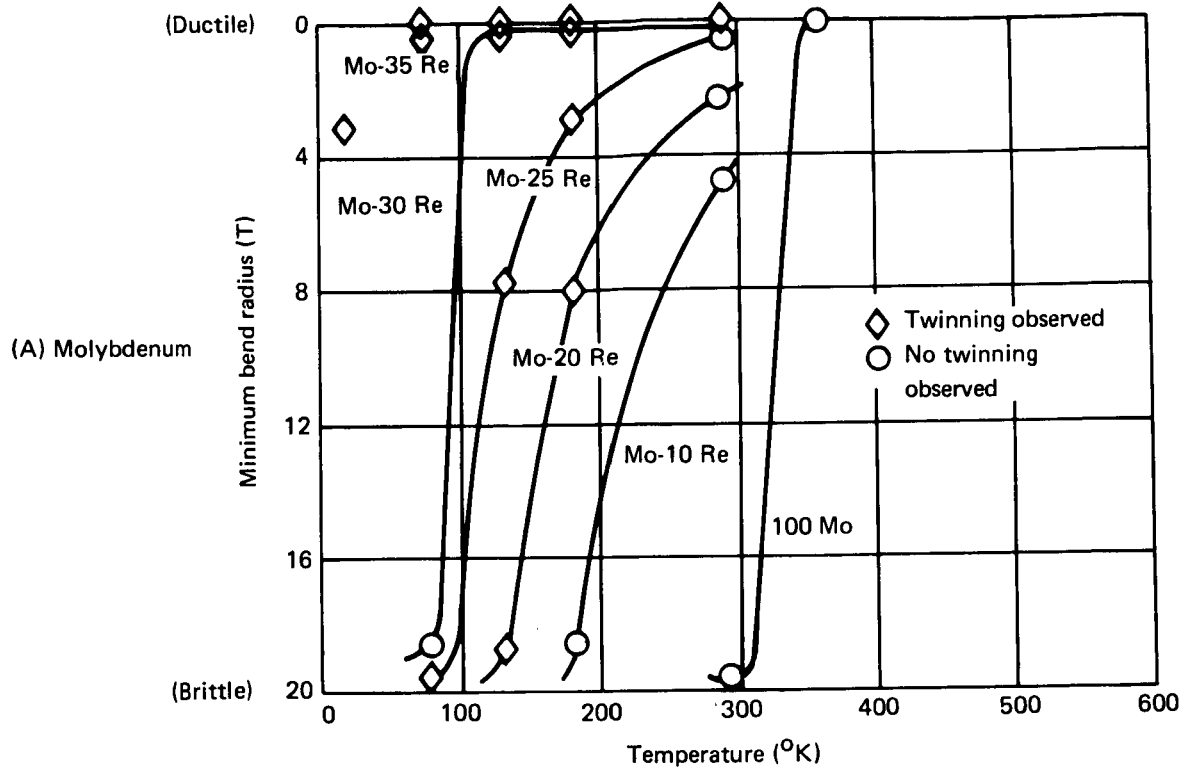
Figure 4. Effect of Rhenium on Ductile-To-Brittle Bend Transition Temperature (ref. 4)

Sublimination: A primary factor to be considered in determining the life expectancy of resistojet thrustor is the sublimation of metal from the heat-exchanger walls. The following presents the estimated life of the 10 mlb resistojet.

Thickness and mass loss rates are given for the critical thrustor parts. These rates are used to calculate the time necessary to reduce thickness or mass by 10% (the work statement definition of thrustor life).

The losses from the 10-mlbf unit were calculated with the use of sublimation data in the presence of a flowing gas from calculations by Zima of the Lawrence Radiation Laboratory (ref. 5). These data are for vacuum and forced convection with helium at 1 atm and 100-fps velocity. Conversion factors for other gases are given. Since mass and thickness loss rates are inversely proportional to the square root of the pressure, pressure effects can be found from the 1-atm data by applying the following equation:

$$\text{loss rate at pressure P} = \text{loss rate at 1 atm} \times \left(\frac{P_1}{P}\right)^{0.5} \qquad (1)$$

The effect of gas velocity is

$$\text{loss rate at velocity V} = \text{loss rate at 100 fps} \times \left(\frac{V}{V_{100}}\right)^{0.5} \qquad (2)$$

As shown in figs. 5 and 6, the rate of mass loss caused by sublimation is greatly reduced by the presence of a gas. At $2500^{\circ}K$, for example, the rate in vacuum is greater than that at 1 atm by a factor of 100.

The temperature distribution used for these calculations is found in the performance predictions section. The outer case is exposed to a vacuum on one side and pressure on the other; however, its temperature is so low that sublimation is negligible. The same is true of the inner case.

The outer heating element has a maximum temperature of $1675^{\circ}K$, which is still low enough that no significant sublimation takes place. The inner heating element, has a high enough temperature even in an H_2 atmosphere to produce significant loss of material by sublimation. A major contribution to the high rate of loss is the high velocity of the gas in the inner element.

17
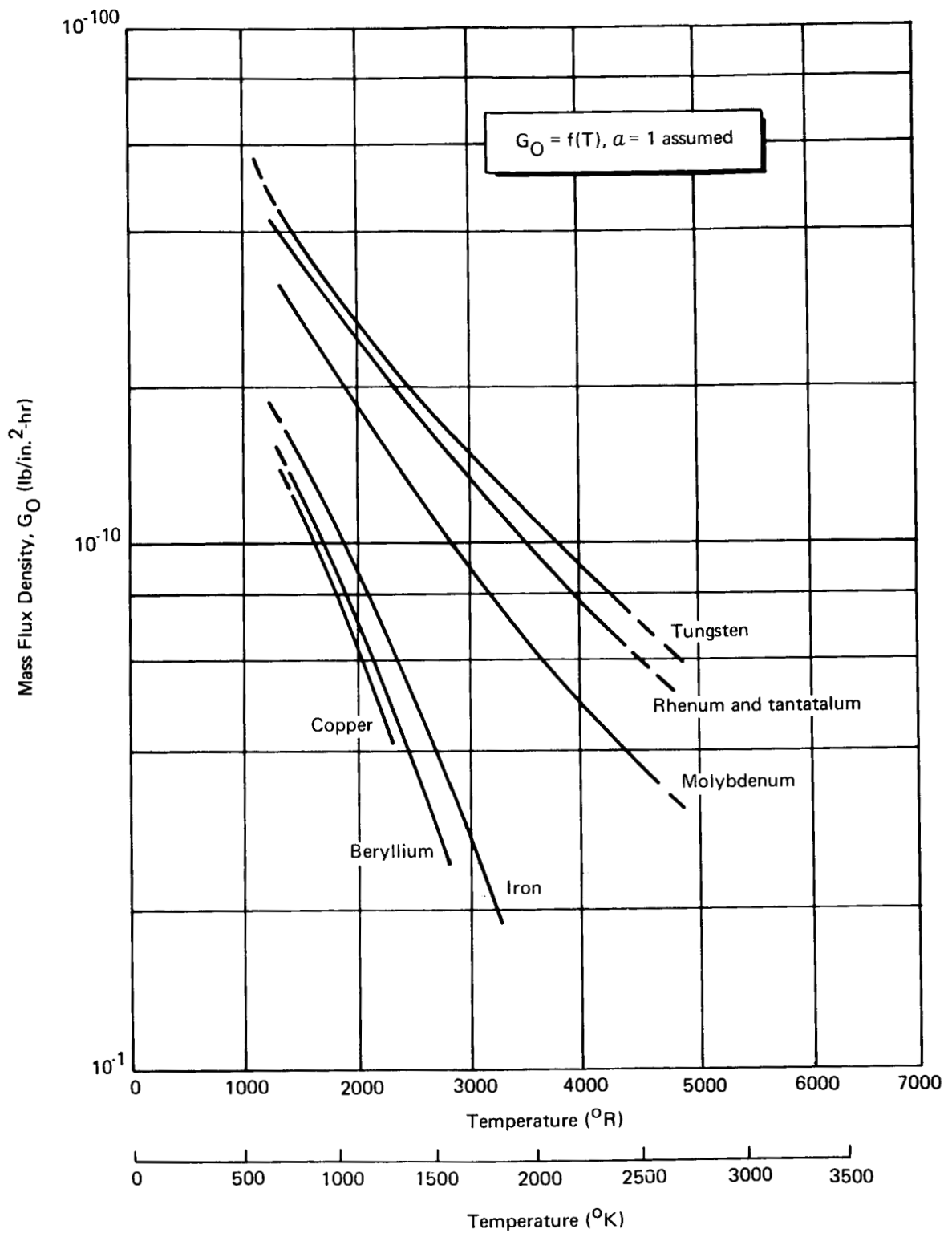
Figure 5. Vaporization Loss vs. Temperature in Vacuum (ref. 5)
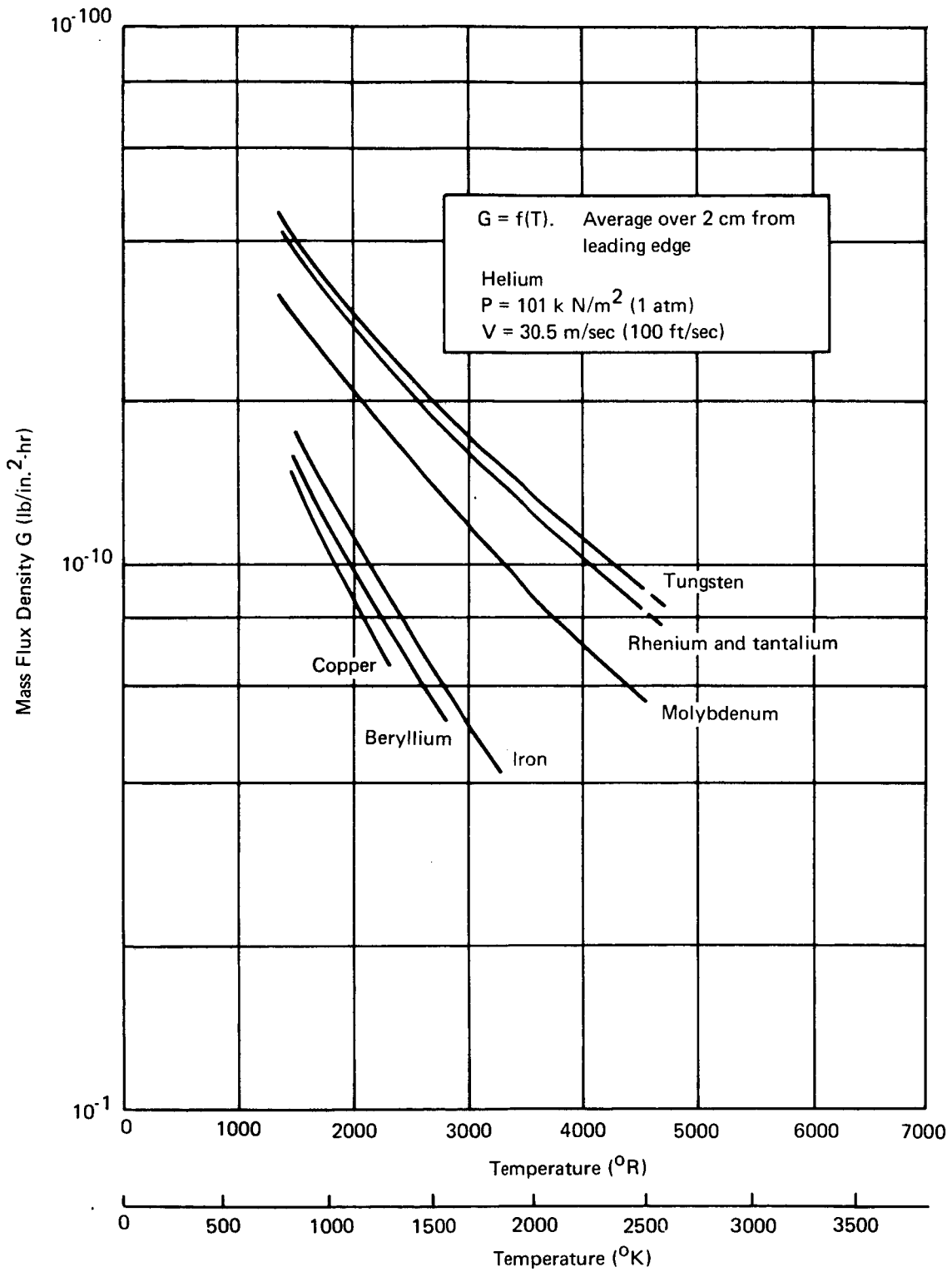
Figure 6. Vaporization Loss vs. Temperature Under Forced Convection (ref. 5)

Table 6 summarizes the erosion rates and resultant life expectancy of the Model I thrustor on H_2.

Since higher erosion rates are predicted for the lower molecular-weight gas, H_2 is taken to be the worst case. Sublimation rates in the presence of NH_3 should be lower by a factor of 0.9. The velocity effect should further reduce the rate by a factor of 0.7 so the erosion rate in NH_3 should be only 60% of the rate in H_2.

The calculations assume laminar flow which is definitely the case in the subject thrustor. Losses in turbulent flow could be considerably higher.

When the thrustor operates in the thermal-control mode (no flow, only sufficient power to maintain temperature), the conditions for sublimation deteriorate because all surfaces are exposed to vacuum. In this mode, it will be necessary to operate at a lower temperature to hold losses to the same level as in normal operation. As shown in table 1, this temperature is 2250°K. If, however, the thermal-control mode constitutes a major percentage of mission time, it may be advisable to operate at even lower temperature to prolong thrustor life.

Electrical resistivity: Rhenium has a higher resistivity than the other candidates (fig. 7). Either higher terminal voltage or thicker heat-exchanger walls result with rhenium as compared to tungsten or 74% tungsten-26% rhenium.

Endurance strength: The pressure stresses on the inner heating element are very low [of the order of 689 kN/m² (100 psia)]. This is primarily because of the relatively low chamber pressure, which is 1 to 2 atm in this type of rocket.

Because of this low stress, the failure criteria by which to compare candidate materials must be those of an endurance nature: (1) endurance stress-rupture, (2) creep elongation, and (3) fatigue. The first two recently have been given a careful comparative evaluation for the materials and temperature range of interest in a H_2 environment (ref. 6). Fig. 8 shows the endurance stress-rupture at 2473°K which is close to the anticipated maximum inner element temperature of 2523°K. No endurance data are available on the refractories as made by the vapor deposition process. The sintered refractory data shown here are believed to be conservative and therefore useful for design purposes. Such data are not available for test times longer than 100 hours. It must be extrapolated to estimate the stress-rupture values of interest of the order of 2000 hours or greater. The basis for the extrapolation is the Larson-Miller relationship [eq. (3)] which indicates a linear relationship on a log-log basis:

$$T (\log t_r + C) = a + b \log \sigma \qquad (3)$$

where

$$T = \text{temperature absolute}$$

$$t_r = \text{rupture life in hours}$$

TABLE 6

SUMMARY OF SUBLIMATION CALCULATIONS--MODEL I (0.044-N) (10-MLBF)
THRUSTOR, RHENIUM HEAT EXCHANGER

Part no.	Name	Max temp (^{O}K)	Mass loss rate (gm/sec)	Thickness loss rate (cm/sec)	Time to 90% mass		Time to 90% thickness	
					sec	yrs	sec	yrs
(fig. 2)			Normal operation, H_2 flow					
1	Outer case	735	10^{-46}	10^{-48}	10^{46}	10^{39}	10^{45}	10^{38}
2	Inner case	735	10^{-46}	10^{-48}	10^{46}	10^{39}	10^{45}	10^{38}
3	Outer heater	1675	3.4×10^{-6}	2.3×10^{-17}	5×10^{14}	1.6×10^7	1.2×10^{14}	4×10^6
4	Inner heater	2520	6.67×10^{-9}	1.67×10^{-10}	1.05×10^7	0.33	9×10^6	0.29
			No-Flow Operation					
4	Inner heater	2250	6.67×10^{-9}	1.67×10^{-10}	1.05×10^7	0.33	9×10^6	0.29
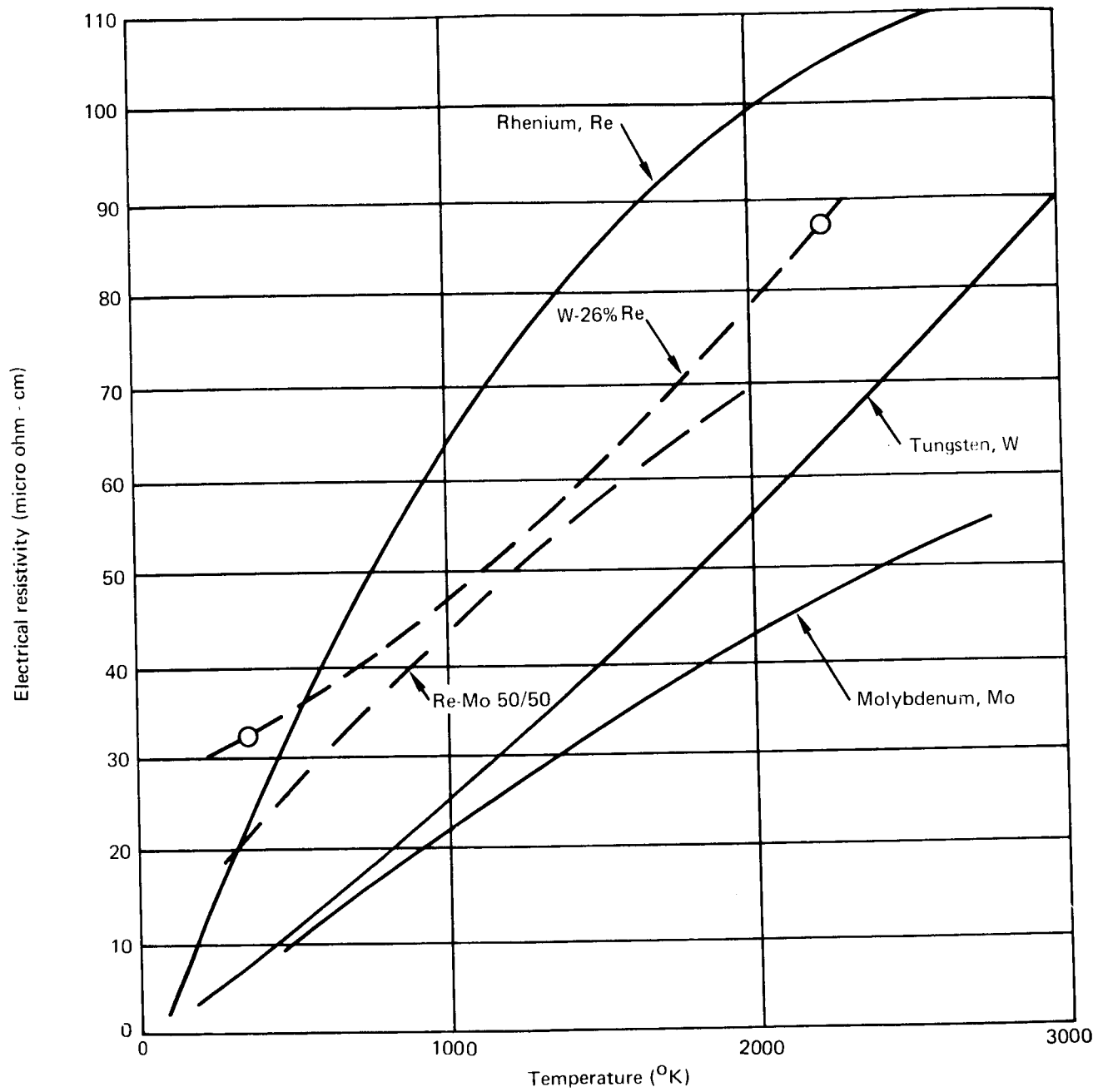
Figure 7. Resistivity of Candidate Materials
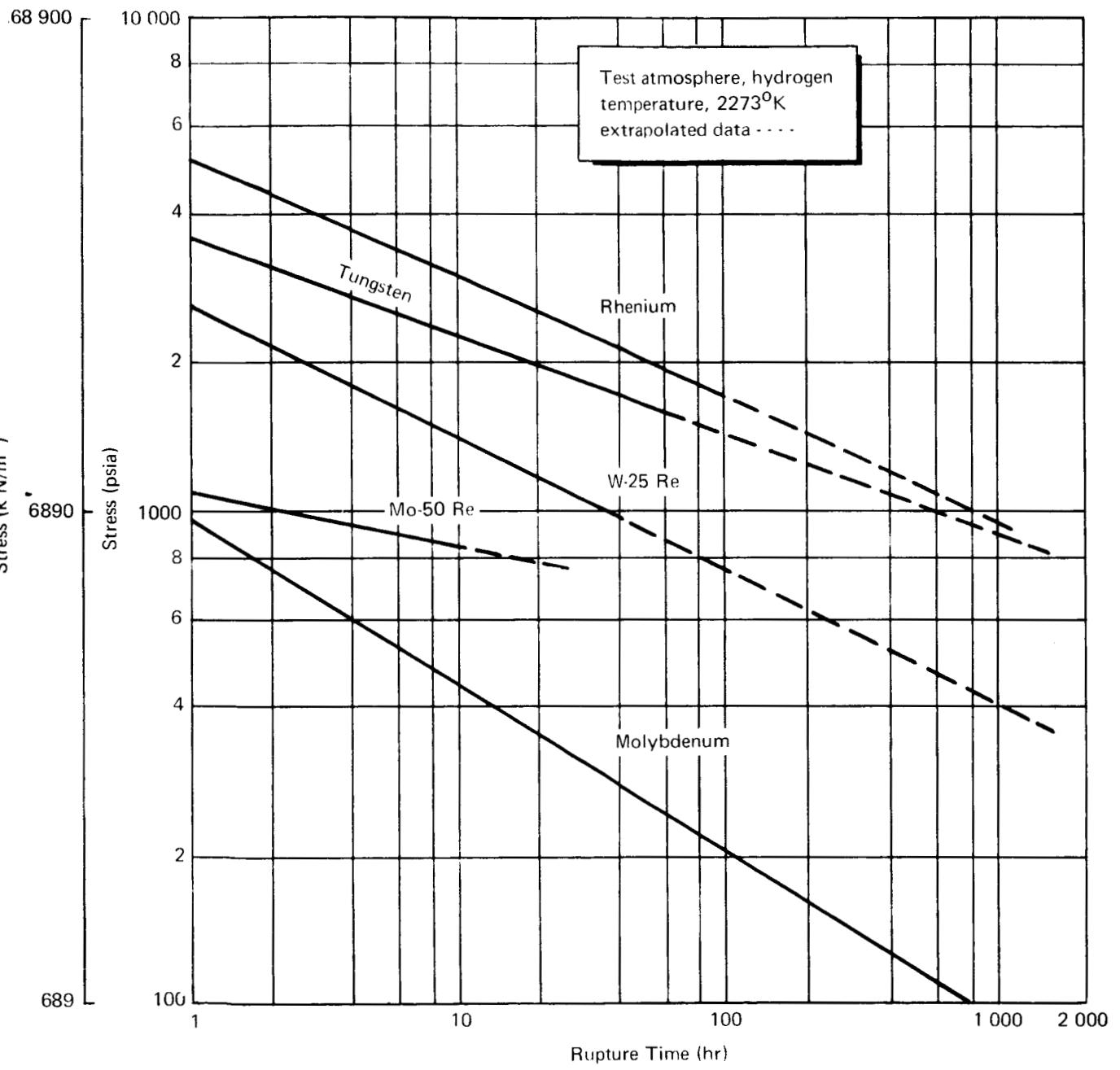
Figure 8. Comparative Stress Rupture of Sintered Refractory Metals and Alloys

C = Larson-Miller constant for given material

σ = stress

and

a and b are constants.

Recent data on rhenium show some unexplainable curvature (see fig. 9), but this is insufficient to invalidate the conclusions here. The order of merit is rhenium-tungsten, 75% tungsten/25% rhenium, 50% molybdenum/50% rhenium, and lastly, molybdenum, with at least one order of magnitude in stress capability between the first and last.

Creep, as measured by elongation rate under stress at $2473^\circ K$ in H_2, is shown in fig. 10. No data could be found for 75% tungsten/25% rhenium at this temperature. Lower temperature data show the latter material to be roughly comparable to rhenium and tungsten. A metal bellows is used to alleviate induced axial stresses from differential thermal expansion. The design permits the inner element to be operated at essentially negligible longitudinal stress at operating temperature but at a definite tensile load under cold-flow condition to ensure straightness.

Creep (yielding) is seen to relieve the inner element at the hot operating condition to negligible operating stress. Creep then is not seen as a governing failure mechanism of the inner element in this device as long as the adjustment is small.

These two factors, rupture and creep, for the selected, rhenium, are shown in fig. 9 over a range of temperature of up to $3073^\circ K$.

The (10-mlbf) resistojet will be subject to cyclic stresses and temperatures. (See Cyclic Performance discussion.) No data were found on high-temperature fatigue of refractories with which to evaluate the effect of operating approximately 10 000 cycles. Cyclic thrustor tests must be conducted to verify this facet, and this is not within the scope of the study. The only criteria for guidance in material choice is that, in general, the higher the creep strength of a material, the higher its high-temperature fatigue strength--indicating rhenium, tungsten, or 75% tungsten/25% rhenium again by this criterion.

Materials of intermediate and low-temperature parts. — It was decided that the outer and inner cases on the initial engines should be of the same material as the heating elements to permit ease of welding and expansion compatability.

Commercially available insulators of ceramic material brazed to metal were chosen for the insulator fitting. These are made from nickel-iron alloy or grade-A nickel, silver brazed to a metalized alumina tube.
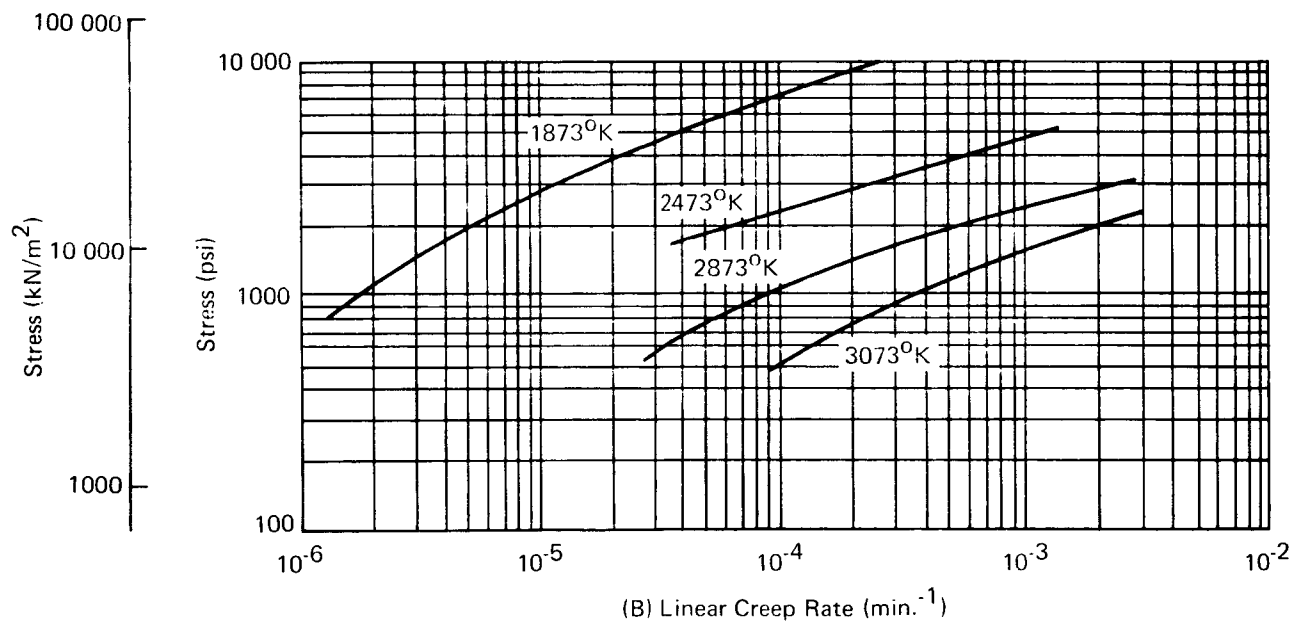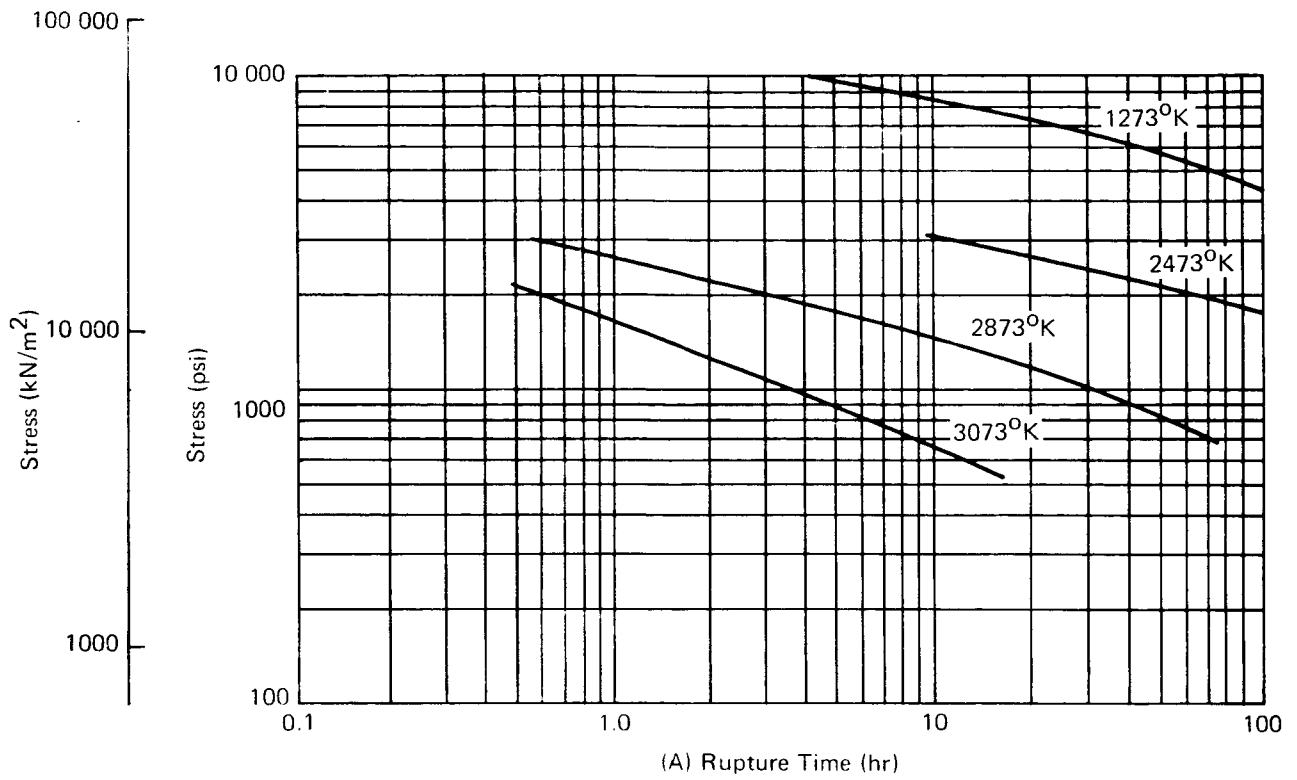
Figure 9 Stress Rupture and Creep Behavior of 0.05 cm Thick Powder Metallurgy Rhenium in Hydrogen (ref. 6)
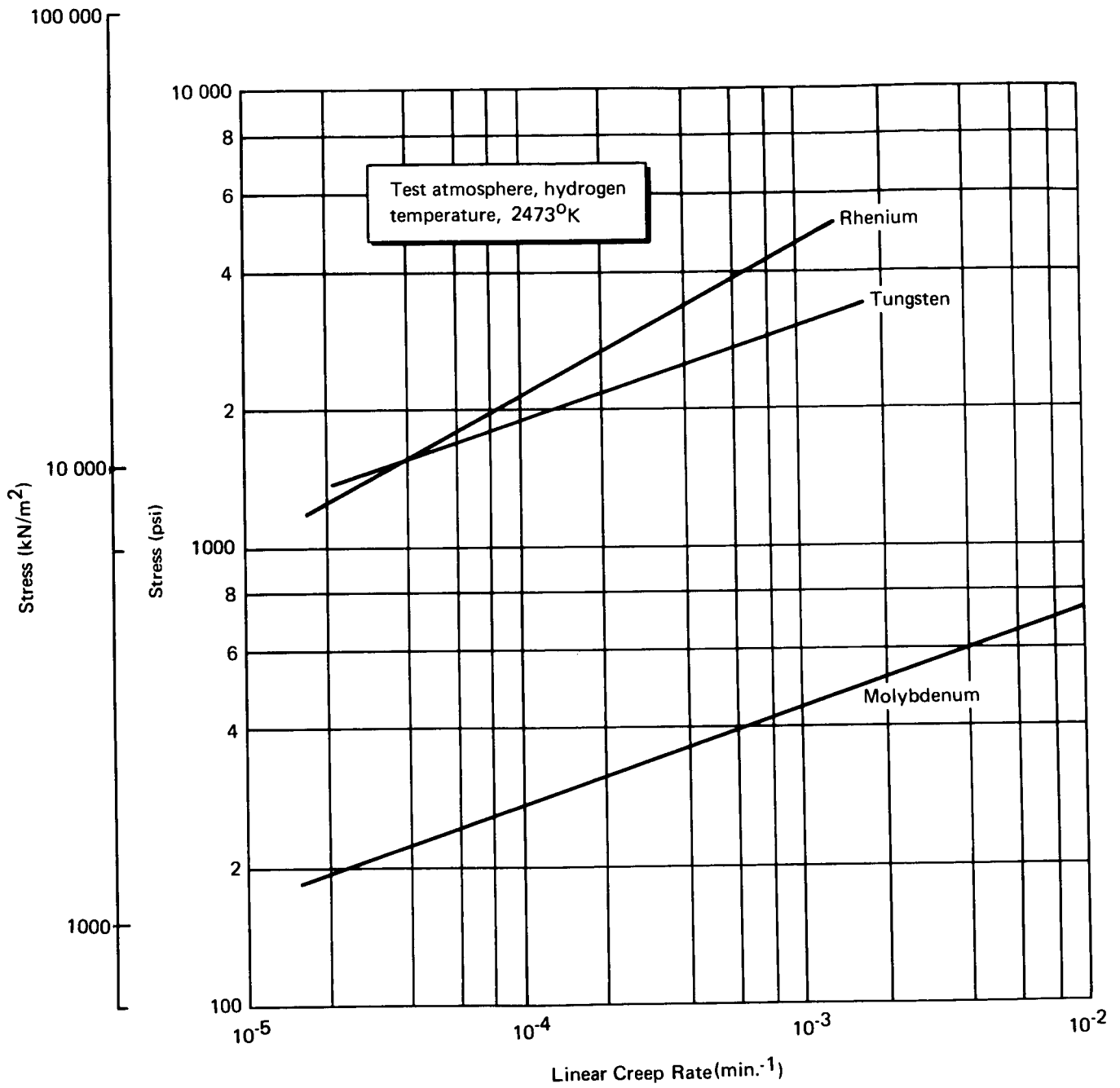
Figure 10. Linear Creep Rate of Sintered Refractory Metals (ref. 6)

The second insulator (6) (see fig. 2) is a tubular shell which prevents a short from the outer heating element (3) to the inner case through the radiation shield (7), should the elements move transversely. The third and fourth insulators are spaced front and rear between the inner case (2) and outer case (1).

Boron nitride has been successfully used in electrothermal devices as an electrical insulator in very-high-temperature service, provided refractory borides are not allowed to form. All boron-nitride insulator sites are located in regions less than $1275^{\circ}K$, which should result in a conservative design.

Either stainless steel or nickel appeared suitable for the tee-fitting; in fact, one engine was built using each material.

Stainless steel was chosen as the bellows material, since a wide variety of stainless-steel bellows, with respect to sizes and spring rates, is available "off the shelf."

The radiation shield in the vacuum jacket plays an important role in preventing the radial loss of heat. The major requirement was that material be available in thin sheets, 0.008 mm (0.0003 in.). Tantalum was the only high-temperature material available in thin sheets. It is believed that at the low pressures involved 20 μmHg, H_2 attack, as discussed earlier, will be inconsequential. The total emissivity of the refractories considered are comparable.

The thermal insulation (11) chosen is Min-K-2000.* It was successfully used previously and has a low thermal conductivity (see fig. 11) along with a high-temperature capability of $1366^{\circ}K$.

Parts Fabrication

Vapor deposition. — Rather sophisticated inside shapes can be formed by the vapor deposition method with the refractories. Rhenium may be deposited (at a temperature of $975^{\circ}K$) on a sacrificial material, such as titanium, which is later removed with a hydroflouric acid solution. This is done by passing H_2 and $ReCl_5$ (usually) gas over the induction-heated mandrel. The reaction,

$$5H_2 + 2ReCl_5 \rightarrow 2Re + 10H\,Cl \qquad (4)$$
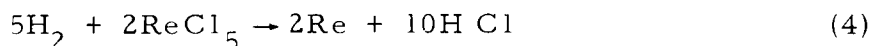
takes place depositing the rhenium on the mandrel.

Mandrels (fig. 12) which have been fabricated from titanium (A-55) bar stock (which conforms to Aerospace Materials Spec No. 4941) were stress-relieved after machining. This annealing process is required to prevent distortion of small parts due to residual stresses during subsequent processing. Parts are annealed in a vacuum retort furnace (10^{-3} torr) at $815^{\circ}K$ and held there for 1 hour.

---

*Johns-Mansville Industrial Insulation Division.
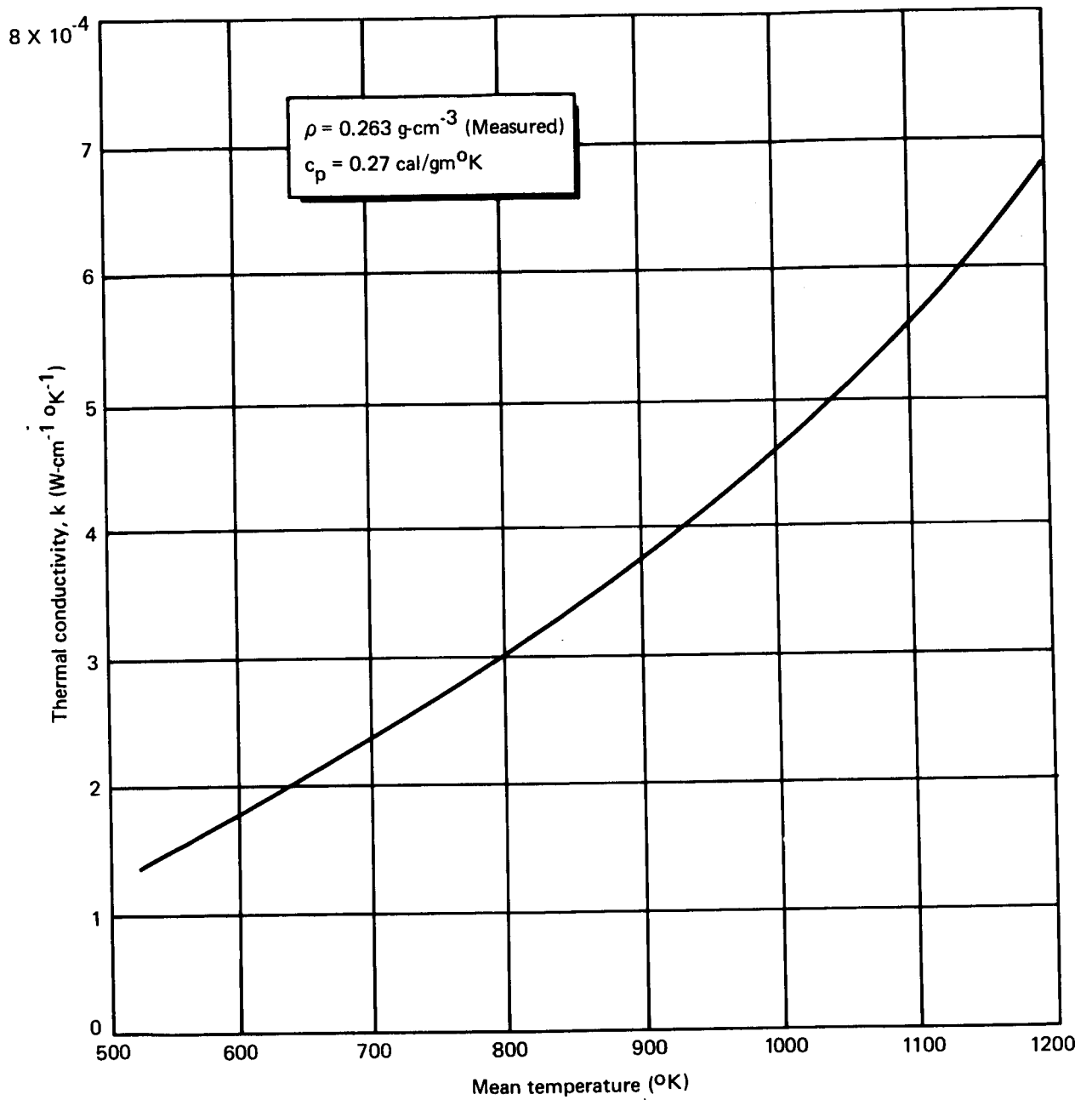
Figure 11.   Thermal Conductivity of Min-K-2000
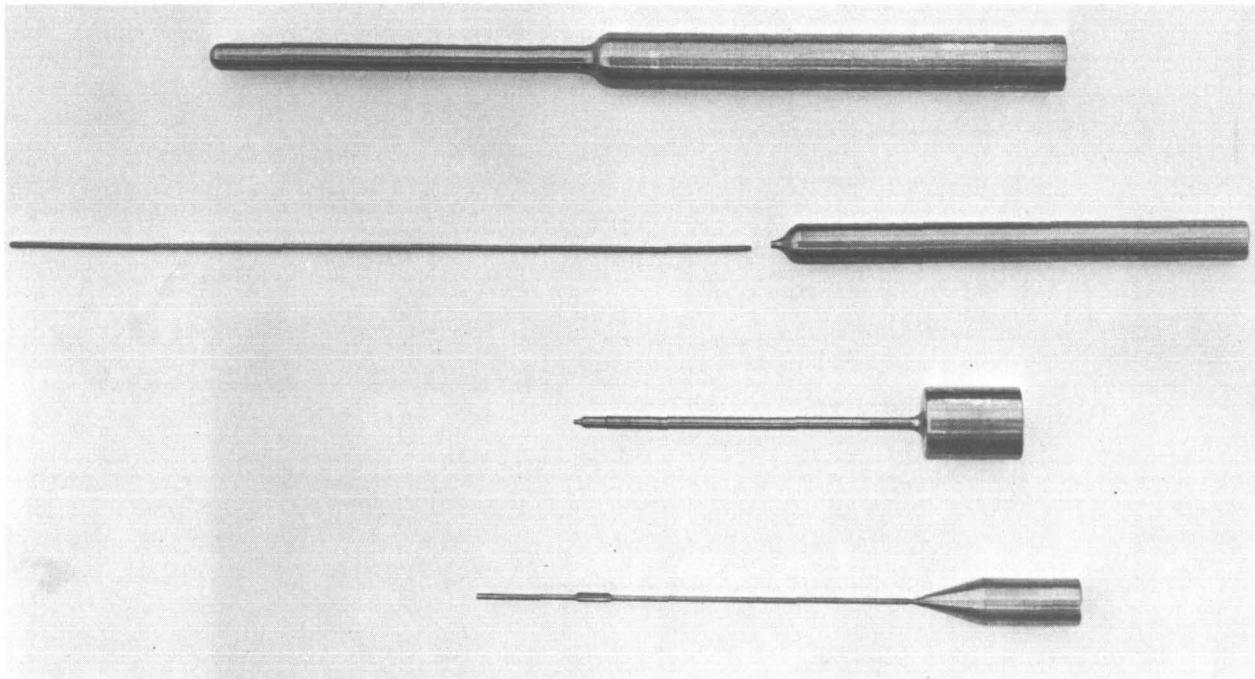
Figure 12. Titanium Mandrels for Vapor Deposition of Rhenium Parts for Model I Resistojet

The vapor deposition technique provided the major breakthrough in allowing the use of this material in the necessary shapes. This process is not currently without fault, however, and qualifies somewhat as an art. As larger quantities are produced, it is believed that reliable quality and delivery times will improve significantly. Some parts are shown, as deposited, in fig. 13.

Machining. — The lack of success in mechanically machining pure rhenium appears to be its sole drawback. Pure tungsten and molybdenum are not particularly easy to machine, either, but some additives, such as 2% thoria and 1/2% titanium, make substantial improvements.

Because of its fantastic coefficients of work hardening, rhenium rapidly turns over even carbide-tipped tools and drills. Rough machining can be accomplished, however, by torch-heating the work while turning.

Drilling can be accomplished by eloxing (electro-discharge) and by using diamond-core tools. Outside diameters and contours may be ground readily with aluminum oxide, and sometimes silicon carbide, wheels.
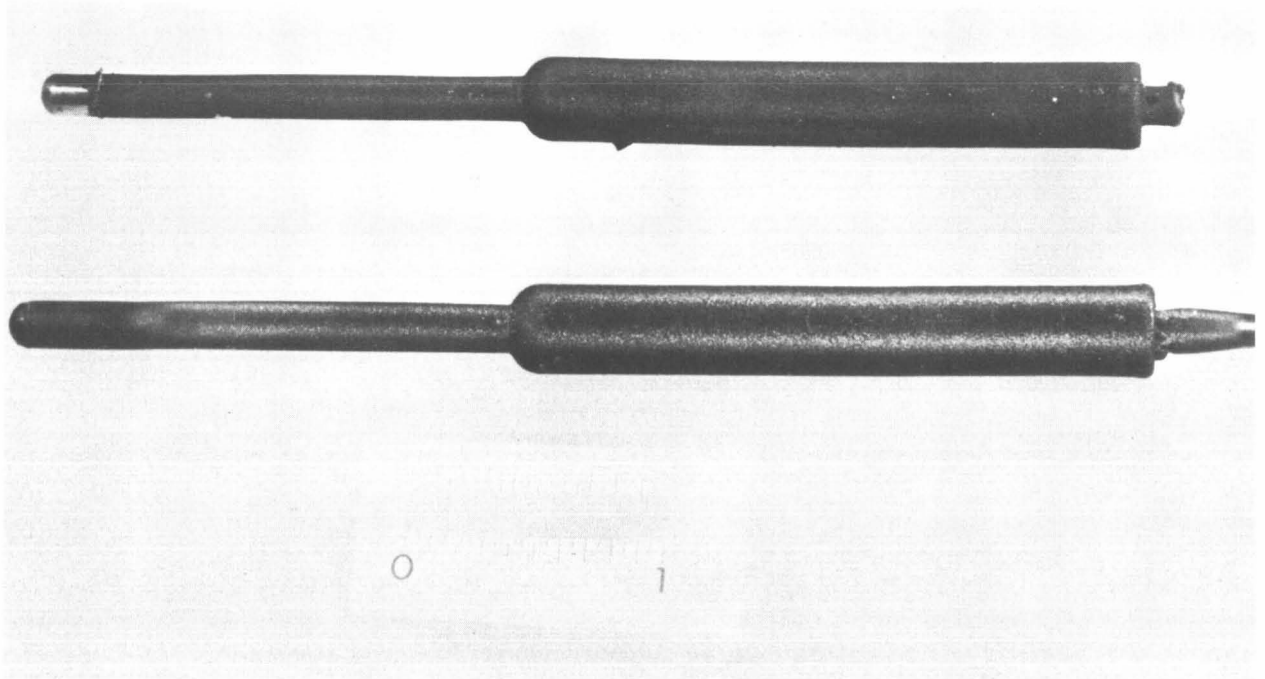
Figure 13. Typical Vapor Deposited Rhenium Parts (Before Grinding)

Rhenium has one of the highest coefficients of work hardening of any of the metals and, therefore, must be annealed quite often. Annealing can be accomplished for the 0.005- to 0.120-in. materials as low as 1775°K for 10 min. to 1 hour. A furnace temperature of 1925°K for 5 to 30 min. is recommended.

Assembly

The rhenium parts of the Model I thrustors were assembled by electron-beam welding; all other joints were made by brazing.

Electron-beam welding. — The progress in resistojets has been paced by the development status of joining refractory metals and to a lesser extent by the ability to form desired part shapes.

There is a marked contrast in electron-beam welding (which is perhaps the best technique known for joining refractories) of rhenium as opposed to that of tungsten. The choice relates to the previous discussion of room temperature ductility. Rhenium is extremely tolerant to electron-beam and TIG welding and subsequent reworking. Because of the brittle nature induced in the weld area, tungsten is prone to sudden fractures for no visible outward reason. In this respect, molybdenum is more like tungsten than rhenium.

The electron-beam welding of molybdenum and tungsten can be summarized as follows: for tungsten, the metallurgical effects induced by welding raise the ductile-to-brittle transition from 475°K to 675°K and relative tensile strength at room temperature is reduced to 50% of the base metal, but the high-temperature properties are unaffected. Molybdenum is similar, but with less reduction in strength to 80% of the original material values.

Because little information was available in the electron-beam welding of rhenium at the beginning of this project, typical joints were made at Marquardt and at EBW, Inc., to establish weld schedules for the Model I thrustor (table 7). Some welds are shown in figs. 14 and 15.

Brazing. — The propellant/electric feedthrough assembly of Model I consists of a bellows, a ceramic seal, and a tee-fitting. The bellows is type 347 stainless steel, while the end adapter is type 321 stainless steel. The insulator portion of the seal is 96% Al_2O_3 with a glazed outer surface. The ceramic seal stud and end connector are made from a 42% Ni/58% Fe alloy with expansion characteristics similar to the alumina insulator with silver-copper eutectic braze (72% Ag/28% Cu) which has a melting point of 1055°K. The tee-fitting is type 316 stainless steel which has a nominal alloy composition of 18% Cr, 12% Ni, and 2% Mo. As designed, the feedthrough assembly is jointed to the outer rhenium tube at the tee-fitting and to the inner rhenium tube at the bellows end adapter. In all, four dissimilar metal joints (Re/321 SS, 321 SS/42% Ni-Fe, 42% Ni-Fe/316 SS, and 316 SS/Re) are required to attach the feedthrough assembly to the resistojet engine.

Brazing was selected as the method for joining these parts for a number of reasons, the most important being that it offers the highest probability of success from a fabrication and service standpoint. While welding was considered initially, it was eliminated because of the high probability that the weld joints would crack on cooling or in service because of the formation of brittle intermetallic compounds. The situation was further complicated by the fact that the 300-series stainless steels contract about three times as much as rhenium on cooling, which would create very high residual stresses in the weld. Further, welding these metals would be difficult because of the large difference in their melting characteristics. For example, type 316 SS melts over the range 1645°K to 1675°K while rhenium melts at 3455°K. The case for brazing the parts is quite strong if one considers the inherent advantages of this method:

(1) If, a good leak-tight joint is not obtained, one can usually disassemble the parts, remove the braze, and braze them again.

(2) Brazed joints are leak-tight and usually remain so during thermal cycling because of the inherent ductility of the joint. Further, internal stresses resulting from fabrication are low because the joining temperature is usually significantly lower than that required for welding.

(3) Braze joints can be made quite strong, if they are designed properly and an appropriate braze is selected. Although braze strengths may be of the order of 6890 kN/m^2 (1000 psi), the joint area can be made quite large so that large forces can be reacted.

TABLE 7

ELECTRON-BEAM WELDING SCHEDULE FOR RHENIUM

Joint	Thickness	Voltage (kV)	Current (mA)	Spot Diam (Div)*	Travel (cm/min)
Tee	0. 5 to 0. 5 mm (0. 020 to 0. 020 in.)	130	2. 5	0. 15 mm (0. 006 in.)	50
Tee	0. 5 to 0. 125 mm	130	3. 05	0. 25 mm (0. 010 in.)	50 - 70% joint pickup during a repair
	(0. 020 to 0. 005 in.)	130	3. 6	0. 25 mm (0. 010 in.)	50 -100% penetration
Lap	0. 25 to 0. 125 mm (0. 010 to 0. 005 in.)	90	2. 2	0. 15 mm (0. 006 in.)	18. 3-accomplished by circle generator

*Div on optics equals 0. 036 mm for the 150-mm work distance used.

Tee joint 0.051 cm (0.020 in.) to 0.013 cm (0.005 in.)
thickness rhenium sheet
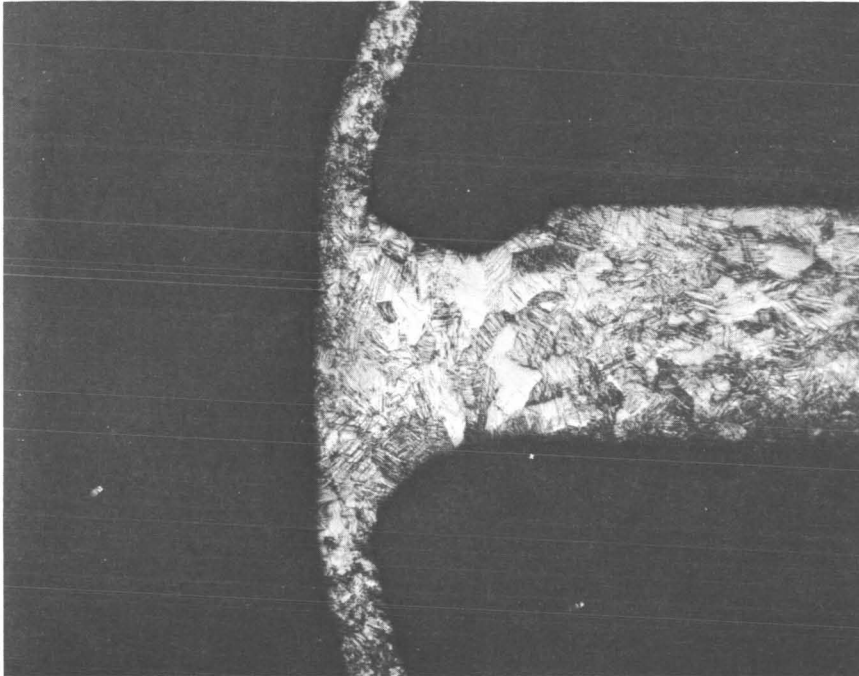
Cross section   (50X)

Figure 14. Electron Beam Weld
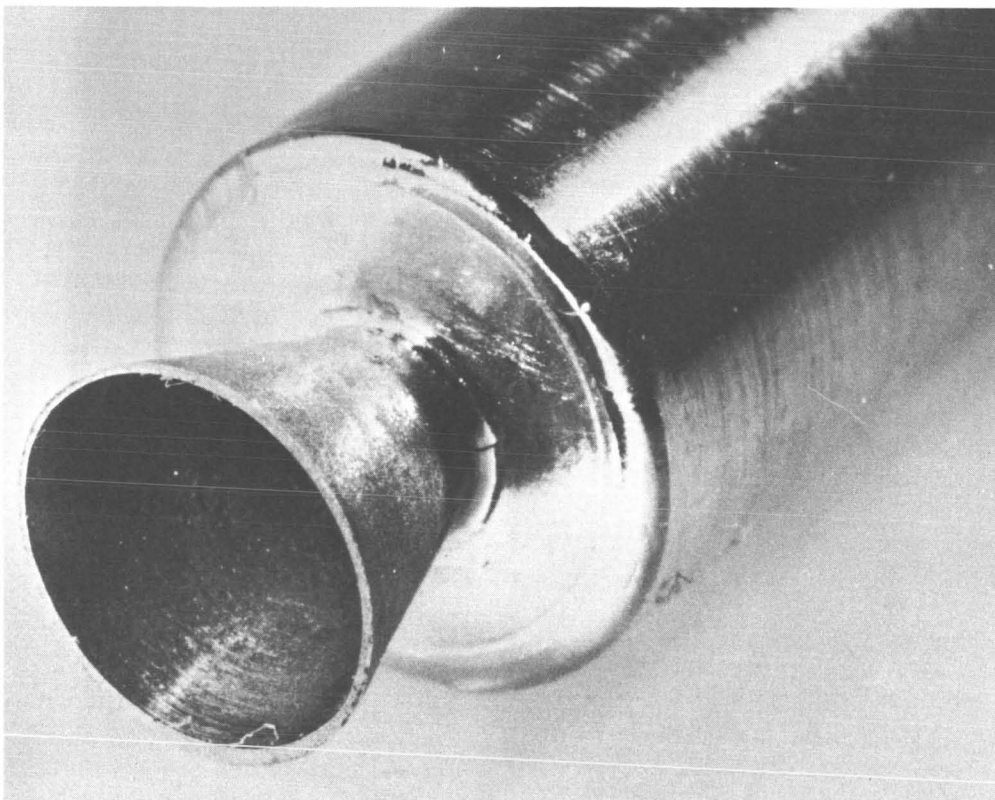
Figure 15. Electron Beam Welds

Factors governing the selection of braze metal and brazing process: The selection of the braze metal and the brazing process was dictated by the material properties of the engine components and the anticipated operating conditions of the engine. The requirements of each are enumerated below.

(1)   Braze base metal.

(A)   Braze must wet rhenium, 316 SS, 321 SS, and 42% Ni-Fe.

(B)   Penetration and solution of component metal parts must be minimal.

(C)   Metal should contain no volatile constituents such as zinc and cadmium which could interfere with vacuum operation of engine.

(D)   Braze should require no fluxing agent.

(E)   Melting temperature should be higher by several hundred degrees than the anticipated operating temperature, but below that temperature which would cause the ceramic seal to deteriorate.

(2)   Braze process.

(A)   Because rhenium and tantalum oxidize readily, the engine must be brazed in an inert vacuum or H_2 atmosphere.

(B)   Close control of the heating cycle is required so that over-heating of the ceramic seal does not occur.

After considering all of these factors, it was decided to furnace braze the assembly, and several potential braze base metals were selected and ordered. A tubular furnace retort which could be operated with a vacuum or H_2 atmosphere was used.

The primary parameter that had to be established was the upper temperature/time limit that the ceramic seal could be subjected to and still remain leak-tight at the brazed joints. After a number of the seals had been heated to specified temperatures and for selected holding times, it was established that seals remained leak-tight when heated to temperature not exceeding $1075^\circ K$ for times not exceeding 10 min. Such was the case, although the braze joints were remelted during this process. Seals which were heated to higher temperatures or for longer times often leaked at the joints. These tests established the upper limits of the braze process.

There was a complete lack of information on the brazing of rhenium metal in the literature; therefore, in the selection of potential base metals, heavy reliance was placed on the fact that rhenium and tungsten are similar. Thus, brazes that wet tungsten should also wet rhenium and so forth. With this in mind, brazes were selected and studied. The composition of the brazes, melting characteristics, and results of the studies are given in table 8. As indicated in the table, the best results were achieved with the BT braze in H_2 and with the Lithobraze BT in vacuum. A considerable time at temperature

TABLE 8

BASE BRAZE METAL PROPERTIES

Braze	Composition weight %	Melting point		Flow point		Remarks
		°R	°K	°R	°K	
BT	72Ag-28Cu	1895	1053	1895	1053	Readily wets rhenium and 42% Ni-Fe in vacuum or H$_2$. Wets 300-series SS in clean, dry H$_2$ if braze time is long or temperature high. Wets 300-series SS in vacuum only if stainless has been acid pickled and vacuum is hard.
Litho-braze BT	71.8Ag-28Cu, 0.2 Li	1895	1053	1895	1053	Readily wets rhenium, 42% Ni-Fe, and type 300-series SS in dry H$_2$ or vacuum. Improved wetability on 300-series SS due to self-fluxing action of lithium.
Prema-braze 615	61.5Ag-24Cu, 14.5 In	1616	898	1760	978	Readily wets rhenium and 42% Ni-Fe in vacuum or H$_2$. Wets 300-series SS only slightly.
Prema-braze 603	60Ag, 30Cu	1571	873	1787	993	Readily wets rhenium and 42% Ni-Fe in vacuum or H$_2$. Wets 300-series SS slightly.
Prema-braze 130	82Au, 18 Ni	2201	1223	---	---	Readily wets all above materials. Has higher temperature capability. Can be used in separate braze operation only, since ceramic-metal insulator braze will not stand high temperature.

was required for the H_2 to reduce the oxide on the stainless steels, thus, prolonged braze times were required with the BT/H_2 process. This situation was not considered compatible with the aim of maintaining the integrity of the ceramic seal; it was therefore decided to braze the first engine assembly with Lithobraze BT in a hard vacuum (10^{-5} mm Hg). Initial checkout runs with a dummy assembly proved the feasibility of this approach. Prebraze cleaning procedures for the various component parts were also established.

Based on the results of this study, the resistojet engine was successfully joined to the feedthrough assembly on the first attempt. The joints were helium leak-checked and found to be completely leak-tight. The procedures followed in successfully brazing the first resistojet engine and recommended for others of the same type are set forth below.

All joints should be snug fits with a 0. 125-mm (0. 005-in.) radial gap located back of the fit. The gap serves as a reservoir for the braze material. In placing the braze material in the gap, one should see that the 0. 005-mm (0. 002-in.) sheet extends no more than 3 mm (1/8 in.) beyond the joint and no less than 3 mm (1/8 in.) into the joint. Th e idea is to provide just enough braze to join the parts and preclude the possibility of braze material flowing down the parts and causing electrical shorts.

Machined parts that have been annealed for 1 hour at 1873°K in vacuum require no further cleaning, provided they are handled with reasonable care afterward. Since the oxide sublimes when heated above 1273°K, the metal surfaces of the annealed parts are bright and free of oxide contamination. Where required, metal parts may be cleaned chemically by placing them for a time in a 30% H_2O_2 solution. If the parts are particularly dirty, they may be electrolytically cleaned in the pickling solution described below.

The bellows assembly and tee-fittings are all type-300-series stainless steel. The oxide films on surfaces to be brazed must be removed prior to brazing. A nitric acid electrolyltic pickling solution is used for this purpose. The bath composition and other particulars are:

    (1) Composition--HNO_3, 10% by volume; HF, 5% by volume.

    (2) Operating Conditions--

        (A) Temperature, 325°K

        (B) Current density, 0. 038 A/cm^2.

        (C) Cell voltage, 5 V.

(D) Immersion time, 60 to 90 sec.

(E) Electrodes, stainless steel.

The ceramic seal should be washed in acetone to remove any oil or grease from the glazed surface. If the grease is not removed, it will be fired into the glazed surface.

The assembly is brazed with the Lithobraze BT in a hard vacuum. All joints must be held for 10 min in the temperature range $1053^{\circ}K$ to $1073^{\circ}K$. The vacuum should be below 2×10^{-5} mm Hg, initially. Outgassing and other reactions will drive this up to 5×10^{-5} at temperature. The sequence of events for the successful braze run is detailed in table 9.

If the furnace is opened too soon, the parts will be slightly oxidized. This discoloration can be removed by placing the feedthrough assembly in the HNO_2-HF solution described above. This solution will also remove any discoloration on the insulator. After brazing, the entire assembly must be leak-checked with the helium leak detector.

TABLE 9

BRAZING LOG

Time (min.)	Temperature		Vacuum (mm Hg)	Remarks
	$^{\circ}K$	$^{\circ}R$		
0	298	536	6×10^{-6}	---
12	373	671	1	Release of water of hydration from boron nitride insulator.
23	423	761	50×10^{-3}	Ag_2O on braze sublimes.
50	1033	1859	4×10^{-5}	---
54	1053	1895	2×10^{-3}	Lithium boiling out of molten braze.
64	1073	1931	2×10^{-5}	Power off.
120	473	851	8×10^{-6}	Power off.
180	353	635	8×10^{-6}	Admitted air to furnace and removed assembly.

PERFORMANCE PREDICTIONS

Heat-Transfer Analysis

H_2 heat transfer. — A detailed thermal and gas dynamic analysis of the Model I, 0.044-N, (10-mlbf), H_2 resistojet heat exchanger (fig. 2) is summarized herein.

Introduction: A detailed thermal-resistance network was developed for the system so that an electrical analog method could be used. This network was simplified to include the major factors influencing the transfer of thermal energy within the system. (See fig. 16.) A two-dimensional "relaxation" procedure was used to solve the thermal network under steady-state operating conditions. Successive approximations were made until the final solution was obtained ($\Sigma Q \sim 0$ at nodal points). These results are believed to be within ±4% of the actual values, based upon the material properties for rhenium made available by Dr. Rollfinke of Chase Brass and Copper Company (table 10).

A digital computer program for the thermal analysis of such hardware is available at Marquardt. For the present development circumstances, the preliminary hand-calculation phase which precedes a machine program was considered to be adequate enough to allow a sufficiently close scrutiny of the significant heat-transfer features of this design.

Background: Since this resistojet differs from previous concentric-tube designs, it required a new thermal analysis. Among the main differences which affect this analysis are (1) the use of rhenium instead of tungsten for the Joule-heated elements, (2) a vacuum "insulator," and (3) a remotely located gas seal. The basic heat exchanger, which will be assembled by electron-beam welding, is a three-pass annular configuration (parallel-flow, counter-flow, parallel-flow), wherein the inner wall of pass 2 is physically the same part (wall 4) as the tubular (outer wall) passage of pass 3 (fig. 17). Since the volume between pass 1 and pass 2 is exposed to the space vacuum (or a simulated vacuum in the test chamber), the conduction and convection heat-transfer modes were negligible. In addition, a multiple-layered radiation shield was inserted in the vacuum jacket to reduce the radiation heat-transfer term to a minimum.

To obtain accurate, convective-heat-transfer coefficient values for the laminar flow of H_2, a search of the literature was made, and some pertinent references were evaluated. The resulting calculations gave local values of the film coefficients along with the modified Graetz and Nusselts number values (tabulated in table 11) and, for the most part, approach the asymptotic value of 4.36 for fully-developed laminar flow of a compressible fluid.
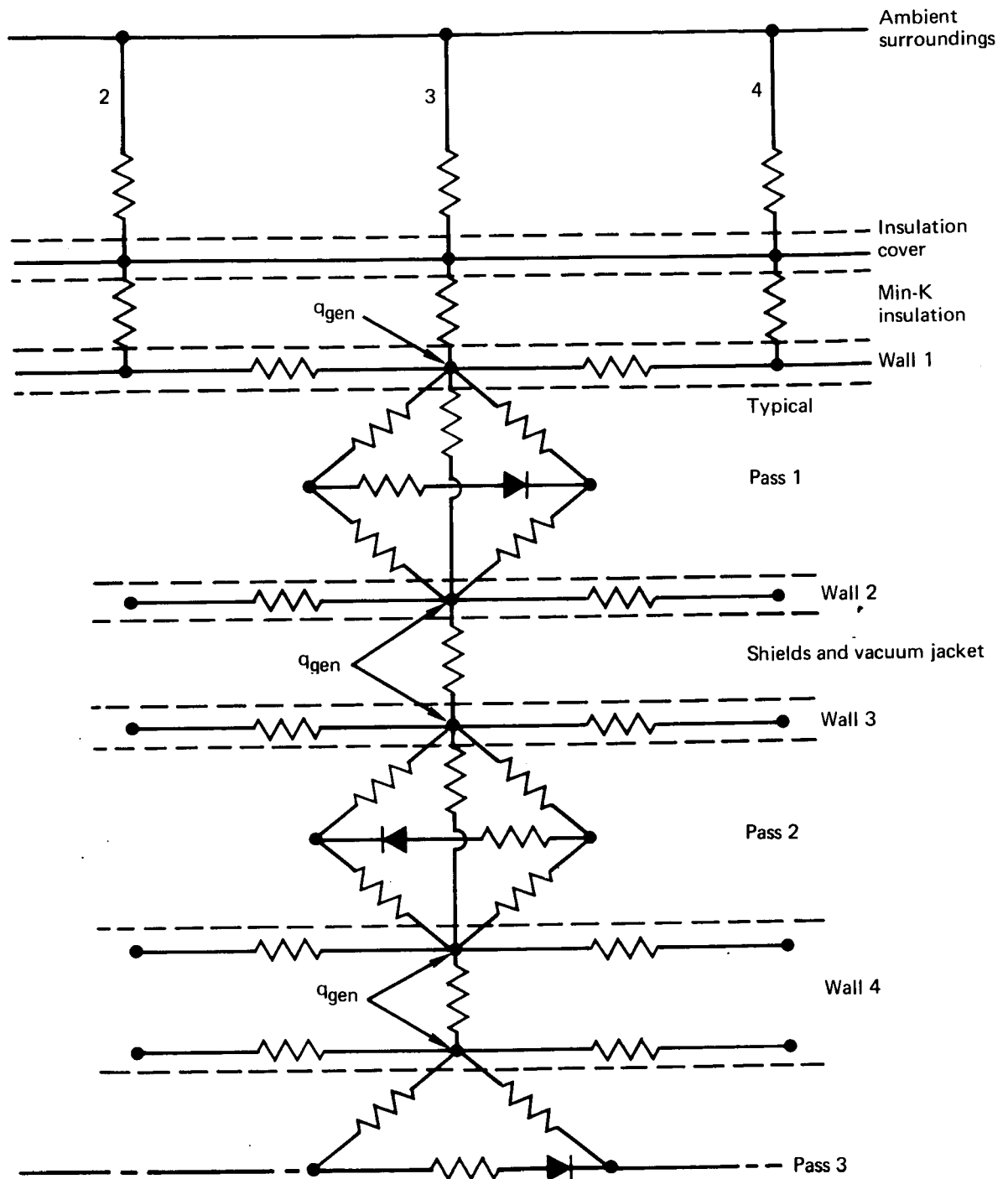
Figure 16. Thermal Resistance Network (Typical Section)

TABLE 10

PROPERTIES OF RHENIUM AS A FUNCTION OF TEMPERATURE

Temperature (^{O}K)	Specific heat (cal/gm^{O}K)	Electrical resistivity (micro-ohm-cm)	Thermal conductivity (watts/cm^{O}K)
300	0.0331	19.0	0.380
500	0.0338	34.3	0.364
1000	0.0372	64.9	0.382
1500	0.0409	84.5	0.439
2000	0.0450	99.0	0.502
2500	0.0492	108.8	0.510
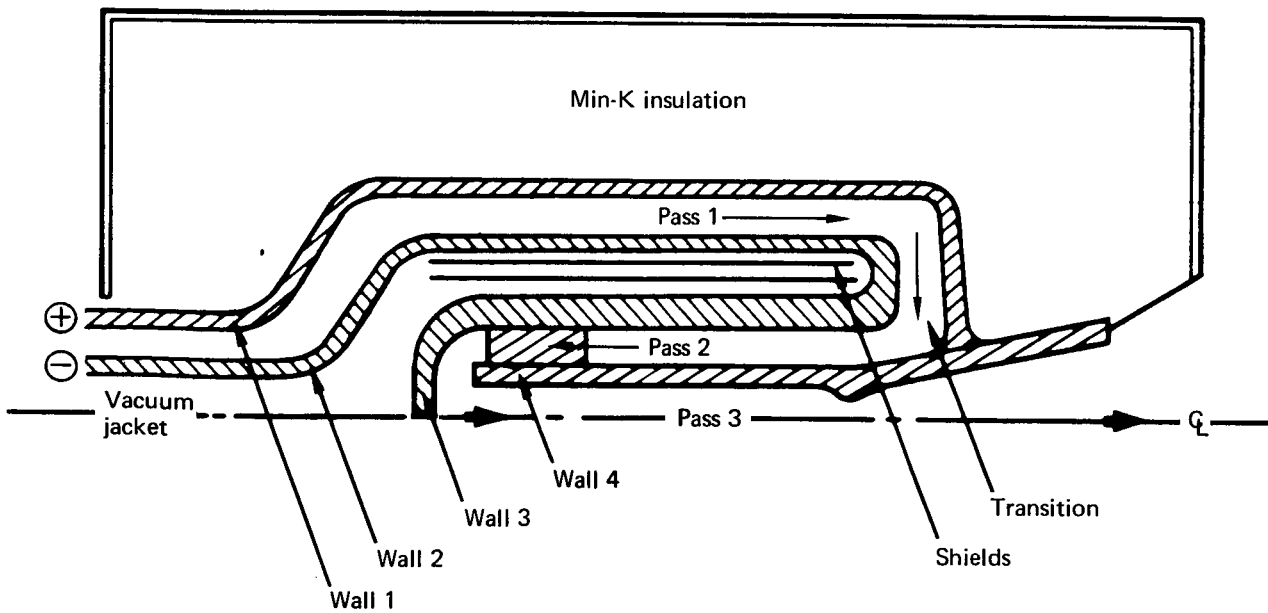
Figure 17. Nomenclature

TABLE 11

SUMMARY OF CONVECTIVE HEAT-TRANSFER COEFFICIENTS AND RELATED PARAMETERS (H_2)

Pass no.	N_{Re}	X/D	$\dfrac{X/D}{N_{Re}N_{Pr}}$	N_{Nu_X}	$h_o = \dfrac{N_{Nu}k}{D_h}$ (watts/cm^2°K)
(1 cm from tee)	167	6.9	0.058	4.97	0.062
Inlet avg	145	13.3	0.125	4.75	0.061
No. 1 inlet	47	56	1.55	4.38	0.118
Avg	40	80	2.55	4.37	0.135
Out	35	104	3.67	4.37	0.151
Transition, Avg	41	143	4.22	4.37	0.095
No. 2 inlet	138	149	1.31	4.39	0.252
Avg	111	165	1.84	4.38	0.342
Exit	109	255	2.94	4.37	0.528
No. 3 inlet	343	181	0.665	4.41	0.400
Avg	310	208	0.820	4.40	0.445
Chamber	288	234	0.955	4.40	0.597

Method: In solving this complex heat-transfer problem, consideration must be given to the simultaneous values for the enthalpy rise of the gas, the heat dissipated within the metallic walls, and the heat transfer from the walls by the modes of conduction, convection, and radiation heat transfer. It can be shown that because of the thin cross-sectional areas (with relation to surface area), the axial conduction term is several orders of magnitude less than the convective term and can be neglected for the first approximation. Similarly, if a radiating surface is adjacent to one having a high-temperature thermal insulation or multiple-layered radiation shields, this can be neglected for the first iteration to get a faster covergence, and the problem can be solved by an iterative method with the neglected terms reintroduced.

Transient and steady-state heat-transfer problems have been solved for many years through the use of an electrical analogy for Ohm's law. For this technique, the heat flow is equivalent to the electrical current, I, the temperature is equivalent to the electrical potential, E, and the thermal resistance is equivalent to the electrical resistance, R. Thus, the corresponding physical relationships in the electrical network can be related to a thermal analysis as follows:

$$I = \frac{\Delta E}{R_T} \quad ; \quad Q = \frac{\Delta T}{R_T} \tag{5}$$

for conduction:

$$\frac{1}{R_T} = \left(\frac{k A_{c.s.}}{\Delta X} \right) \tag{6}$$

for convection:

$$\frac{1}{R_T} = (h_o A_s) \tag{7}$$

for radiation:

$$\frac{1}{R_T} = (h_r A_s) \quad ; \quad h_r = f \left(\frac{T_1^4 - T_2^4}{\Delta T} \right) \tag{8}$$

where

$A_{c.s.}$ = cross-sectional area

A_s = surface area

k = thermal conductivity

X = distance

h = heat transfer coefficient

A longitudinal section of the 0.044-N (10-mlbf) resistojet is shown in figs. 2 and 17. The walls were initially given an estimated temperature which varied with passage length. Similarly, the gas (H_2) temperature was initially estimated as a function of passage distance from inlet, and received energy by convective heat transfer from the resistance-heated rhenium walls. The net energy in each wall segment depends on the Joule heating within the segment, heat transferred to the segment by conduction and/or radiation, and/or heat transferred from the segment by conduction, convection, and radiation.

Probably the most important thermal resistances in the network are the convective or film heat-transfer coefficients which control the amount of energy transferred from the hot walls to the gas throughout the flow passages. Although previous analyses have sometimes calculated these values on the basis of a constant Nusselt number, this analysis obtained local values based on a modified Graetz number which includes the effects caused by velocity and pressure distributions for a laminar flow in concentric annuli. Tabulated values for these parameters are given for this design at various locations in table 11.

The boundary conditions imposed on this heat-transfer problem were the ambient temperature (25°C) and the maximum temperature of the insulation cover (121°C). A maximum value for the electrical energy dissipated during thrustor operation was given as 240 watts, while an inlet-bulk mean gas temperature of 300°K and a chamber bulk mean gas temperature of 2420°K were used for this analysis.

With these specified conditions and the properties of H_2 compiled by King (ref. 7), successive temperature values were obtained until the final solution was accomplished. Approximately six iterations of calculations were made until it was considered accurate enough ($\pm 4\%$) for use as a guide in the hardware development phase.

Initially, the estimated temperature distribution for each heat-exchanger pass was based on an estimated gas-temperature variation with passage length, and the electrical and thermal resistivity of the rhenium elements was based on the above temperature distributions. To obtain the final solution, the various temperature values had to be "relaxed" in order to satisfy a thermal balance at each node, as well as to satisfy the conservation of energy within the system.

Gas dynamic summary: The gas dynamic characteristics associated with the thermal analysis is summarized in table 12. The calculated pressure drop through the thrustor totaled 38.6 N/m^2 (5.6 psia). For the plenum-chamber gas-pressure design value of 152 kN/m^2 (22 psia), the required inlet (tee) gas pressure was projected to be 190 kN/m^2 (27.6 psia). Experimental values were found to be higher, 303 kN/m^2 (44 psia). This difference is not yet fully understood. Another interesting result of the flow-passage gas-dynamic calculations is that the average Mach number for the first two heat-exchanger passes is extremely low (because of the large flow areas in these two sections) and is still relatively low (M = 0.26) at the plenum chamber. Since the foregoing analysis was based on nominal dimensions of this resistojet, measurements will have to be made to determine the influence of flow passage variations on the actual hardware.

Results: The resulting temperature distribution in the metal and gas volumes is shown in fig. 18 and table 13. Energy-balance terms and element-resistance values are summarized in tables 14 and 15. The fact that about 80% of the total input energy is dissipated in the innermost element (wall 4) has both advantages and disadvantages. The main advantage is that most of the energy is dissipated in the centerline of the heater, so that all concentric walls outside would intercept the "losses" of heat from the inner elements and, thus, increase the thermal efficiency of this design. The primary disadvantage would be that there could be a large radial-temperature gradient across the nozzle support which might limit its structural life.

The maximum wall temperature to maximum gas temperature difference is 100°K in this design. The thermal efficiency or the percentage of the energy of that supplied which is transferred to the gas is 91.6%.

TABLE 12

SUMMARY OF FLUID FLOW PARAMETERS (H_2)

Pass no.	Pressure drop (kN/m^2)	(psia)	Mach no. (avg)	Flow area, A_f (cm^2)	$\dfrac{\dot{W}}{A_f}$ (gm/cm^2-sec)
Inlet	0.028	0.004	0.004	0.070	0.087
No. 1	0.186	0.027	0.005	0.091	0.067
Transition	0.014	0.002	0.005	0.121	0.050
No. 2	8.34	1.210	0.049	0.014	0.435
No. 3	29.9	4.340	0.220	0.0045	1.344
Plenum	---	---	0.260	0.0045	1.344
Throat	---	---	1.000	0.0022	3.18*

*Since $C_d = A_f/A^*_{geom} = 0.865$, $\dfrac{\dot{W}}{A^*_{geom}} = 2.75$ for the given mass flow rate.

Note: The geometric nozzle area ratio, A/A^*, was varied from 100:1 to 25:1 incrementally by machining the divergent cone. The purpose was to allow experimental optimization of the nozzle/heat exchanger system.

One area of possible heat loss is the nozzle support section which electrically connects the inner element with the outer case (fig. 17). Fortunately, approximately 70% of the energy in this section is transferred to the gas in this transition between pass 1 and pass 2; however, unless the thickness of this part is carefully controlled, excessive losses may occur since thermal conduction is directly proportional to cross-sectional area.

On the basis of a thermal analysis, the corresponding resistivity values of rhenium and the nominal cross-sectional areas given in the reference drawing, the current and voltage values at the steady-state operating condition for an input power of 240 watts were calculated to be 40 amps and 6.0 volts. The thermal inventory, which indicates the thermal capacity of the rhenium parts, resulted in a total of 1714.3 watt-sec.

Thermal insulation capability of vacuum jacket. — Limiting the high temperature to the core and particularly to the vicinity of the nozzle inlet is desirable for thermal efficiency. Because of its small radial size, hence, severe temperature gradients, the millipound-class thrustor requires the introduction of additional radial-thermal insulation techniques over those previously used successfully in the larger concentric engines. The vacuum jacket about the central heating element is shown here to be sufficient as an additional technique to ensure an efficient (10-mlbf) thrustor design.
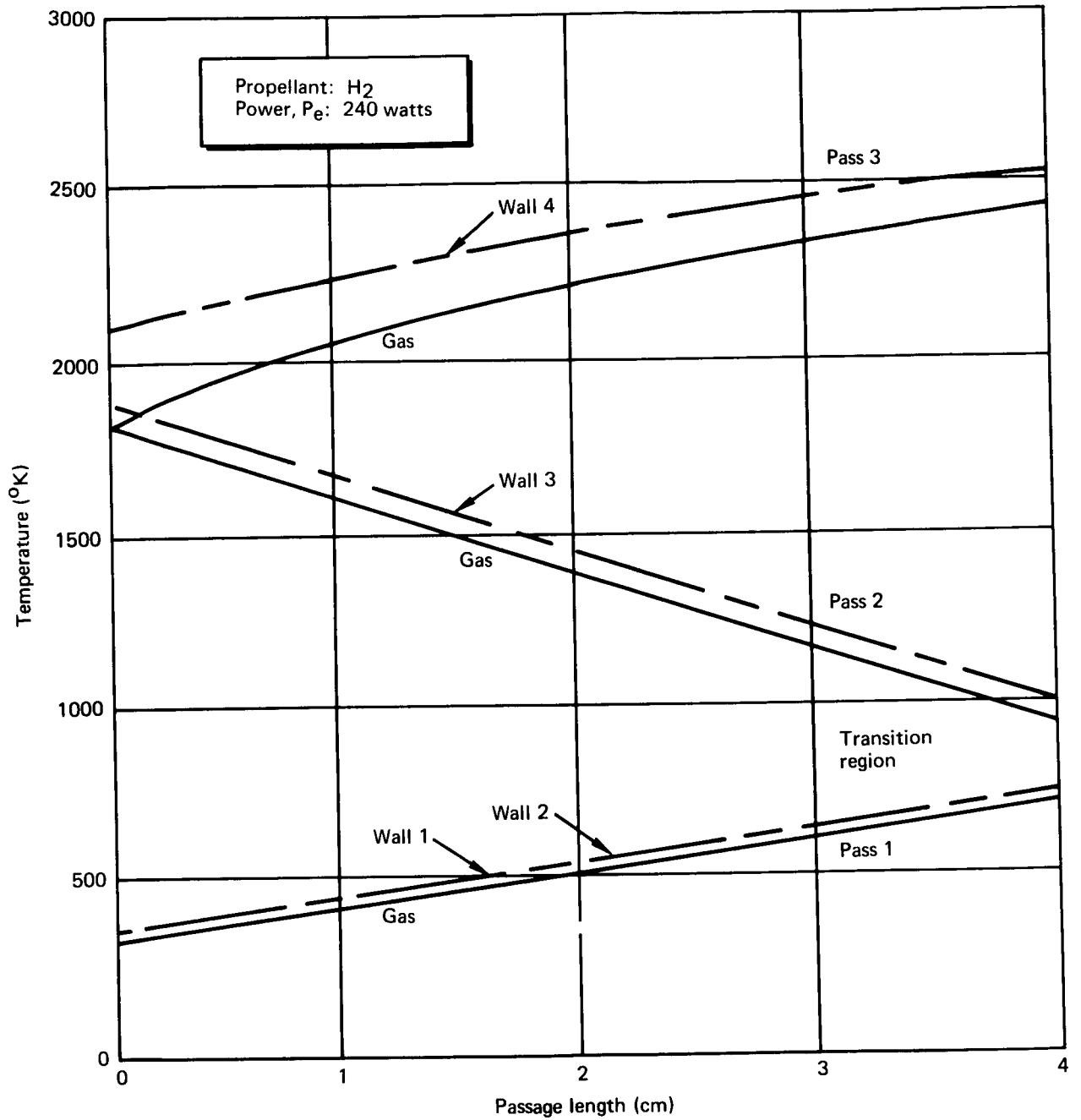
Figure 18. Heat Exchanger Thermal Analysis Model I Resistojet (H_2)

TABLE 13

SUMMARY OF TEMPERATURE DATA (H_2)

Pass no.	Gas temperature ($^{\circ}$K)	Wall no.	Wall temperature ($^{\circ}$K)
Stem	300	2	400
Inlet exit	450	1	460
		2	500
No. 1 in	460	1	465
		2	470
No. 1 out	700	1	710
		2	705
Transition	800	2-3	810
		1-4	935
No. 2 in	960	3	1005
		4	2520
No. 2 out	1840	3	1875
		4	2080
No. 3 in	1845	4	2080
No. 3 out	2420	4	2520

In the hard vacuum of space, the radial-gaseous-conduction term is shown to be infinitesimally small across the jacket. The only problem during development testing is to ensure that this is simulated. This section presents an analysis of this problem for the Model I thrustor (fig. 2) in relation to the Electrothermal Laboratory, the facility to be used for life testing.

Fig. 19 summarizes the heat conducted (by gaseous conduction only) across the jacket from the outer heating element to the inside of the case as a function of jacket pressure. This assumes four interposed, equally spaced radiation shields and uses the outer annulus as a basis of conservative estimation of this mode of heat-flux contribution. That is, this mode of heat flux is from shield to shield. The largest-area lowest-temperature level which is the last annular space represents the largest (most conservative) heat flow from a free-molecule point of view.

TABLE 14

SUMMARY OF MAJOR ENERGY BALANCE TERMS

Pass no.	Wall no.	Gas enthalpy rise per pass (watts)	Internal heat generated per wall (watts)	$h_o A_s$ avg (watts/$^\circ$K)
Stem	2	0.7	5.68	
	1		2.54	0.25
Inlet		14.6		
	2		1.28	0.14
	1		2.11	0.50
No. 1	2	21.2	3.00	
Transition	2-3	27.0	1.02	0.14
	1-4		1.11	0.16
	3		32.00	0.27
No. 2		82.3		
	4		67.80	0.17
No. 3	4	74.4	123.62	0.15
Total		220.2	240.16	
Losses to surroundings		19.8		
		240.0		

TABLE 15

CALCULATED ELEMENT RESISTANCES AND THERMAL INVENTORY

Pass no.	Wall no.	Electrical resistance at steady-state temperatures (micro-ohm)	Electrical resistance in "cold" state (micro-ohm)	Thermal capacity (watt-sec)
Stem	2	3 500	3 000	
	1	1 571	1 101	63.1
Inlet	2	796	3 122	49.1
	1	1 305	715	490.0
No. 1	2	1 850	930	414.5
	2-3	632	84	84.1
Transition				
	1-4	682	50	166.4
	3	19 750	4 900	301.5
No. 2	4	37 450		
			23 075	145.6
No. 3	4	80 650		
		148 186	36 977	1 714.3

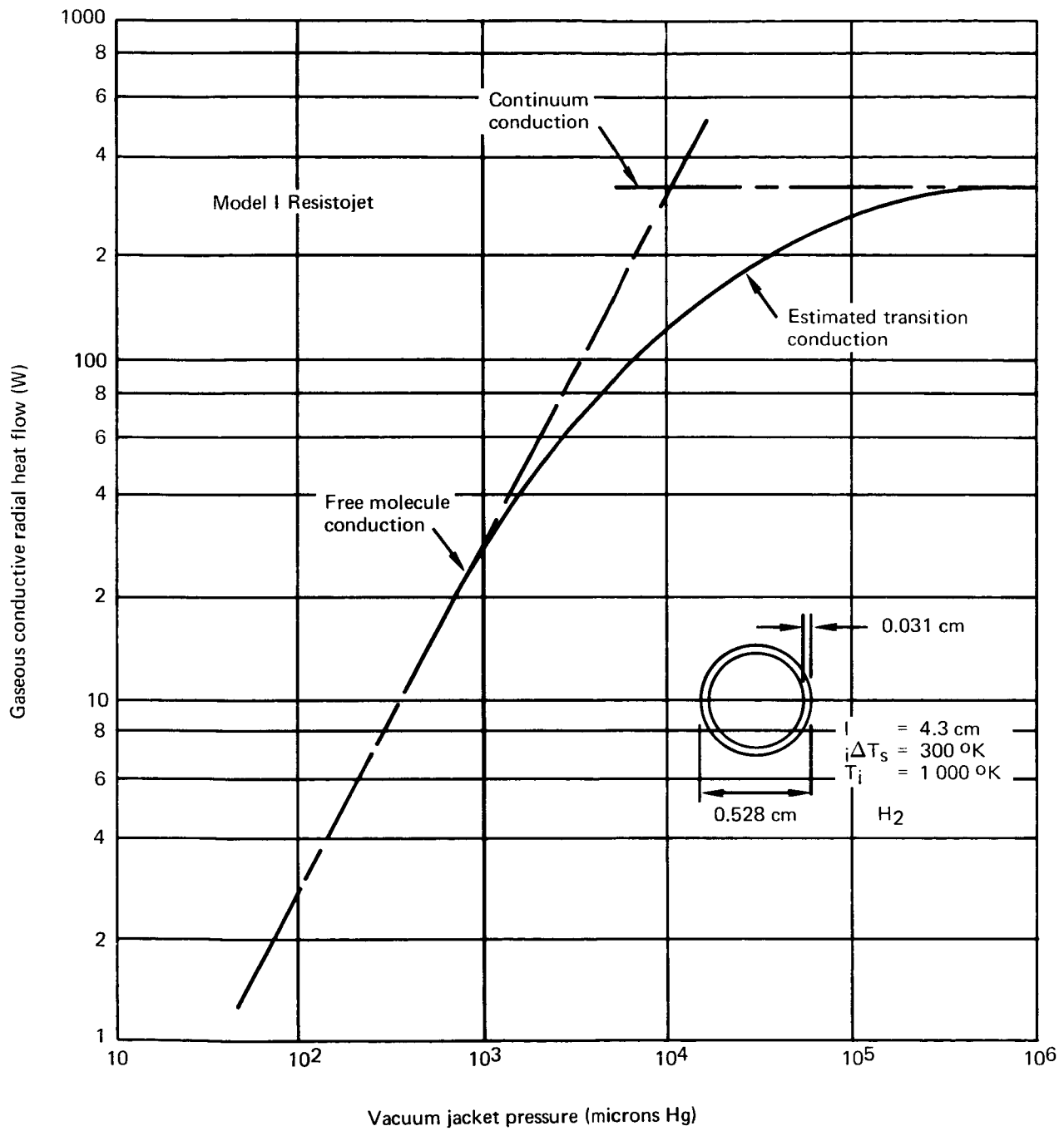$$\frac{R \text{ cold}}{R \text{ hot}} = \frac{36\ 977}{148\ 186} = 0.250$$

Figure 19. Gaseous Conductive Radial Heat Flow with Jacket Pressure (H_2)

There are three regimes of gaseous conductive heat flow (fig. 19): continuum, transition, and free molecule. As is well known from a kinetic theory point of view (Maxwell, circa 1860), gaseous thermal conduction (continuum) is independent of pressure. It is a somewhat weak function of temperature directly related to the 0.69 power of the temperature to a first approximation. The effective temperature used in fig. 19 is 1000°K for all regimes.

Gaseous conductive flux under free molecule flow is proportional to pressure as shown by eq. (9) taken from ref. 8 using the original notation.

$$\frac{Q}{A} = \tilde{\alpha} \ \Lambda_o P_\mu \left(\frac{273.2}{T_i}\right)^{\frac{1}{2}} (T_s - T_i) - watts/cm^{-2} \tag{9}$$

where

Λ_o = free molecule heat conductivity at 273°K

$$\Lambda_o = \frac{1.468 \times 10^{-5}}{M^{(1/2)}} \left(\frac{\gamma + 1}{\gamma - 1}\right) watts/cm^{-2} \ deg^{-1} \ micron^{-1} \tag{10}$$

The conductive flow under continuum assumptions, as governed by the Fourier Law, is given in eq. (11) for flow between two concentric cylinders,

$$\frac{Q}{A} = \frac{\lambda \left(T_s - T_c\right)}{a \ ln \ (r/a)} \tag{11}$$

The intersection of the extrapolated two-linear relationships from eqs. (9) and (11) for the specific problem occurred at a Knudsen number around 1.0. From kinetic theory it can be shown that Knudsen number where this occurs is

$$Kn_x = \left(\frac{L}{d}\right)_x = \frac{3}{4} \tilde{\alpha} \ \frac{(\gamma + 1)}{2} \tag{12}$$

As in similar problems, the "transition zone" is too complex to compute easily and is approximated by a faired curve beginning at a Knudsen number of two orders of magnitude either side of the "cross-over" value.

The radial radiation term across the jacket is approximately 10 watts. A gaseous conduction term of this same order would not be severe. It is seen from fig. 19 that jacket pressures of the order of 360 μmHg are required. Slightly lower pumping pressures (200 μmHg) are required because of the thermal transpiration effect, or

$$P = \sqrt{\frac{T}{T_i}} \ P_i \tag{13}$$

50

The geometry upon which fig. 19 is based is the Model I development thrustor. The important dimensions of the problem are summarized in table 16.

A temperature level of 1000°K, with a temperature difference of 300°K, was assumed from preliminary heat-transfer analysis.

The accommodation coefficients used were assumed to be close to the 0.54 of clean tungsten in H_2 at 1273°K. The Knudsen numbers were evaluated using a mean free path, L, near Maxwellian velocity distribution, by eq. (14).

$$\bar{L} = 8.589 \times 10^3 \frac{\eta}{P_\mu} \left(\frac{T}{M}\right)^{\frac{1}{2}} cm \tag{14}$$

The viscosity, η, of H_2 at 1000°K was taken at 1.999×10^{-4} g/cm sec and the earlier-used thermal conductivity of 1.047×10^{-3} cal/cm sec $^{\circ}$K were taken from Grier (ref. 9).

Simulation in the laboratory: Fig. 20 gives the pumping-station capability (manufacturer's data) of the Electrothermal Laboratory. The requirement of one H_2 engine at a specific impulse of 720 sec is 6.3×10^{-3} g/sec; for NH_3 at 320 sec, it is 1.42×10^{-2} g/sec. The resulting cell pressure for H_2 is projected to be 30 μmHg, giving a jacket pressure of 54 μmHg. The resulting gaseous conduction term, from fig. 19, is 1.5 watts or approximately 0.6% of the total input power, an insignificant term. NH_3 is seen to incur even less loss.

TABLE 16

PERTINENT MODEL I THRUSTOR DIMENSIONS

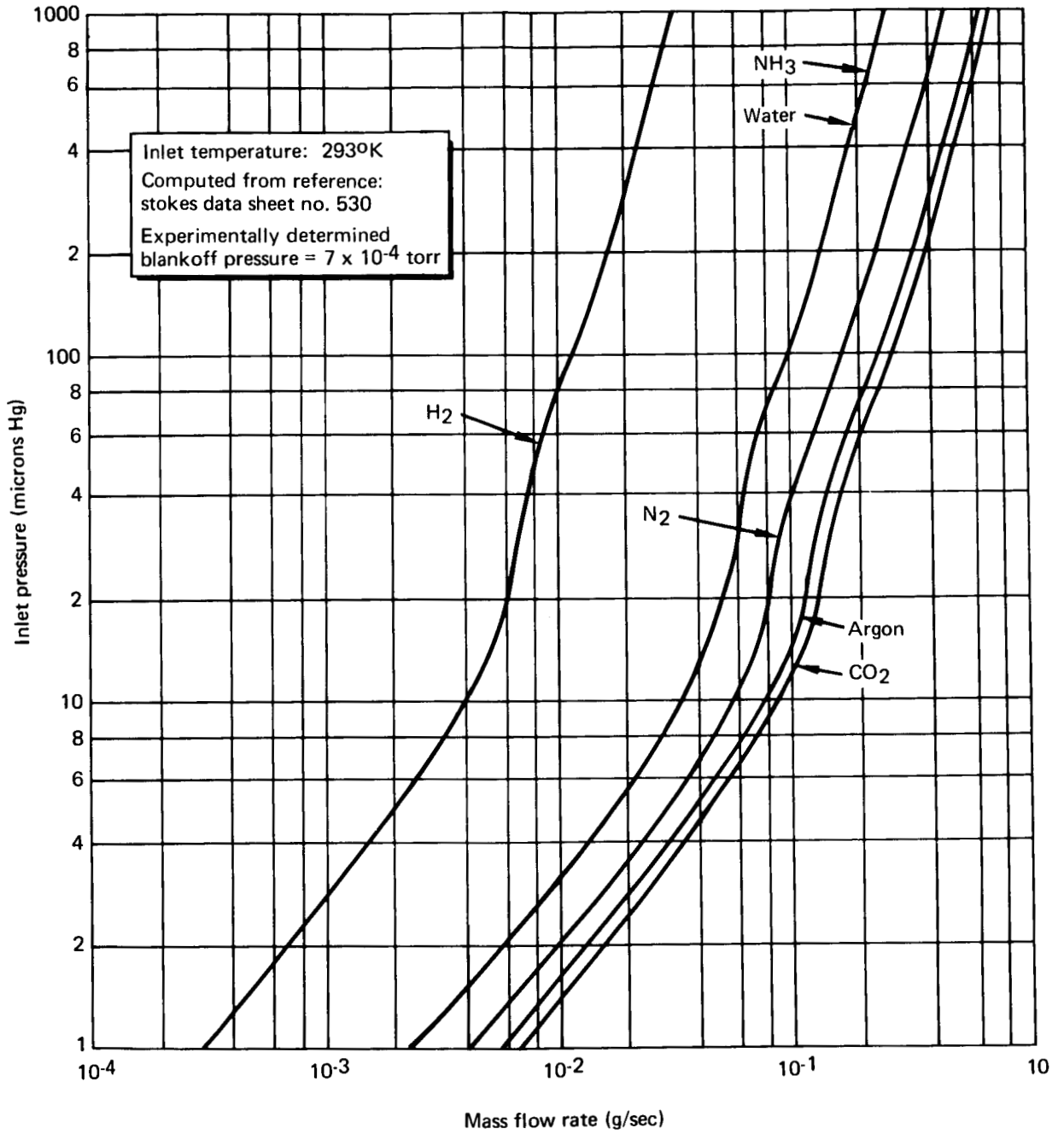| Part no.	Name	Surface diameter (cm)	Length (cm)	Material
3	Inner case	0.528	4.3	Rhenium
7	Shield (five, equally spaced)	---	4.3	Tantalum
4	Heating element	0.230	4.3	Rhenium

Figure 20. Inlet Pressure of 16-in. Ring Jet Booster With 300 cfm Microvac Forepump as a Function of Mass Flow Rate

Two H_2 and four NH_3 0.044-N (10-mlbf) resistojets are to be life tested on a 50% duty cycle. Table 17 shows the propellant requirements at any one time, that is, half the set above.

The total equivalent flow expressed as H_2 is 0.0130 g/sec. This is seen to result in a cell pressure of 120 μmHg or 220 μmHg jacket pressure. The resulting radial heat flux is 6 watts or 2.5% of input power. By the use of a vacuum line to a separately supplied hard-vacuum pump, the radically conductive heat term can be reduced to essentially nothing if desired. It is anticipated that this vacuum line will not be required.

In the hard vacuum of space with the jacket exposed, the conductive heat term is seen to be of the order of 10^{-7} watts, or an infinitesimal amount.

Fig. 21 shows the capability of an alternate facility at The Marquardt Corporation, Van Nuys, California.

NH_3 heat transfer. — The basic configuration of the 0.044-N (10-mlbf) resistojet using H_2 as the working fluid was described in the thermal analysis. A thermal and gas dynamic analysis was subsequently made using NH_3 as the propellant in order to predict any potential development problems. The same methods, as described earlier, were used to obtain the results summarized in fig. 22 and tables 18 through 22.

The temperature of the two inner-heater elements was slightly higher for the NH_3 case, and the resultant temperature of the stainless-steel insulation cover would be about 80°K higher than with H_2 for the same physical design. The thermal efficiency or the percentage of the electrical energy supplied which is transferred to the gas is 87%.

This early analysis was made for 3 atm, while testing was done later at 1.5. While no direct comparison can be made, the conclusions are presented as being useful.

A summary of such gas-dynamic parameters as Mach number, pressure drop, and flow per unit area, w/a, for NH_3 through the passages, a total pressure drop of only 13.8 kN/m^2 (2.2 psia) was calculated for this thrustor configuration. Therefore, for the design plenum-chamber gas pressure of 304 kN/m^2 (44.1 psia), the required inlet (tee) gas pressure would be about 319 kN/m^2 (46.3 psia).

TABLE 17

PROPELLANT REQUIREMENTS

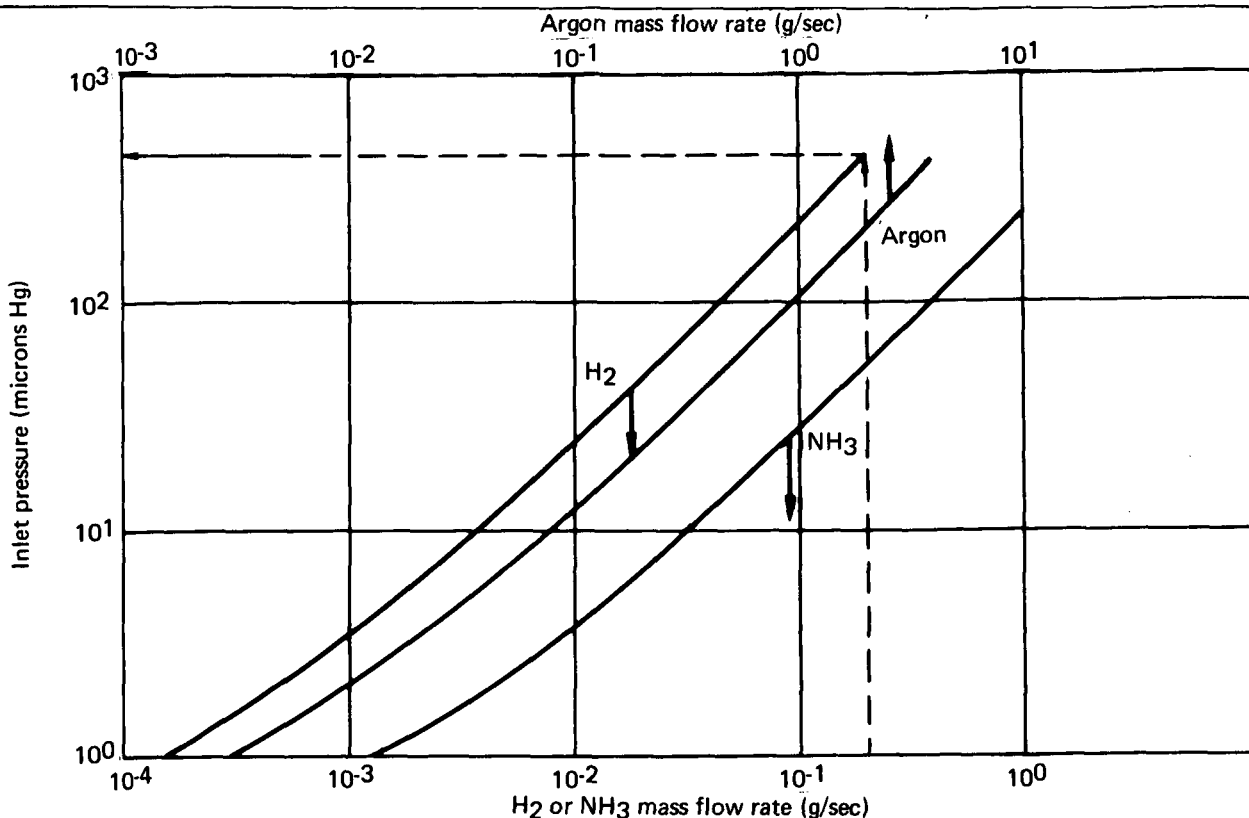| No.	Size	H_2	N_2
1	10 mlbf (H_2)	0.0063 g/sec	---
2	10 mlbf (NH_3)	0.0051 g/sec	0.0234 g/sec
	Total	0.0114 g/sec	0.0234 g/sec

Figure 21. Inlet Pressure of an 18 by 41 High Vacuum Roots Blower as a Function of Mass Flow Rate

The average Mach number values for the first two heat-exchanger passes are essentially constant and extremely low (M = 0.002) because of the large flow areas in these sections. The plenum chamber Mach number with NH_3 is 0.12, as compared with 0.26 for the H_2 operation.

Because of the lower thermal conductivity of NH_3, as compared with H_2, the convective heat transfer coefficients were substantially lower (see table 19). This resulted in a larger gas-to-wall temperature difference and, thus, a slightly lower thermal efficiency (see tables 20 and 21).

On the basis of this thermal and gas dynamic analysis of the Model I thrustor, the resistivity values of rhenium, and the nominal cross-sectional areas of the elements, the overall electrical characteristics (that is, current and voltage values) of the NH_3 thrustor for a steady-state operating condition of 150 watts was calculated to be 31.0 amps and 4.82 volts (see table 22). The corresponding thermal inventory resulted in a total of 1 420.9 watt-sec when using NH_3 in this thrustor.

No-Flow heat transfer. — The heat exchanger configuration of the Model I resistojet was analyzed for steady-state low-power operation, as shown in fig. 23, without propellant flow. The thermal problem is unique in that no heat is transferred by convection, since there is neither a working fluid nor a gaseous atmosphere (vacuum to simulate space environment).
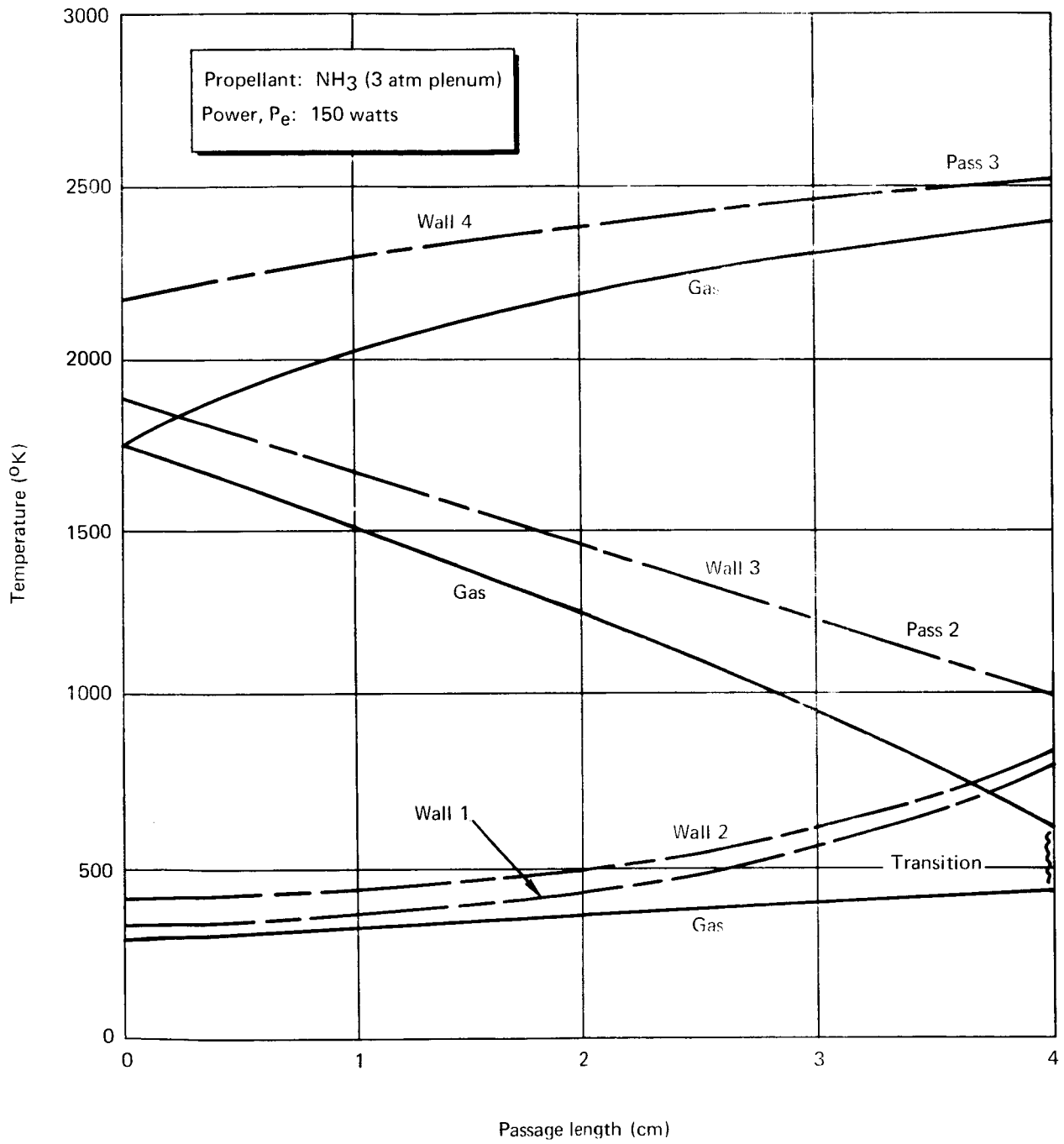
Figure 22. Heat Exchanger Thermal Analysis Model i Resistojet (NH₃)

TABLE 18

SUMMARY OF FLUID FLOW PARAMETERS (NH_3)

Pass no.	Pressure drop (kN/m^2)	(psia)	Mach no. (avg)	Flow area, A_f (cm^2)	$\dfrac{\dot{W}}{A_f}$ (gm/cm^2-sec)
Inlet	0.007	0.001	0.002	0.070	0.171
No. 1	0.034	0.005	0.002	0.091	0.132
Transition	0.002	0.0003	0.002	0.121	0.098
No. 2	3.10	0.450	0.026	0.014	0.858
No. 3	11.80	1.761	0.111	0.0045	2.650
Plenum	---	---	0.120	0.0045	2.650
Throat	---	---	1.000	0.0009	13.26

TABLE 19

SUMMARY OF CONVECTIVE HEAT-TRANSFER COEFFICIENTS
AND RELATED PARAMETERS (NH_3)

Pass no.	N_{Re}	X/D	$\dfrac{X/D}{N_{Re}N_{Pr}}$	N_{Nu_X}	$h_o = \dfrac{N_{Nu}k}{D_h}$ (watts/cm^2°K)
(1 cm from tee)	272	6.9	0.005	7.63	0.013
Inlet avg	240	13.3	0.014	6.75	0.012
No. 1 inlet	83	56	0.099	4.72	0.015
Avg	74	80	0.175	4.56	0.020
Out	67	104	0.242	4.51	0.021
Transition Avg	81	143	0.512	4.43	0.016
No. 2 inlet	267	149	0.247	4.51	0.046
Avg	182	165	1.87	4.41	0.187
Exit	157	255	3.70	4.37	0.350
No. 3 inlet	450	181	0.92	4.40	0.247
Avg	392	208	1.29	4.39	0.349
Chamber	356	234	1.57	4.38	0.421

TABLE 20

SUMMARY OF TEMPERATURE DATA (NH₃)

Pass no.		Gas temperature ($^{\circ}$K)	Wall no.	Wall temperature ($^{\circ}$K)
Stem		300	2	400
Inlet exit		370	1	450
			2	500
	in	375	1	450
			2	520
No. 1				
	out	450	1	790
			2	840
Transition		500	2-3	925
			1-4	1100
	in	565	3	1090
			4	2550
No. 2				
	out	1740	3	1870
			4	2200
	in	1745	4	2200
No. 3				
	out	2420	4	2550

TABLE 21

SUMMARY OF MAJOR ENERGY BALANCE TERMS (NH₃)

Pass no.	Wall no.	Gas enthalpy rise per pass (watts)	Internal heat generated per wall (watts)
Stem	2	1.0	2.30
	1		1.61
Inlet		4.9	
	2		2.00
	1		1.32
No. 1	2	20.0	1.87
Transition	2-3	13.0	0.63
	1-4		0.69
	3		20.0
No. 2		55.0	
	4		50.0
No. 3	4	36.5	69.5
Total		130.4	149.92
Losses to surroundings		20.0	
		150.4	

$$\eta_{th} = \frac{130.4}{150.4} = 0.87$$

TABLE 22

CALCULATED ELEMENT RESISTANCES AND THERMAL INVENTORY (NH$_3$)

Pass no.	Wall no.	Electrical resistance at steady-state temperature (micro-ohm)	Electrical resistance in "cold" state (micro-ohm)	Thermal capacity (watt-sec)
Stem	2	3 500	3 000	
	1	1 745	1 101	63.1
Inlet	2	797	3 122	49.1
No. 1	1	1 020	715	294.5
	2	1 550	930	287.5
Transition	2-3	780	84	86.2
	1-4	605	50	183.5
No. 2	3	19 300	4 900	285.0
	4	37 200	23 075	172.0
No. 3	4	88 720		
		155 217	36 977	1 420.9

$$\frac{R \text{ cold}}{R \text{ hot}} = \frac{36\ 977}{155\ 217} = 0.238$$

No-flow solutions have been shown in table 23, that is, (1) power input required to limit the stainless steel insulation cover to 394°K and (2) power input required to maintain the inner rhenium element (tube) at 2600°K.

One critical operational problem with the no-flow thrustor mode is that dimensional and density variations in the material cross-section of rhenium parts, particularly the inner element and outer element, strongly affect electrical resistivity. If care is not exercised during initial no-flow operation on each unit, a "burn-out" could occur in the inner tube. A second problem has to do with the integrity of the Min-K-2000 thermal insulation material at the high thrustor outer-case temperatures during no-flow operation. A third possible problem area is the high temperature of the thrustor's inlet wall which occurs during no-flow operation.

Steady-state operation of the Model I thrustor at an input power level of 10.5 watts with no propellant flowing through the unit is feasible without damage. At this power level, the maximum temperature of the inner element would be approximately 1990°K, and the mean temperature of the stainless-steel insulation cover would be 394°K. To attain a rhenium-wall maximum temperature of 2600°K, the Min-K-2000 thermal-insulation temperature at the interface with the rhenium outer case would exceed the maximum continuous operating temperature of 1300°K specified by the manufacturer of the material (John Mansville Corp.). This suggests the use of radiation shields between the outer case and insulation.
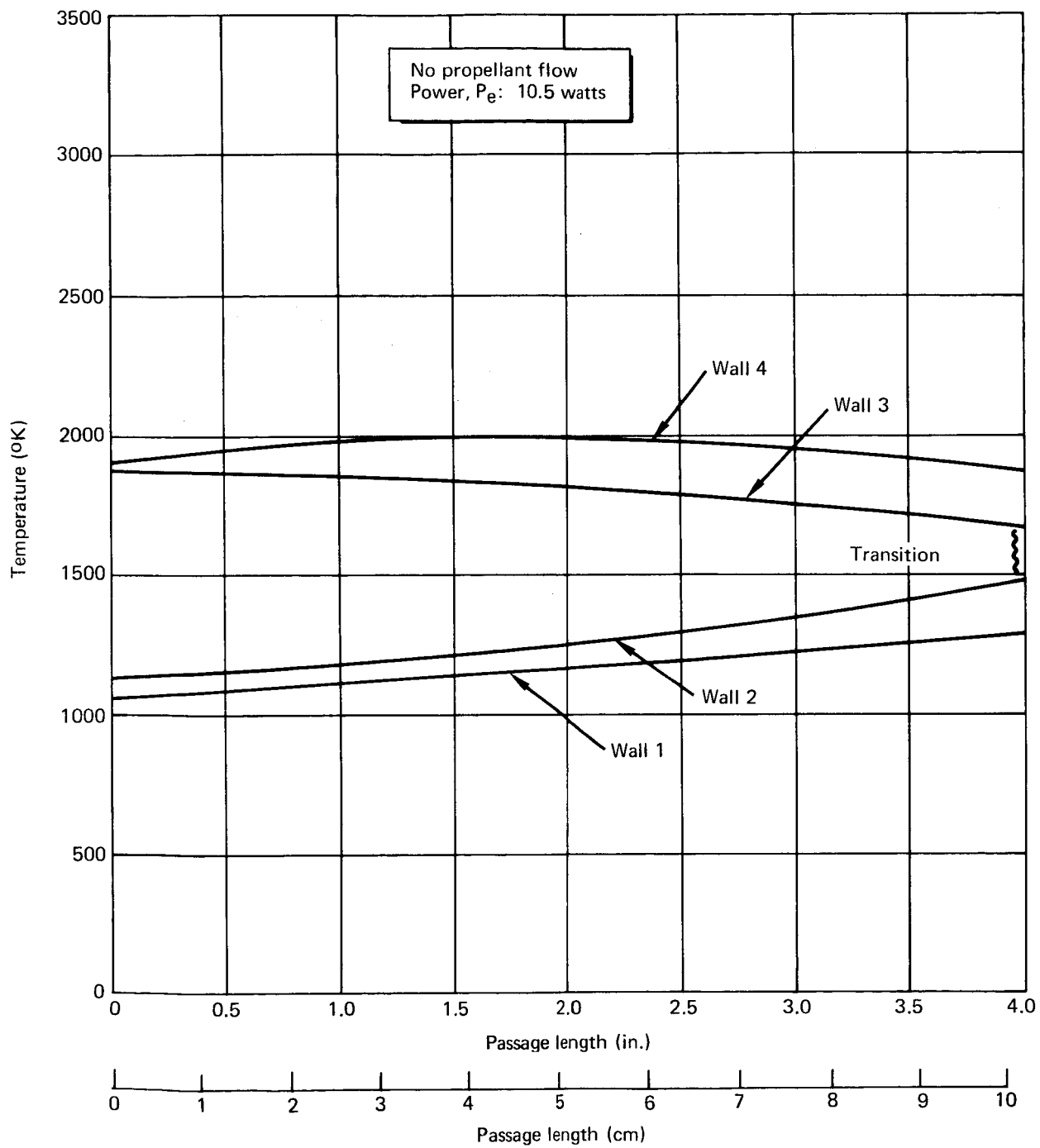
Figure 23. Heat Exchanger Thermal Analysis — Model I Resistojet

TABLE 23

SUMMARY OF TEMPERATURE DATA
(No Propellant Flow)

Pass no.		Wall no.	Case (1) Mean wall temperature, (P_e = 10.5 W) (^{O}K)	Case (2) Mean wall temperature, (P_e = 16.75 W) (^{O}K)
Stem		2	600	950
Inlet exit		1	1000	1900
		2	1050	1940
No. 1	in	1	1050	1960
		2	1100	2000
	out	1	1275	2035
		2	1450	2090
Transition		2-3	1600	2125
		1-4	1500	2100
No. 2	in	3	1675	2200
		4	1860	2525
	out	3	1870	2290
		4	1900	2500
No. 3	in	4	1900	2500
	max.	4	1990	2600
	out	4	1860	2525

Nozzle Performance Analysis

Nozzle efficiency. — An accurate prediction of the resistojet's propellant utilization (thrust per unit of mass flow rate) requires an accurate prediction of the kinetic-energy-conversion efficiency of the thrustor nozzle. This efficiency, η_N, is the square of the ratio of the delivered specific impulse to the ideal specific impulse of the thrustor.

$$\eta_N = \left(\frac{I_{sp_{F, E, D, V}}}{I_{sp_{ideal, equilibrium}}} \right)^2 \tag{15}$$

The subscripts are used to indicate that the specific impulse includes losses caused by frozen flow, F, incomplete expansion, E, divergence of the flow leaving the nozzle, D, and viscous effects, V. The nozzle efficiency then, is the product of the efficiencies which account for these four effects.

$$\eta_N = \eta_F \, \eta_E \, \eta_D \, \eta_V \tag{16}$$

The product $\eta_E \; \eta_D \; \eta_V$ can be optimized for given thrustor sizes and operating conditions (pressure and temperature). Optimum values of this product can be correlated with Reynolds number.

The frozen flow efficiency is given by

$$\eta_F = \left(\frac{I_{sp_{ideal,\; frozen}}}{I_{sp_{ideal,\; equilibrium}}} \right)^2 \tag{17}$$

Combining eqs. (15), (16), and (17), the Reynolds-number-dependent product is found to be

$$\eta_E \; \eta_D \; \eta_V = \frac{\eta_N}{\eta_F} = \left(\frac{I_{sp_{F,\; E,\; D,\; V}}}{I_{sp_{ideal,\; frozen}}} \right)^2 \tag{18}$$

$I_{sp_{F,\; E,\; D,\; V}}$ is the specific impulse with all losses considered; therefore, it is the actual delivered specific impulse of the thrustor in space and is given by

$$I_{sp_{F,\; E,\; D,\; V}} = \sqrt{\eta_E \; \eta_D \; \eta_V} \; I_{sp_{ideal,\; frozen}} \tag{19}$$

The ideal frozen-flow specific impulse which, in the subscript notation is simply I_{sp_F}, is accurately determined from IBM computer resistojet performance solutions.

An extensive survey and correlation of experimental data for pure gas rocket was conducted and compared with analytical nozzle performance models to arrive at the Reynolds-number-dependent product

$$\sqrt{\eta_E \; \eta_D \; \eta_V} = f \; (Re_D*) \tag{20}$$

From these data, the optimum value of the efficiency product in eq. (20) was established (fig. 24). The experimental data used were from Marquardt, AVCO, Rocket Research, and NASA thrustor tests. Also used were extensive data from thrustors using two propellants and having various nozzle geometries. These latter data are proprietary and will be published later.

Nozzle discharge coefficient and specific impulse ratio

1.0

0.9

0.8

0.7

0.6

0.5

0.4

C_D

$I_{sp_{F,E,D,V}} / I_{sp_{IDEAL, FROZEN}}$

H_2

N_2H_4 & NH_3

CO_2

H_2O

3   10^1 10^2 10^3 10^4
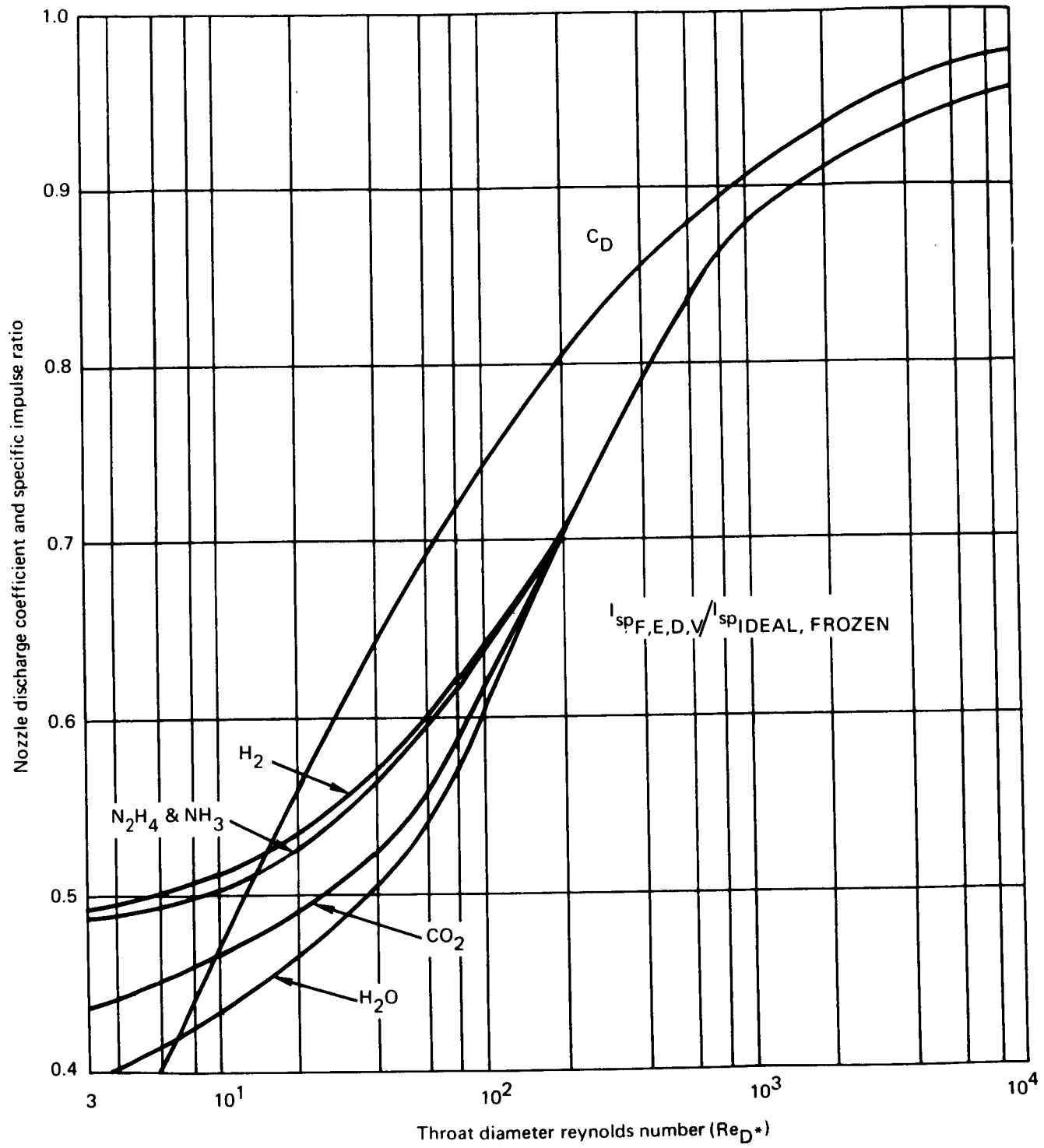
Throat diameter reynolds number (Re_{D^*})

Figure 24. Predicted Resistojet Nozzle Performance

The described approach relies primarily on experimental data to define the optimum overall nozzle efficiency (eq. 16). It does result, therefore, in a more realistic evaluation of the nozzle performance. The usual methods involve a separate evaluation of the expansion divergence and viscous efficiencies. It is difficult to establish each of these values accurately, let alone the optimum product $\eta_E \, \eta_D \, \eta_V$.

Calculated specific impulse: The actual specific impulse is calculated from eq. (19) with the ideal frozen-flow specific impulse. An iterative procedure is used to determine the nozzle-throat-diameter Reynolds number, which, in turn, defines the efficiency product, $\eta_E \, \eta_D \, \eta_V$, from the optimum nozzle performance correlation.

Two equations are used in the iteration. The first of these defines the nozzle throat diameter and is derived from mass continuity and the specific-impulse definition resulting in

$$D^*_{geom} = \sqrt{\frac{4}{\pi} \frac{F}{C_D \, I_{sp_{F, \, E, \, D, \, V}} (\dot{m}/A^*_{eff})}} \qquad (21)$$

In eq. (21), F is the thrust in pounds force, C_D is the dimensionless nozzle discharge coefficient (fig. 24), m is the thrustor mass flow rate in pounds mass per second, and A^*_{eff} is the effective area of the nozzle throat in sq ft. The equation gives the geometric throat diameter in feet. The mass flow rate per unit of throat effective area is accurately given by the IBM rocket-nozzle-program computer solutions. A Reynolds-number estimate is made to evaluate the nozzle discharge coefficient and actual specific impulse.

The second equation in the solution is the definition of Reynolds number at the nozzle throat.

$$Re_{D^*} = \frac{(\rho u)^* \, D^*_{geom}}{\mu^*} \qquad (22)$$

The denominator is the viscosity at the nozzle throat, while $(\rho u)^*$ is the mass-velocity at the throat which is equivalent to the mass flow rate per unit of throat area. For convenience in interpreting experimental data, the mass flow rate is ratioed to the geometric throat area. Using the specific impulse definition,

$$\dot{m} = \frac{F}{I_{sp_{F, \, E, \, D, \, V}}} \qquad (23)$$

the Reynolds number becomes

$$Re_{D}^* = \frac{2.274 \times 10^8 F}{I_{sp_{F, E, D, V}} D^* g \mu^*}$$ (24)

with viscosity in micropoise units.

The throat diameter calculated from eq. (21) is used in eq. (24) to obtain a corrected Re_D^*. Equation (20) is re-evaluated, and the procedure is repeated until a Reynolds-number closure is obtained.

Figs. 25 and 26 present the actual specific impulse for 10-mlbf resistojet thrustors for H_2 and NH_3.

Calculated required power. — The electric power that must be supplied to the resistojet thrustor depends on (1) the power intially in the propellant, (2) the power required in the propellant, and (3) the thermal efficiency of the heater. The heater efficiency, η_H, is defined as the ratio of the power in the gas leaving the nozzle, P_{gas}, to the total input power. The total input power is the sum of the electric power, P_{elec}, and the power initially in the propellant, P_{prop}. Thus,

$$\eta_H = \frac{P_{gas}}{P_{elec} + P_{prop}}$$ (25)

Solving eq. (25) for the electric power required

$$P_{elec} = \frac{P_{gas}}{\eta_H} - P_{prop}$$ (26)

The values of heater efficiency will change with each vehicle installation. For general applicability, the minimum power requirements are presented here, that is for $\eta_H = 100\%$. In application studies, preliminary design values of heater efficiency permit the actual electric-power requirements to be readily calculated.

Considering eq. (26) in more detail, the power in the gas and initially in the propellant can be expressed as a product of propellant mass flow rate and corresponding enthalpy changes.

$$P_{gas} = \dot{m} (h_2 - h_o)$$ (27)
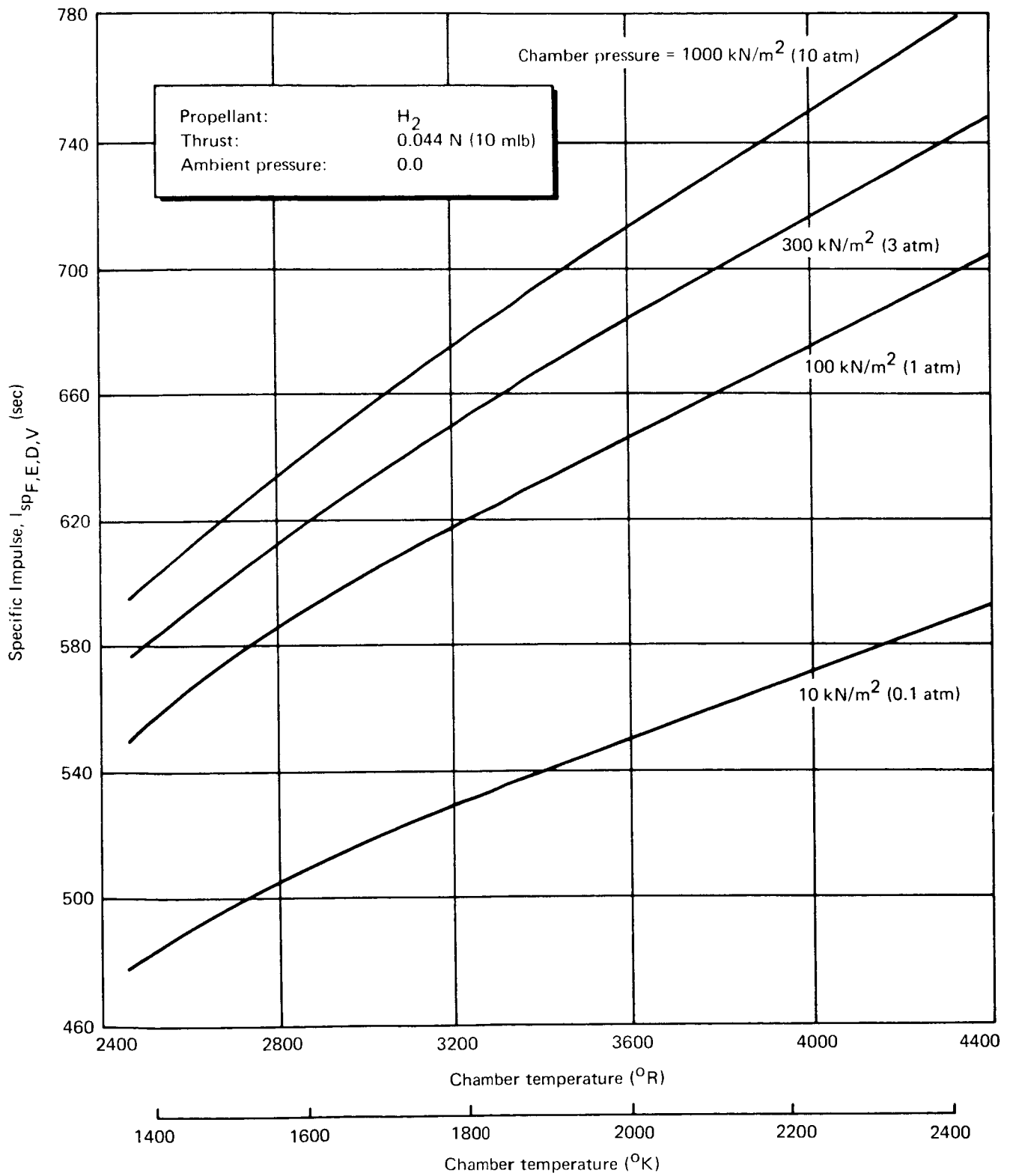
$$P_{prop} = \dot{m} (h_1 - h_o)$$ (28)

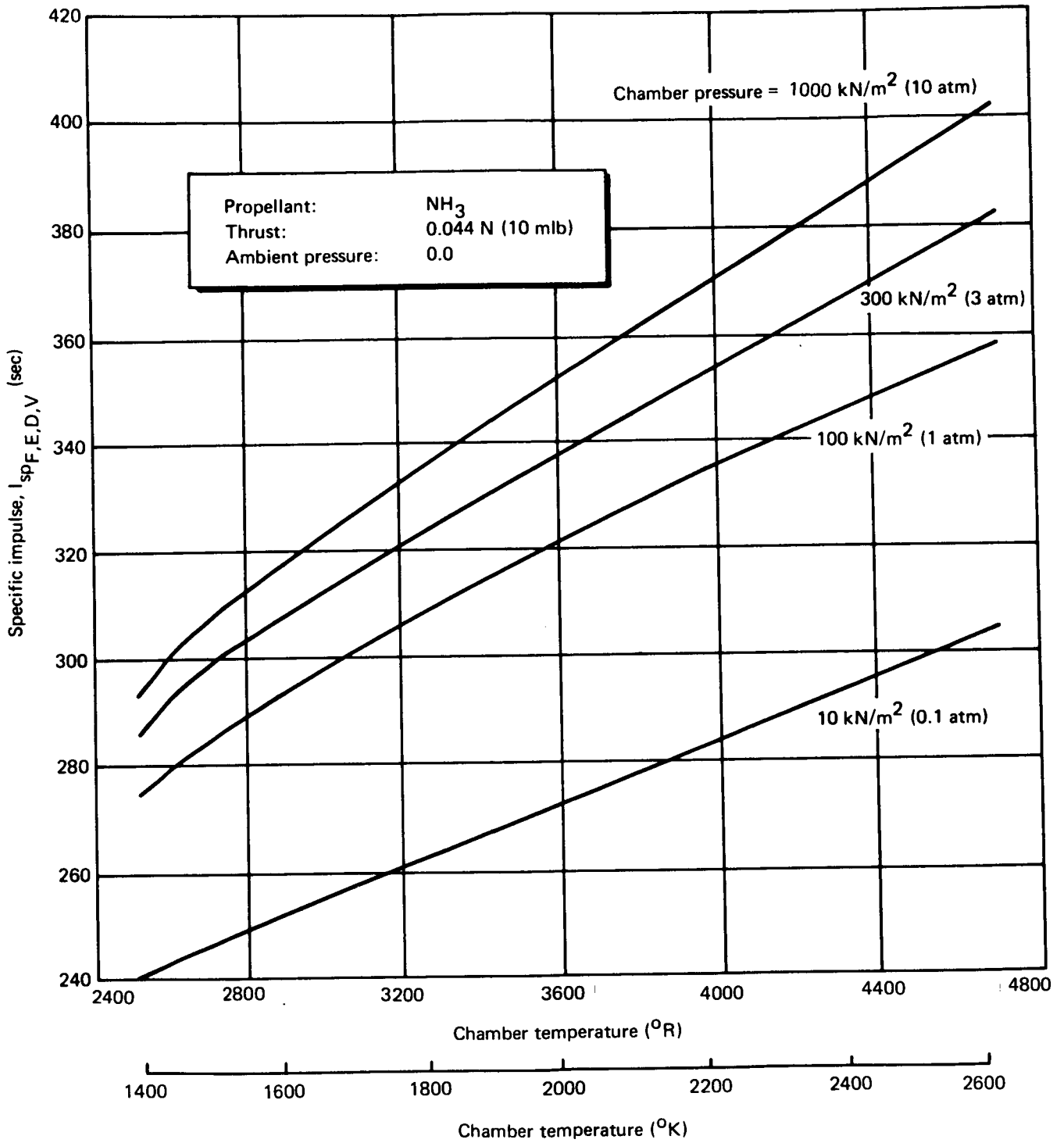Figure 25. Resistojet Delivered Specific Impulse (H_2)

Figure 26. Resistojet Delivered Specific Impulse (NH₃)

The mass flow rate may be readily computed from the specific-impulse definition eq. (23) in each case. In eqs. (27) and (28), h is the enthalpy of the propellant. Subscript (o) refers to a reference enthalpy at $0^O K$. Subscript (1) refers to the initial (as-supplied) propellant condition, while subscript (2) refers to the final chamber condition of the gas. To avoid having to evaluate initial power in the gas, for preliminary design purposes, the heater efficiency values (denoted η'_H) supplied in this section are based upon h_1 taken equal to $298^O K$ ($536^O R$). For cases where h_1 is equal to $298^O K$ eq. (26) is simplified to

$$P_{elec} = \frac{P_{gas}}{\eta'_H} \tag{29}$$

the actual electric power is readily evaluated by dividing the minimum required power, P_{gas} in eq. (29), by η'_H.

The minimum required powers presented in figs. 27 and 28 correspond to initial propellant (1) taken at $298^O K$. Therefore, for the curves in figs. 27 and 28, electric power requirements can be found by dividing by the respective heater efficiencies. Preliminary design values of the heater efficiencies (η'_H) are included as fig. 29.

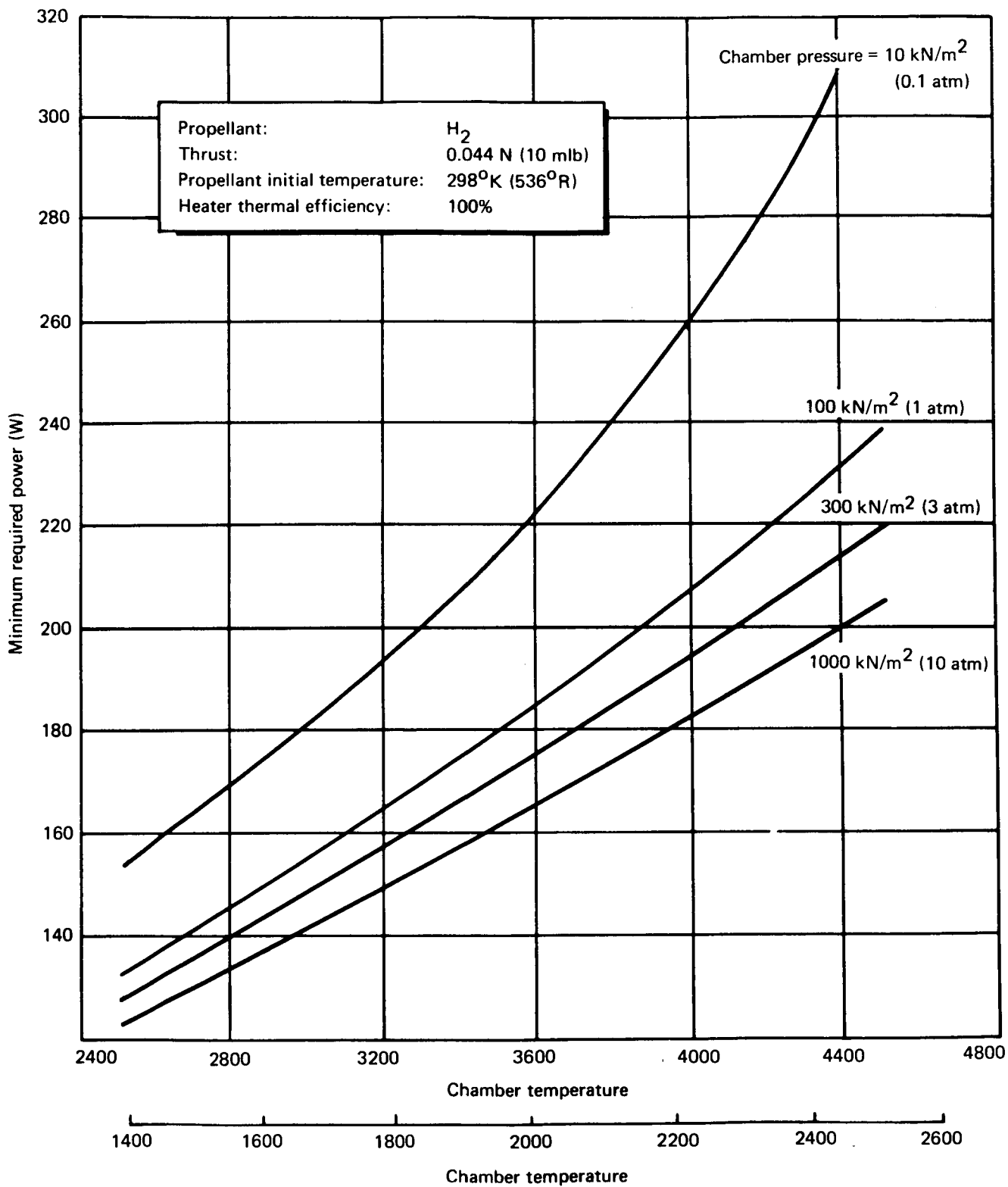Table 24 presents a summary of the design conditions for the Model I thrustor.

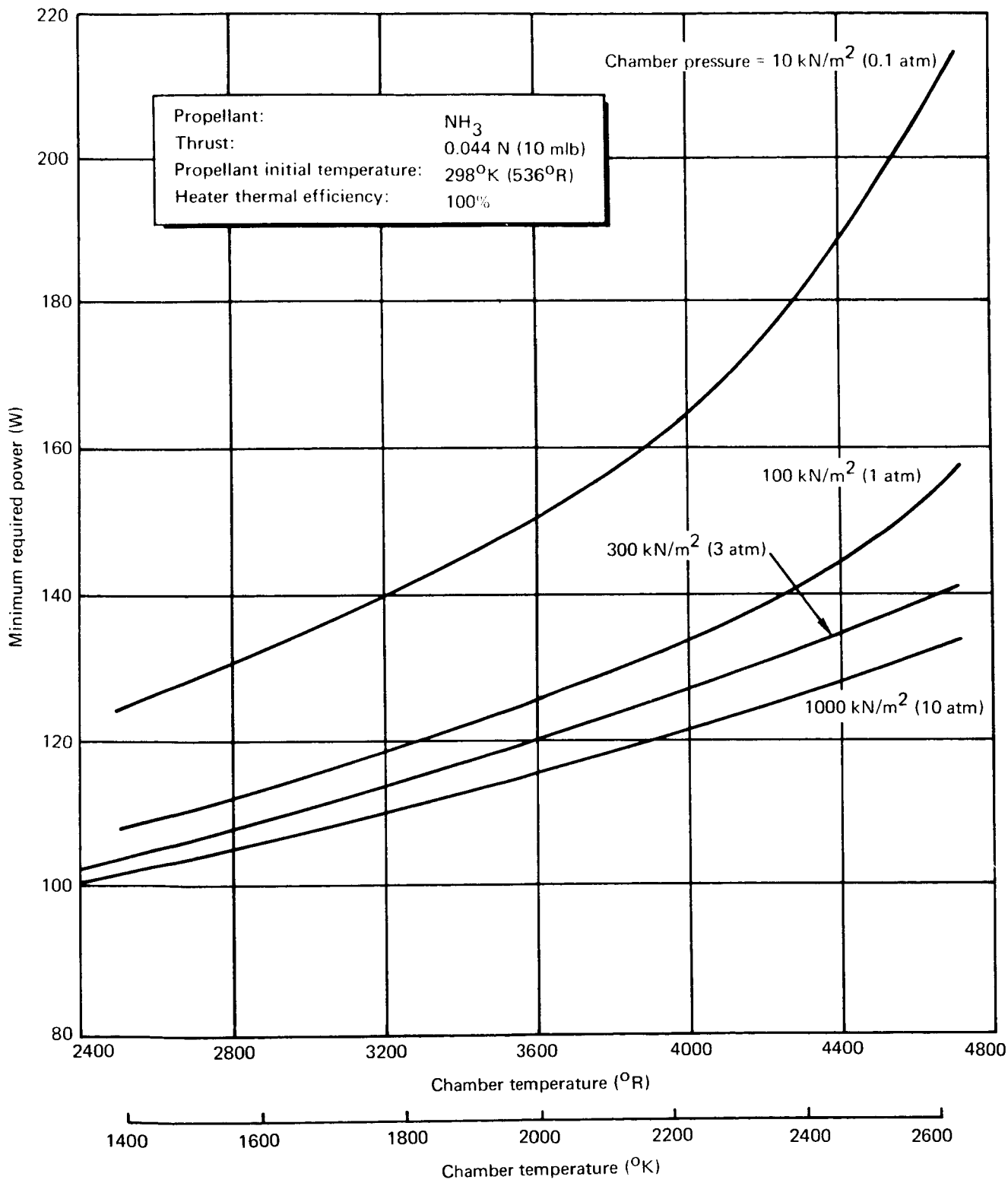Figure 27. Resistojet Minimum Power Requirement (H_2)

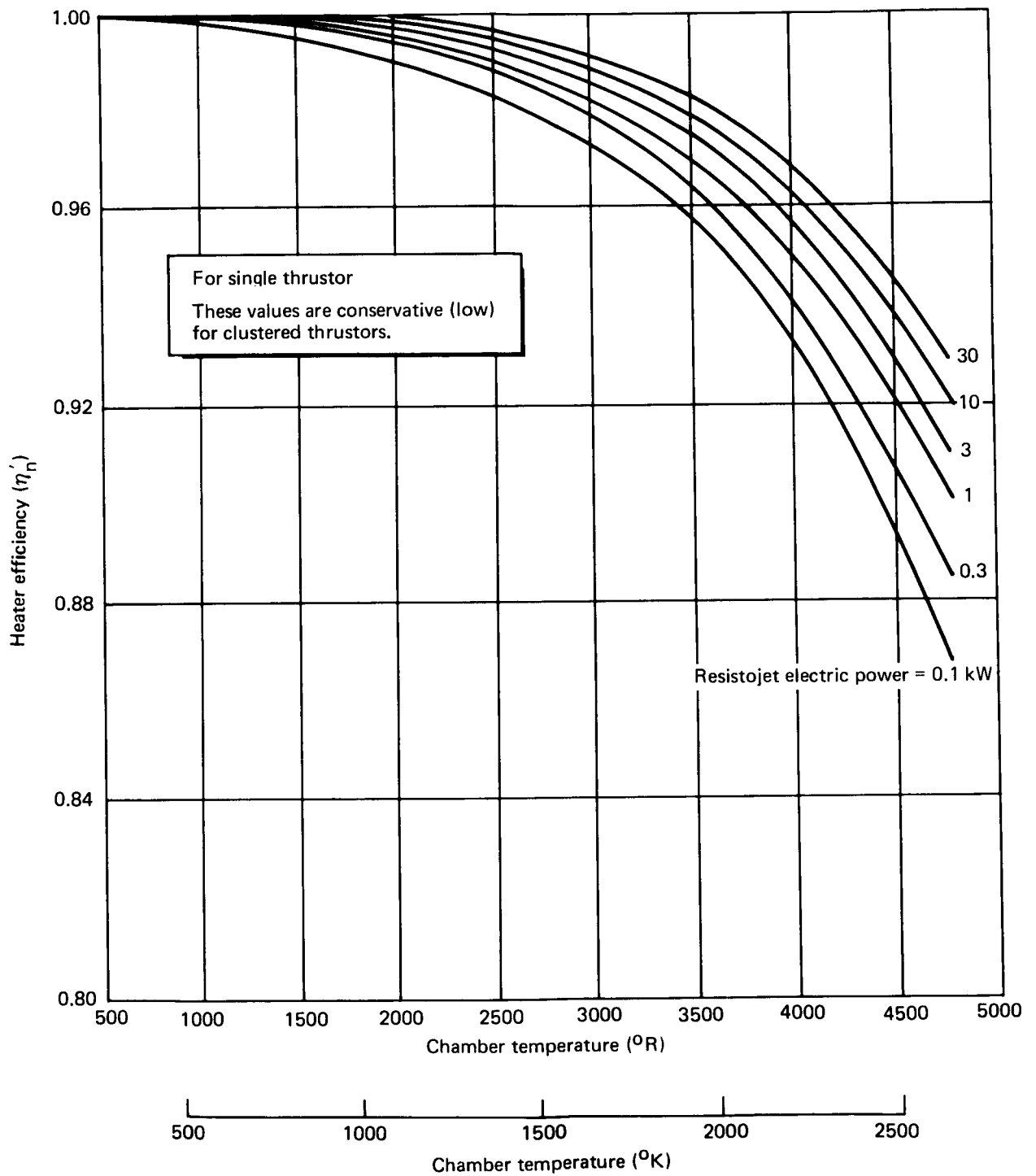Figure 28. Resistojet Minimum Power Requirement (NH_3)

For single thrustor

These values are conservative (low) for clustered thrustors.

Resistojet electric power = 0.1 kW

Figure 29. Preliminary Resistojet Heater Efficiencies (H_2)

TABLE 24

MODEL I DESIGN PARAMETERS

Chamber	H$_2$	NH$_3$
Pressure, atm	1.5	1.5
Gas temperature, ^{O}K	2420	2420
Exit Reynolds number	288	356
Exit Nusselts number	4.4	4.4
Film factor, w/cm^{2O}K	0.4 to 0.6	0.25 to 0.42
Exit Mach number (avg)	0.26	0.26
Element wall, mm		
Inner heating	0.15	0.15
Outer heating	0.30	0.30
Inner element length, cm	4.2	4.2
Inner element ID, mm	0.78	0.78
Throat diameter, mm	0.53	0.53
Nozzle half-angle, rad (^{O})	0.306 (17.5)	0.306 (17.5)
Area ratio	20 to 110	20 to 110
Throat radius, mm	0.63	0.63

MODEL I TESTS

Test Plan

Test facility and instrumentation. — The facilities and instrumentation used in development testing of the prototype 0.044-N (10-mlb) thrustor are shown in fig. 30. The electrothermal laboratory at The Marquardt Corporation has 65.2 m^2 (702 sq ft) of floor space. The heart of the laboratory is the vacuum chamber, which is 0.9-m diam and 2-m long. The chamber pumping system consists of a 0.40-m (16-in.) Stokes ring-jet booster backed up by a 140-ℓ/sec (300 cfm) mechanical pump. Without cooled baffles, the ultimate vacuum of the system is about 0.3 µm Hg.

Either of the two propellant systems, may be used in constant mass flow or constant pressure mode by valving the flow controller in or out of the circuit. The maximum error in the mass flow system is estimated to be approximately 1.5%. This error is mainly in the rotameter flowmeter readout.

Power is provided by a 20-volt, 125-A, silicon-controlled rectifier with two selective modes of operation: constant voltage and constant current. The latter mode eliminates catastrophic failures in case of shorting during development testing. The supply voltage is regulated to ±0.08% in the constant voltage mode.

The primary-electric-power indicator is a digital voltmeter. The accuracy of the voltmeter is 0.01%; however, since it is used to measure both voltage and current separately, the error in the electric power measurement will be larger. Because of time lag in reading voltage and current separately, there will be a maximum error in each of 0.1%, giving 0.2% error for electric power measurement.

Thrust has a maximum error of 0.8% in the dynamometer and 0.5% in readout, giving a maximum error of about 1.3% in the thrust measurement.

Thermal losses from the exterior of the thrustor are calculated from temperatures indicated by thermocouples.

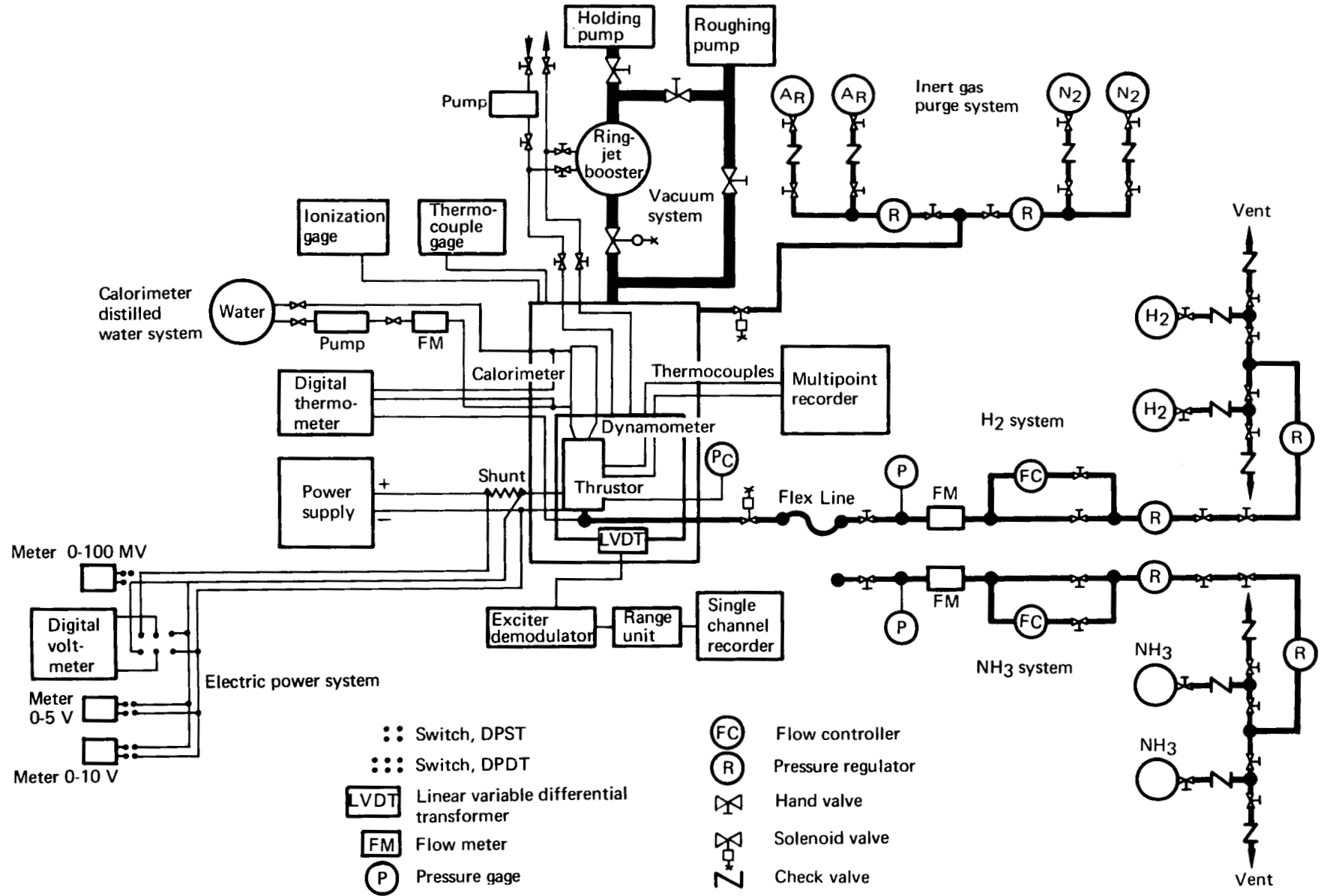The instrumentation list with ranges and estimated accuracies is shown in table 25.

Figure 30. Resistojet Development Test System Schematic

TABLE 25

ELECTROTHERMAL LABORATORY INSTRUMENTATION LIST

Instrument	Range	Accuracy
Brooks rotameter, H_2	0.0015-0.018 g/sec	±1%
Brooks rotameter, NH_3	0.005-0.055 g/sec	±1%
Brooks rotameter, water	0.8-8.0 g/sec	±1%
Grove pressure regulators (2)	0 to 300 psia	- - -
Brooks flow controllers (2)	- - -	- - -
Magnevac gage (pressure in test chamber)	1 μm to 500 mm Hg	±0.5 μm Hg
Digital voltmeter (thrustor power)	10^{-4}-10^3 V	±0.1 mV
Triplett meters (current and voltage, secondary measurement)	0-10 V 0-100 A	2% of full scale
Sorenson power supply	0-20 V 0-125 A	±0.075% ±125 mA
Honeywell strip chart recorder (thrust record)	0-5 mV	±0.25%
Honeywell multipoint recorder (temperatures)	0-1273°K	±0.25%
Low-thrust dynamometer	0.1 mlb - 1.5 lb	±3.5% ±0.8%
Heise pressure gages (2)	0 - 100 psia 0 - 100 psia	±0.1% of full scale
NRC ionization gage	10^{-3} to 1 μm Hg	±2%

Calibration procedures. — Many of the instruments, such as gages and meters, used in the development tests of the 0.044-N (10-mlb) thrustor are calibrated in the Marquardt Standards Laboratory using normal procedures. Special calibration procedures for instruments used to make performance measurements are described in the following paragraphs.

Dynamometer: The first step in calibration of the flotation-type, low-thrust dynamometer is to adjust the body of the linear variable differential transformer (LVDT) so that the output is linear over the range to be used. This occurs when the core moves symmetrically about the midpoint of the transformer.

The dynamometer is calibrated by means of hanging precision weights on a line connected to a pulley. The pulley is attached to the thrustor by means of a fine monofilament line concurrent with the thrust axis. The pulley rotates (through a small angle) on a Bendix flexure. The dynamometer is calibrated before and after each thrustor test. A typical calibration curve is shown in fig. 31.

Rotameters: The rotameters used to measure propellant flow rate present a problem because of the low flow rates used and the differences in the densities of the propellants relative to air. Two methods are used to calibrate the H_2 rotameter. In the first method, the gas is exhausted through the rotameter from a small container with a known, fixed volume, and the changes in pressure and temperature with time are noted. The mass flow rate is then

$$\dot{m} = \frac{V\Delta\rho}{\Delta t} \tag{30}$$

where V is volume, Δt is the time interval, and $\Delta\rho$ is the change in density, which is directly proportional to the change in the pressure-to-temperature ratio.

The second method is to attach a large balloon to the table of a laboratory balance and flow H_2 through the rotameter into the balloon. A timer is started when the balance swings through zero and a mass, m_1, is added to the balance. After a time, Δt, has elapsed, the buoyant force on the H_2-filled balloon causes the balance to swing through zero again, at which time the timer is stopped. The mass of H_2 flowing into the balloon in the time, Δt, is $\dot{m}\Delta t$; it is also equal to $\rho_{H_2}\Delta V$. The buoyant force on the balloon is

$$F = Vg\,(\rho_{air} - \rho_{H_2}) \tag{31}$$

where g is the acceleration due to gravity. The change in buoyant force, ΔF, in time, Δt, is

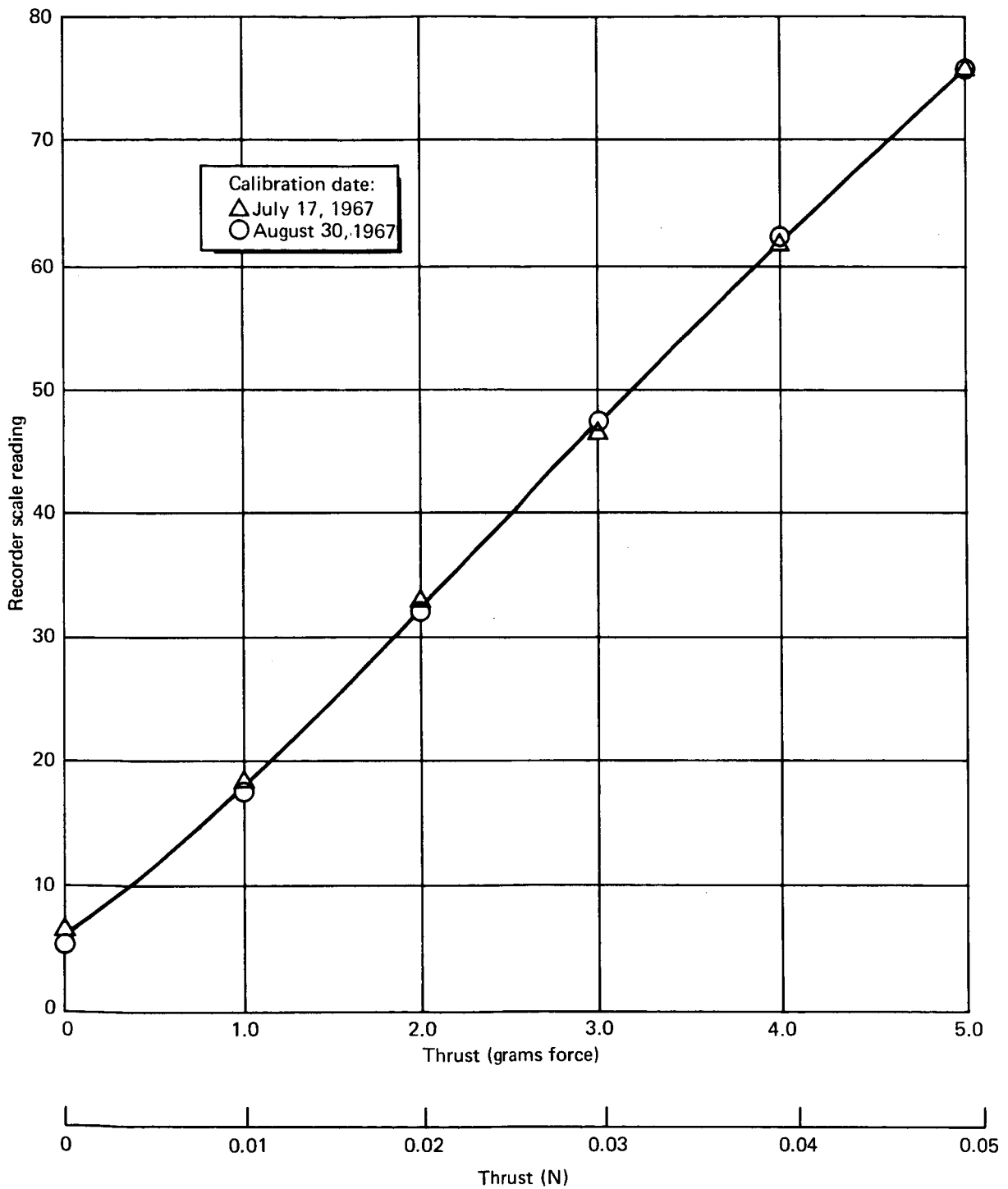$$\Delta F = \Delta Vg\,(\rho_{air} - \rho_{H_2}) \tag{32}$$

76

Figure 31. Dynamometer Calibration Model 128

Substituting for ΔV gives

$$\Delta F = g\, \dot{m} \Delta t \frac{(\rho_{air} - \rho_{H_2})}{\rho_{H_2}} \tag{33}$$

ΔF is also equal to $m_1 g$, or

$$\dot{m} = \frac{m_1}{\Delta t \left(\frac{\rho_{air}}{\rho_{H_2}} - 1\right)} \tag{34}$$

Both methods were used over a flow rates range from 0.002 to 0.018 g/sec and a pressure range from (100 to 300 kN/m^2) (1 to 3 atm).

NH$_3$ presents a different problem. While lighter than air, it is much heavier than H$_2$, and the balloon method is marginal at best. A volumetric flow calibration device, as used in the Marquardt Standards Laboratory, is employed as well as the fixed-volume/pressure-change method used in the H$_2$-rotameter calibration. A typical rotameter calibration curve is shown in fig. 32.

Power measuring devices: Power is measured by combining the measurements of voltage and current. Voltage is measured with a digital voltmeter (primary measurement) and a D'Arsonval meter (secondary). Current is measured by the millivolt output from a precision shunt. This is read on a millivolt meter and on the digital voltmeter (primary).

The shunts are calibrated in the Marquardt Standards Laboratory. All meters are then calibrated in the test system to eliminate line losses.

Thrustor Performance Evaluation. — After the thrustor has been installed and aligned, the entire system is leak-checked. The nozzle is stoppered, and the system is evacuated and then checked on a mass-spectrometer leak detector using helium. Then the stopper is held in the nozzle, and the system is pressurized with H$_2$. The H$_2$ supply is closed off, and the drop in pressure versus time is noted. The maximum tolerable H$_2$ leak rate is 3×10^{-5} g/sec or 0.5% of the design flow rate.

When the system is tight, the dynamometer is calibrated and the cell closed. H$_2$ flow with no electric power is then initiated and adjusted to cold-flow operating conditions. All data are then read and recorded.

All data taken during the application of power are immediately reduced and plotted on control charts so that deviations from expected performance can be noted quickly. Temperatures of such critical areas as braze joints and outer case are continuously plotted versus specific impulse and/or electric power. Specific impulse versus power and resistance versus power are also continuously plotted. This process is repeated with NH$_3$.

The definitions of all the performance parameters are given in the Appendix. Experimentally the heater efficiency, η_H, is found by calculating the thermal power lost, P_1, from the thrustor envelope by means of a temperature survey. The loss terms are thermal radiation from the surface, thermal
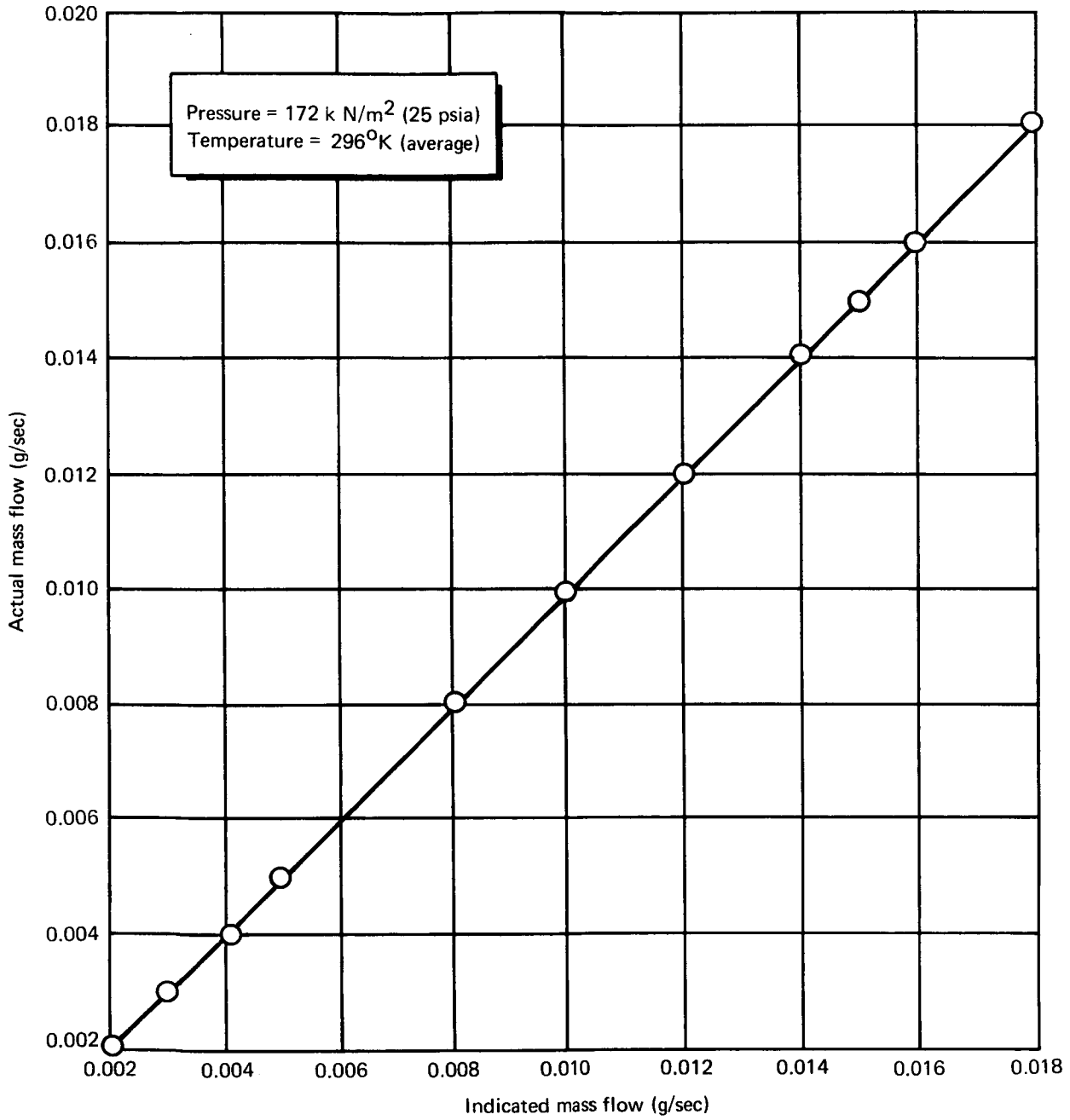
Figure 32. Calibration of H_2 Rotameter

conduction to the mount and down the electrical leads. The power in the jet is found from eq. (6) and η_H from eq. (7). Equation (9) supplies the basis for the nozzle efficiency ηN.

A-2 Thrustor Tests

Fig. 33 shows the Model I instrumented, ready for test.

Initial tests--May 23 to 26, 1967. — In the initial tests on H_2 and NH_3, the thrustor was not taken to the specific impulses for which it was designed. Using the cold resistance and an assumed temperature distribution, the hot resistance of the thrustor was calculated to be 0.15 ohms at $2420^\circ K$ gas temperature. As it turned out, this was too low, and the specific impulses attained were 667 and 325 sec on H_2 and NH_3, respectively.

The heat losses from the exterior of the thrustor were calculated, and the resulting heater efficiency confirmed suspicions that the gas temperature was, in fact, lower than $2420^\circ K$ (probably closer to $2200^\circ K$). Thermal conduction losses through the power leads were much larger than expected. Plotting the previous resistance data versus temperature (calculated from energy consideration) and extrapolating to $2420^\circ K$ gave a new target resistance of 0.156 ohms.

Second test series--June 6, 1967. — For this second test series, an attempt was made to reduce conductive losses by decreasing the conductive area of the power cables and by placing pyrolytic graphite washers between the insulation cover and the mounting bracket. These measures were effective to some extent; later, redesign of the power leads and mounting bracket produced further improvement.

The performance of the thrustors during the second test series is summarized in table 26 and in figs. 34 through 37. Some of the points shown may have been taken before thermal equilibrium was established; however, the maximum points are probably stable. The specific impulses of 739 sec (H_2) and 344 sec (NH_3) compared with theory indicate that the gas temperature is at least $2420^\circ K$, the target temperature.

Extended performance test--June 7 and 8, 1968. — After the second test series on H_2 and NH_3 had shown that predicted performance could be achieved, an extended test was conducted using H_2 propellant. The thrustor operated for 25 hours at specific impulses above 700 sec.

During this test, there were some fluctuations in electric power (of 15 watts magnitude) without any detectable change in resistance. These are as yet unexplained. However, the resultant increase in electric power for the same specific impulse and thrust between the start of the 24-hour test and later measurements indicates a decreasing efficiency. As the test progressed, a change was noticed in the insulation around the nozzle which was visible through the test cell window. Also, one by one, the thermocouples on the outer case failed. The evidence pointed to high case temperatures causing deterioration of the insulation and therefore decreasing heater efficiency.
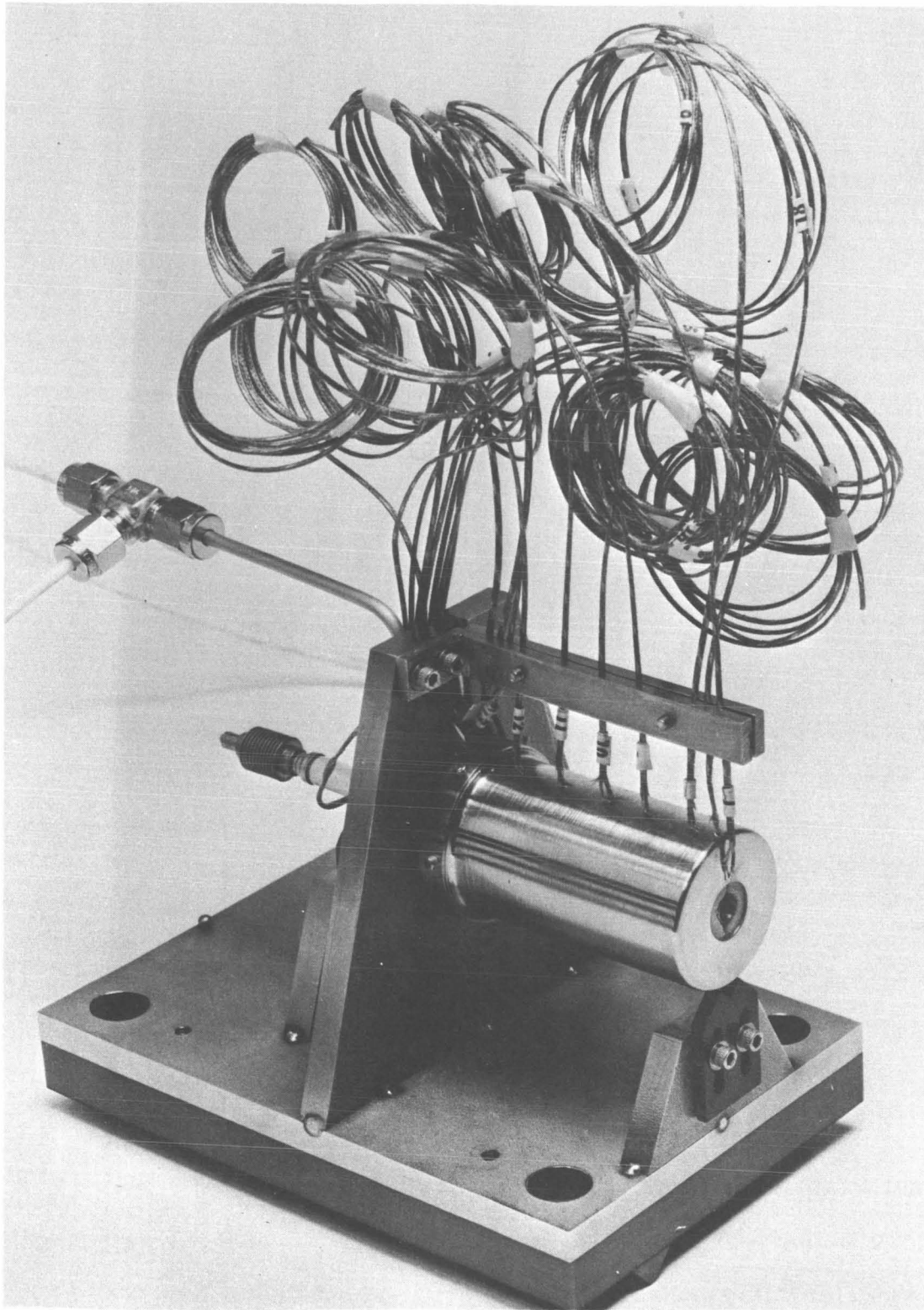
Figure 33. Instrumented (Model I) Resistojet and Mounting Bracket

TABLE 26

PERFORMANCE SUMMARY

| Performance parameters	Data point number			
	150	157	79	88
Thrustor	A-1	A-1	A-2	A-2
Throat diameter, cm	0.0516	0.0516	0.0589	0.0589
Area ratio	110:1	110:1	20:1	20:1
Propellant	H_2	NH_3	H_2	NH_3
Voltage, V	5.88	5.07	6.16	5.50
Current, amps	42.1	34.9	39.9	34.9
Electric power, W	248	177	246	192
Total power, W	278	185	272	200
Thrust, grams force	4.56	4.55	4.58	4.59
Mass flow, grams/sec	0.00705	0.0135	0.0062	0.01335
Specific impulse, sec	647	337	739	344
Chamber pressure, kN/m^2 (atm)	182 (1.80)	172 (1.70)	122 (1.21)	118 (1.17)
Gas temperature, $^{\circ}K$	2306	2320	2203	1970
Maximum exterior temperature, $^{\circ}K$	641	767	598	606
Thrustor resistance, ohms	0.140	0.145	0.154	0.158
Test cell pressure, microns	8	6.5	6	3.5
Electric power efficiency, η_o*	0.573	0.417	0.662	0.395
Overall efficiency, η_o	0.510	0.399	0.599	0.380
Heater efficiency, η_H	0.929	0.808	0.777	0.629
Nozzle efficiency, η_N	0.549	0.494	0.771	0.604
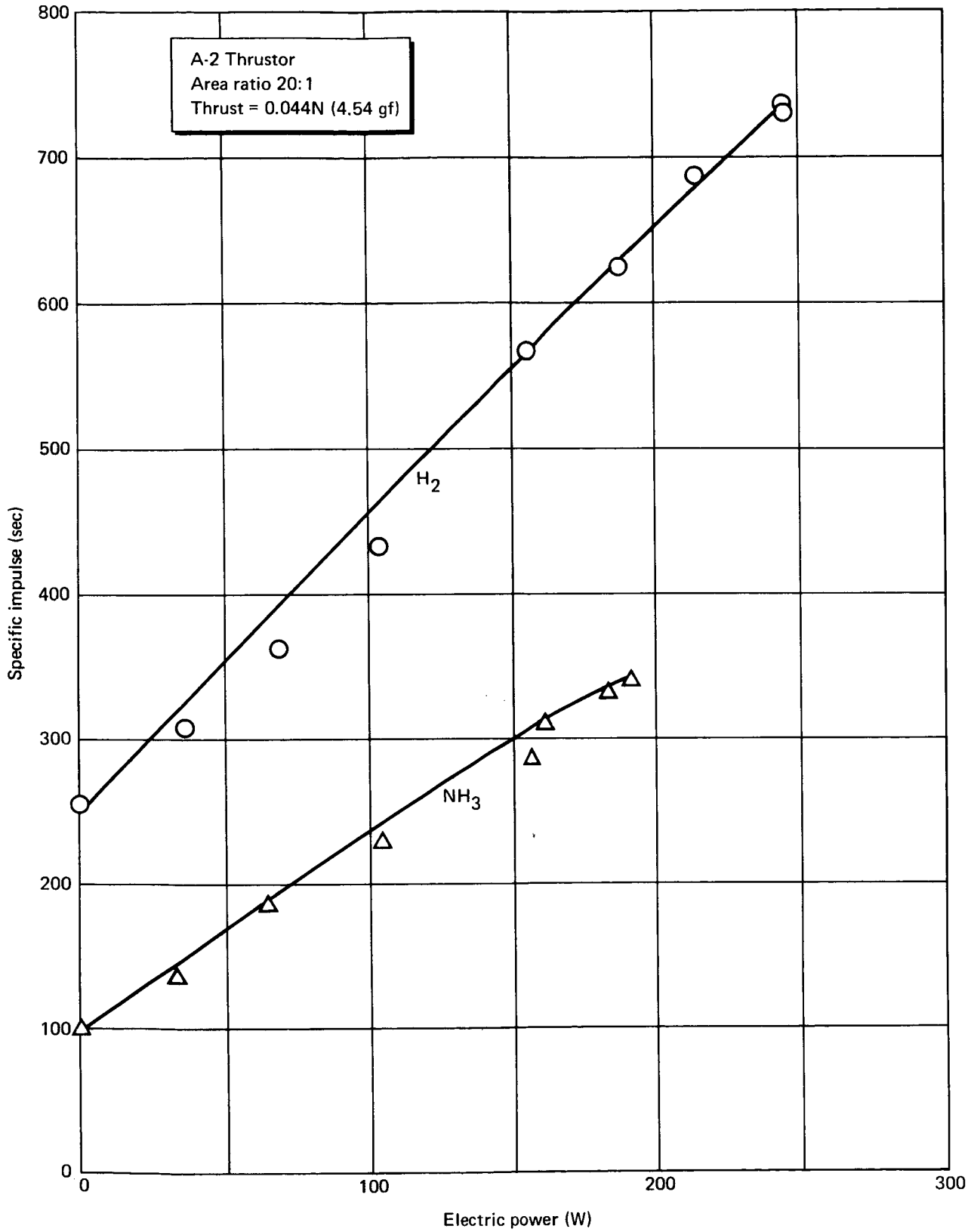
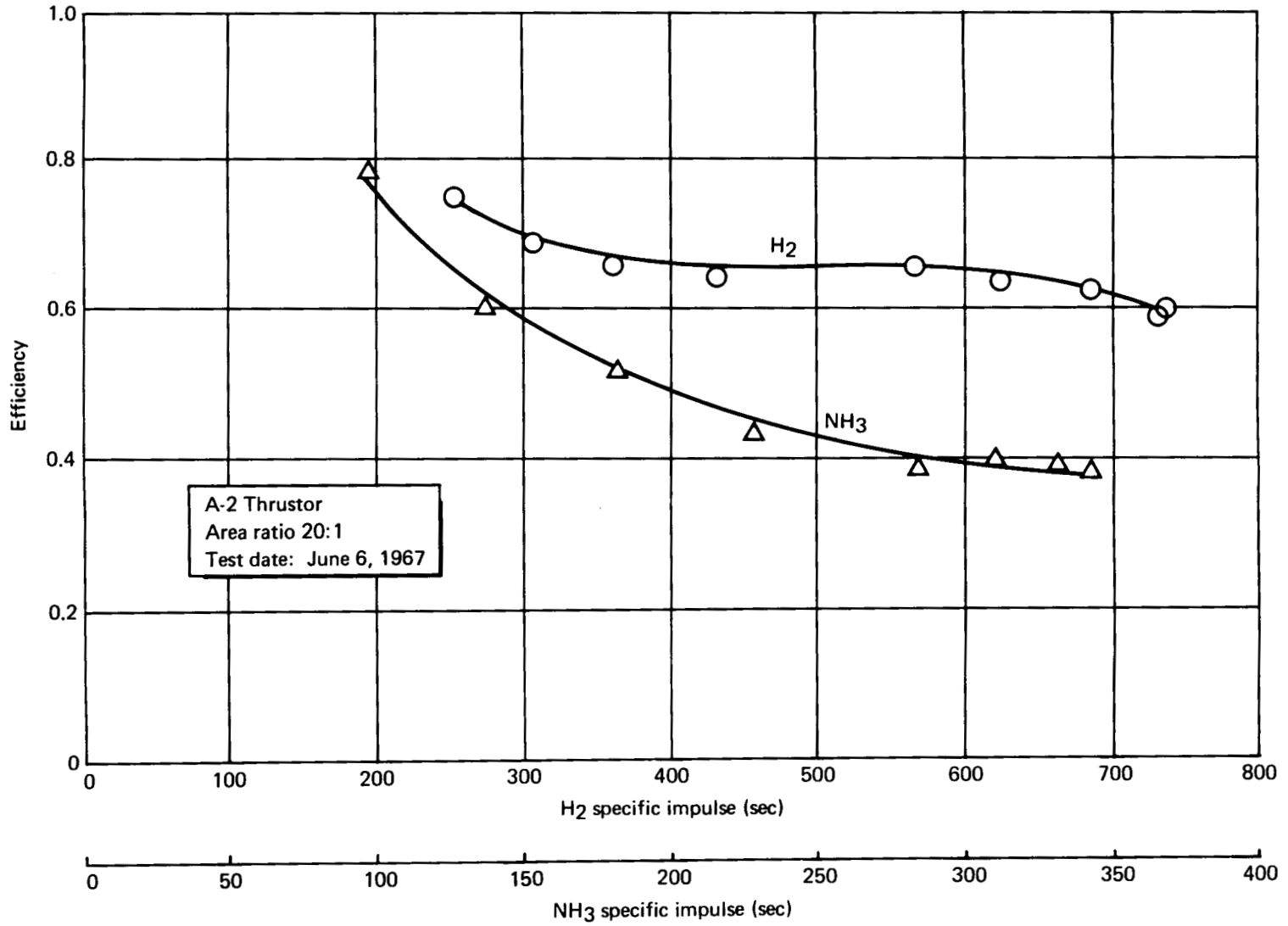Figure 34. Resistojet Specific Impulse vs. Electric Power

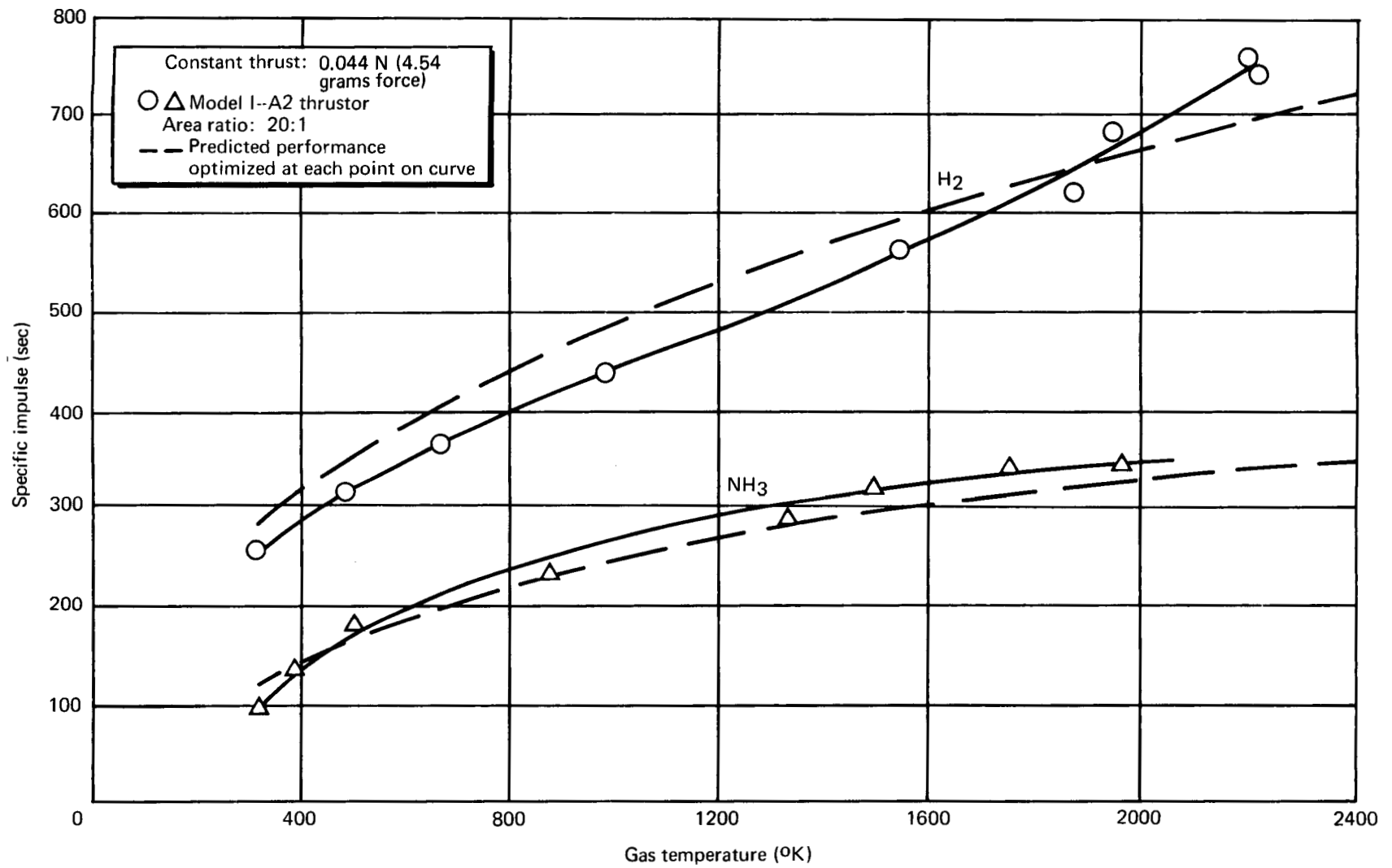Figure 35. Total Power Overall Efficiency
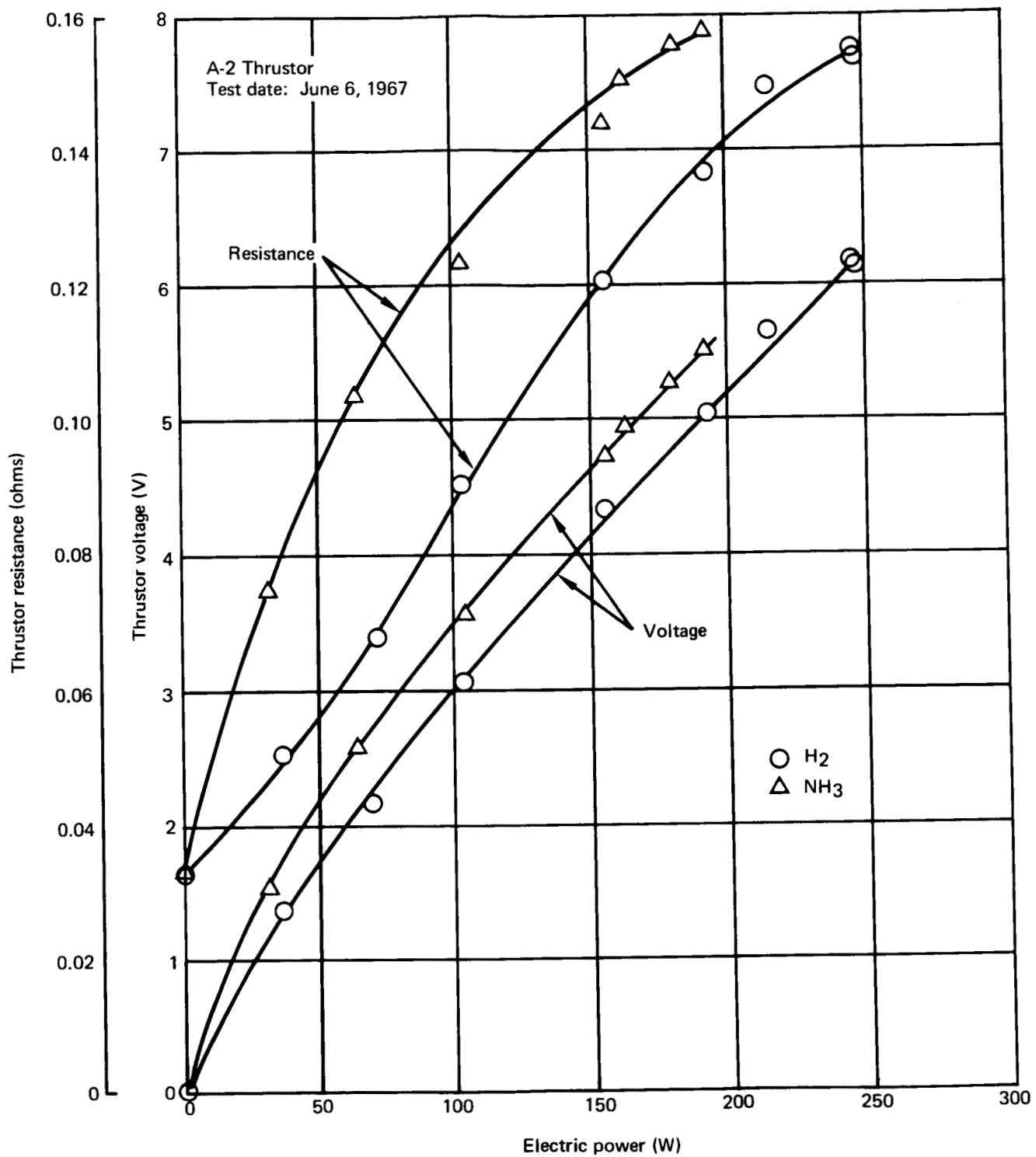
Figure 36. Specific Impulse vs. Gas Temperature

Figure 37. Electrical Characteristics

Post-run inspection confirmed suspicions that the insulation had been overheated; the insulation was charred wherever it had been exposed to temperatures greater than 1270°K (maximum continuous duty temperature for Min-K-2000). The data for the extended test are summarized in figs. 38 and 39.

It was concluded from these tests that:

(1) Efficiencies are somewhat lower than anticipated.

(2) Thermal conduction losses are greater than originally predicted. (This partly accounts for the lower efficiencies.)

(3) The maximum temperatures of the outer case are probably in the 1600°K range, which is significantly greater than predicted.

These conclusions indicated that future tests would require the use of higher temperature insulation near the outer case. Also, the electric leads would have to be modified to reduce conduction losses. These measures increased the efficiency (as subsequent tests verified).

A-1 Thrustor Tests

On July 18 and 19, 1967 the A-1 thrustor was tested on H_2 and NH_3, respectively. During both the H_2 and NH_3 tests, six points were taken at 1-hour intervals to allow ample time for thermal stability.

These tests marked the first use of the new electrical leads with stainless-steel thermal dams. Conduction losses were reduced considerably, and the resultant heater efficiencies were much improved over the earlier tests with thin copper dams of the same dimensions.

The results of these tests are presented in table 27 and in figs. 40 through 43. Decreased nozzle performance, compared to the A-2 engine, with its 20.1:1 area ratio, was observed. This is because of increased viscous loss as compared to the increase in expansion performance from the larger area ratio nozzle.

Model I Test Summary

As shown in figs. 44 through 46 and in table 26 (which summarizes the test results of both the A-1 and the A-2 thrustors), the A-2 thrustor had a significantly higher nozzle efficiency than the A-1. This is because of the higher viscous losses in the longer A-1 nozzle ($A/A^* = 110$). On the other hand, because of lower conduction losses through the modified power cables with stainless-steel heat dams, the heater efficiency of the A-1 thrustor was considerably higher than that of the A-2.

Composite performance curves, using the A-1 heater efficiency and the A-2 nozzle efficiency, were plotted (figs. 47 and 48) in an attempt to predict the performance of the Model II thrustors.
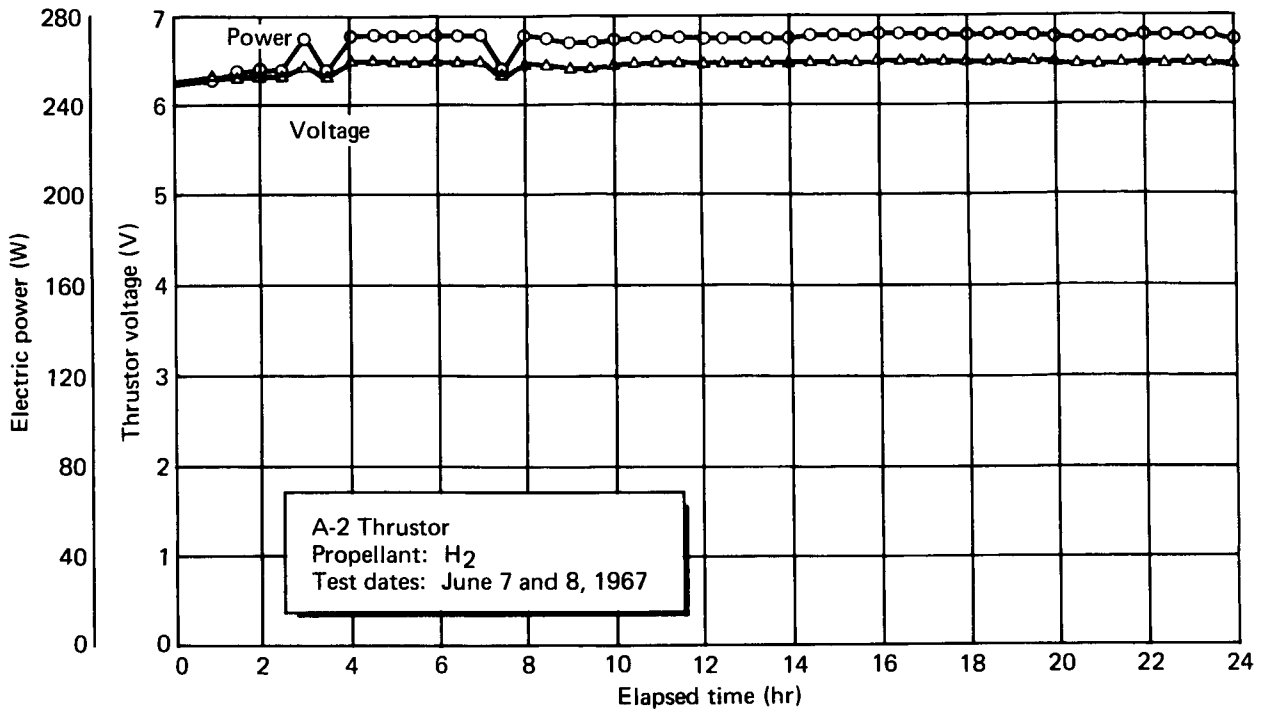
Figure 38. Electrical Characteristics vs. Elapsed Time--24-Hour Test
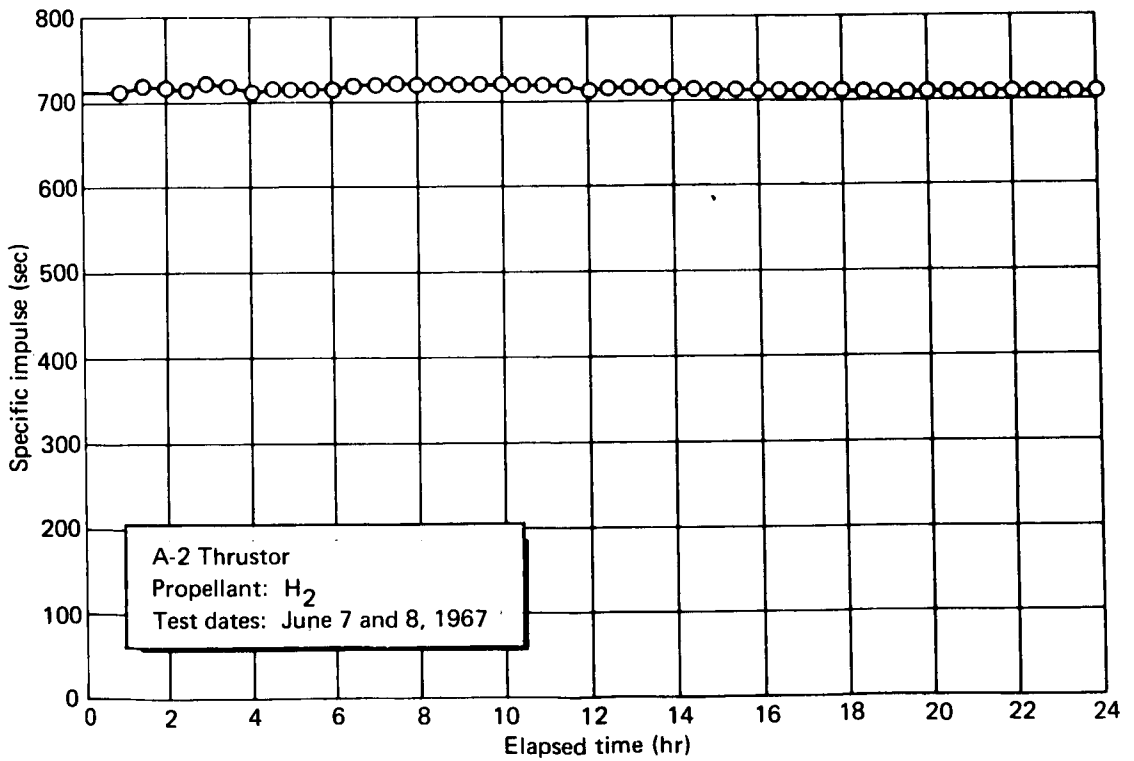

Figure 39. Specific Impulse vs. Elapsed Time--24-Hour Test

TABLE 27

A-1 THRUSTOR PERFORMANCE SUMMARY

| Leading performance parameters	Data point number	
	150	157
Test date	7-18-67	7-19-67
Propellant	H_2	NH_3
Electric power, W*	247.5	176.9
Voltage, V	5.879	5.069
Current, amps	42.1	34.9
Thrust, grams force	4.56	4.55
Mass flow, g/sec	0.00705	0.01350
Specific impulse, sec*	647	337
Metering pressure, kN/m^2 (psia)	336 (48.8)	284 (41.2)
Metering temperature, °K	306.33	304.10
Inlet pressure, kN/m^2 (psia)	332 (48.1)	280 (40.7)
Inlet gas temperature, °K	302.02	300.58
Test cell pressure, μm Hg	9	6.5
Max. temperature, outer shell, °K	521	598
Thrustor resistance, ohms*	0.1396	0.1452
Estimated gas temperature °K	2306	2320
Thrustor chamber pressure, kN/m^2 (psia)	183 (26.5)	171 (24.8)
Electric power efficiency, η_o*	0.573	0.417
Overall efficiency, η_O*	0.510	0.399
Heater efficiency, η_H*	0.929	0.808
Nozzle efficiency, η_N*	0.549	0.494

*Calculated
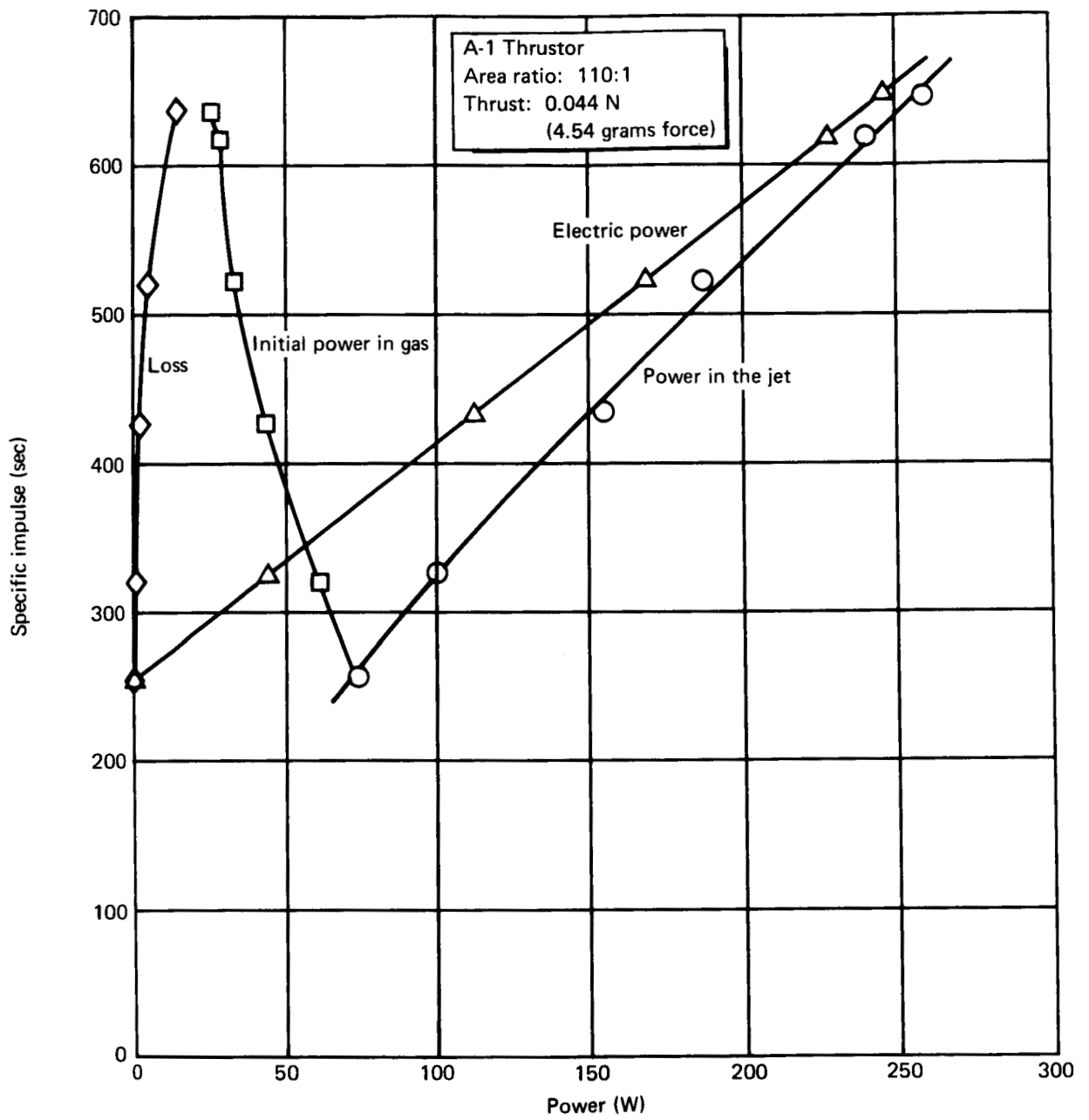
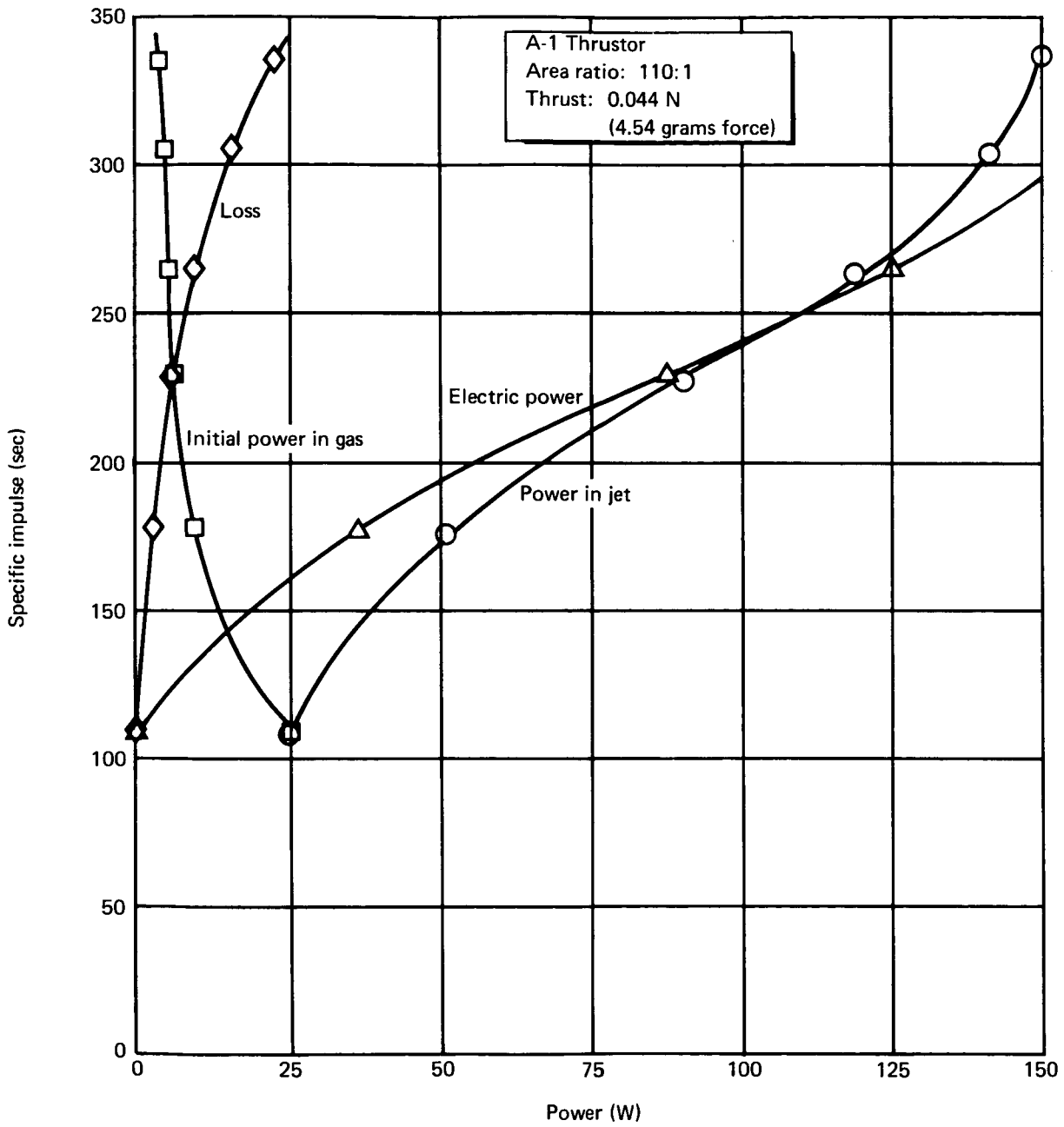Figure 40. Power Summary (H_2)
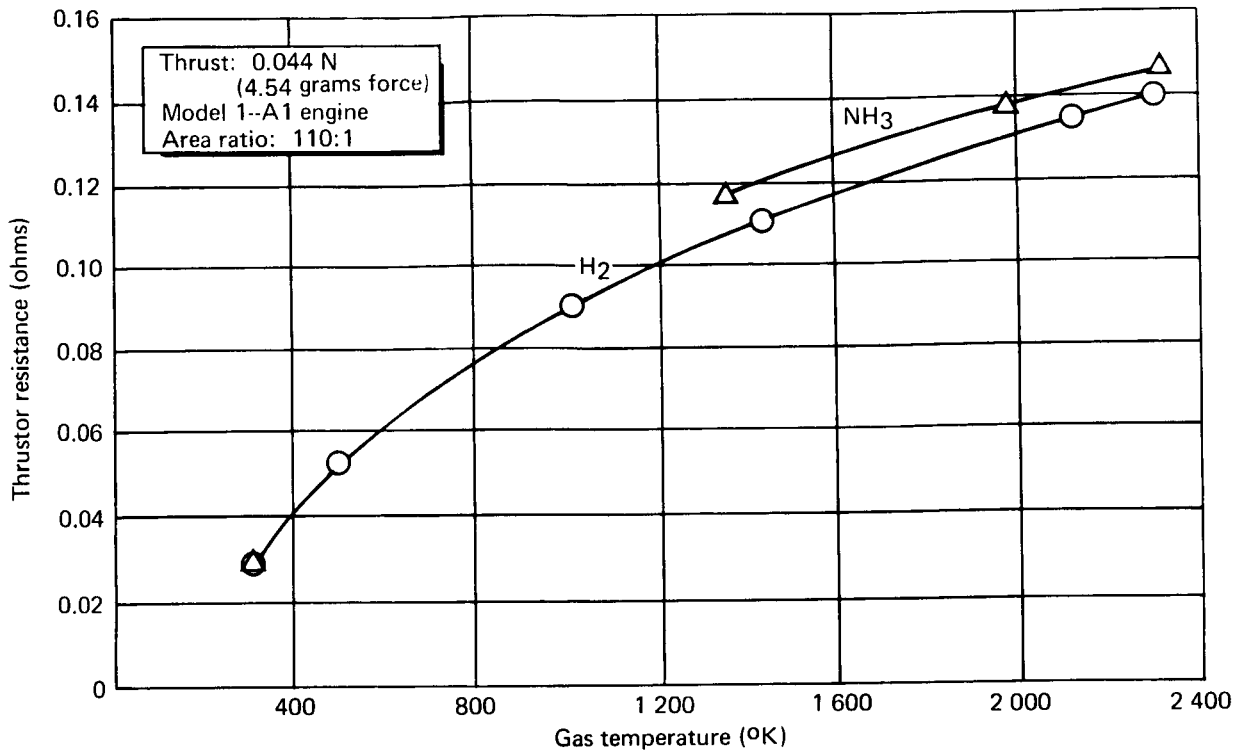
Figure 41. Power Summary (NH_3)
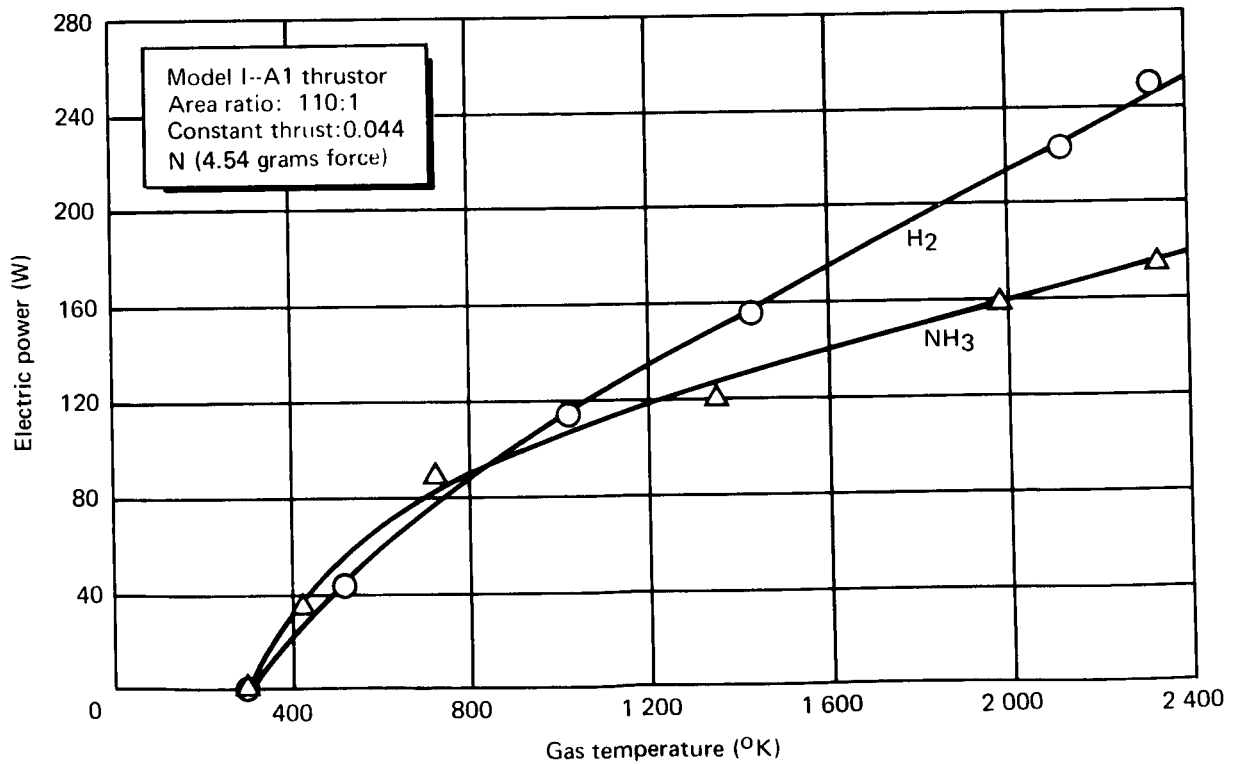
Figure 42. Resistance vs. Temperature

Figure 43. Electric Power vs. Gas Temperature
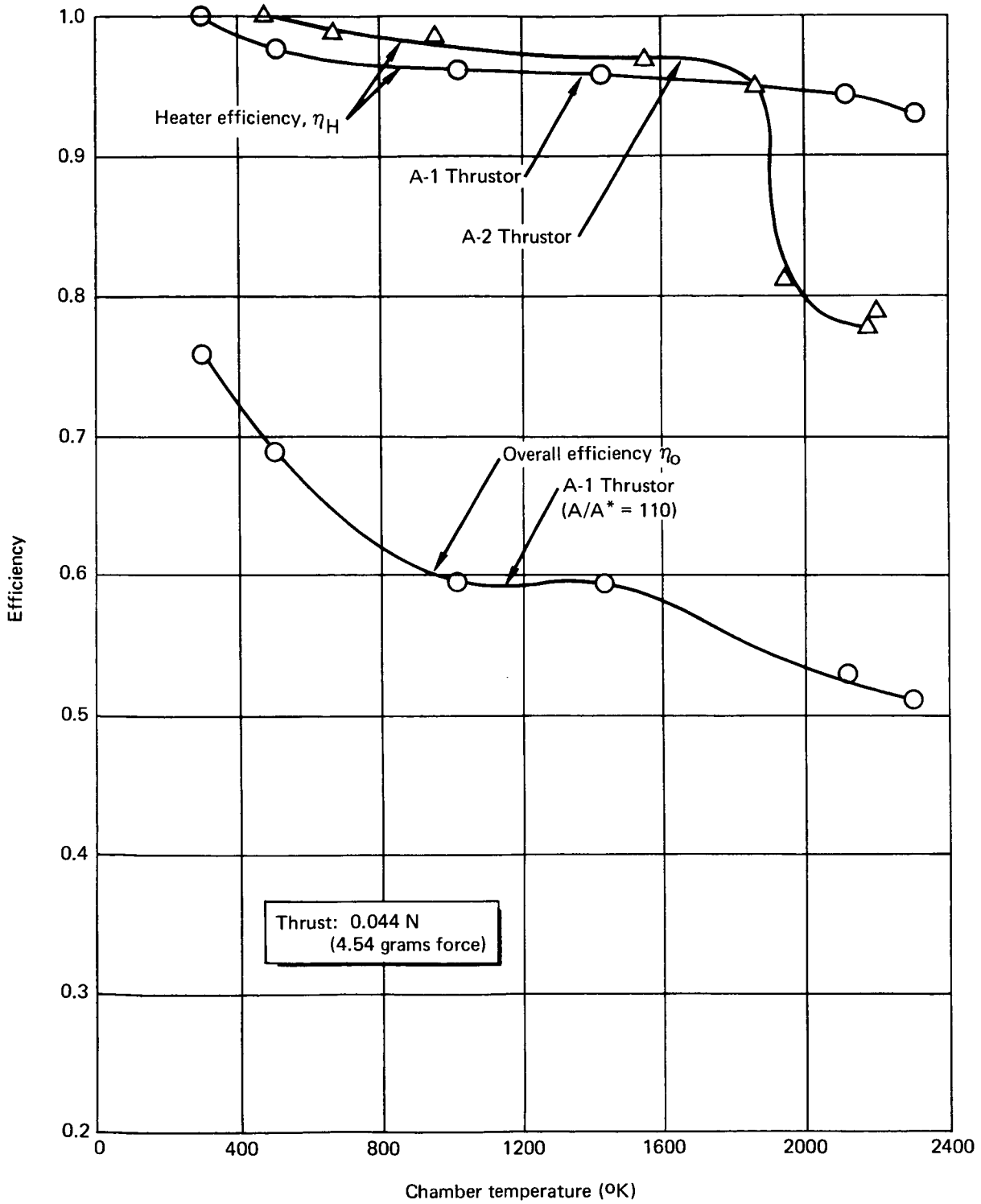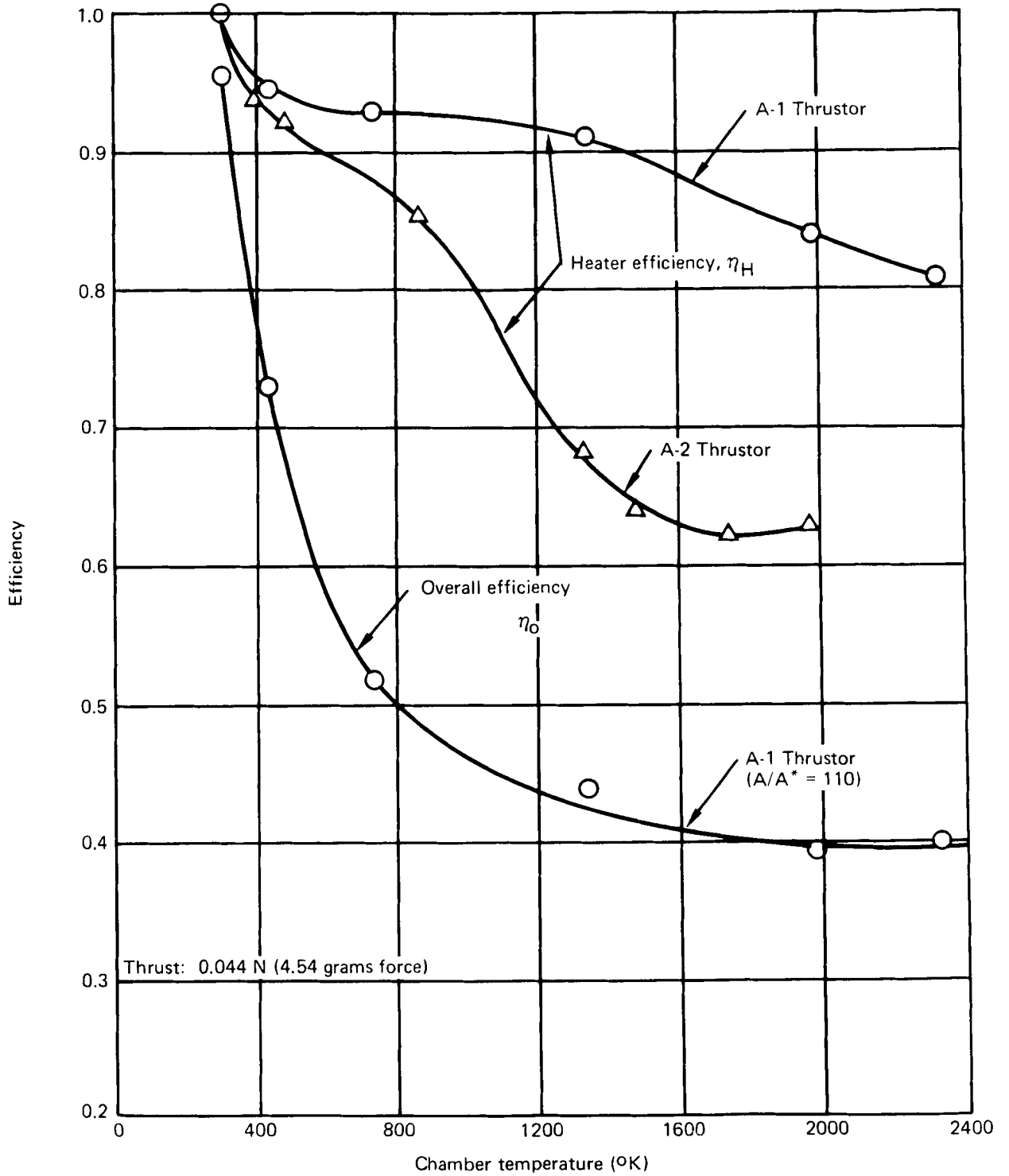
Figure 44. H_2 Efficiencies
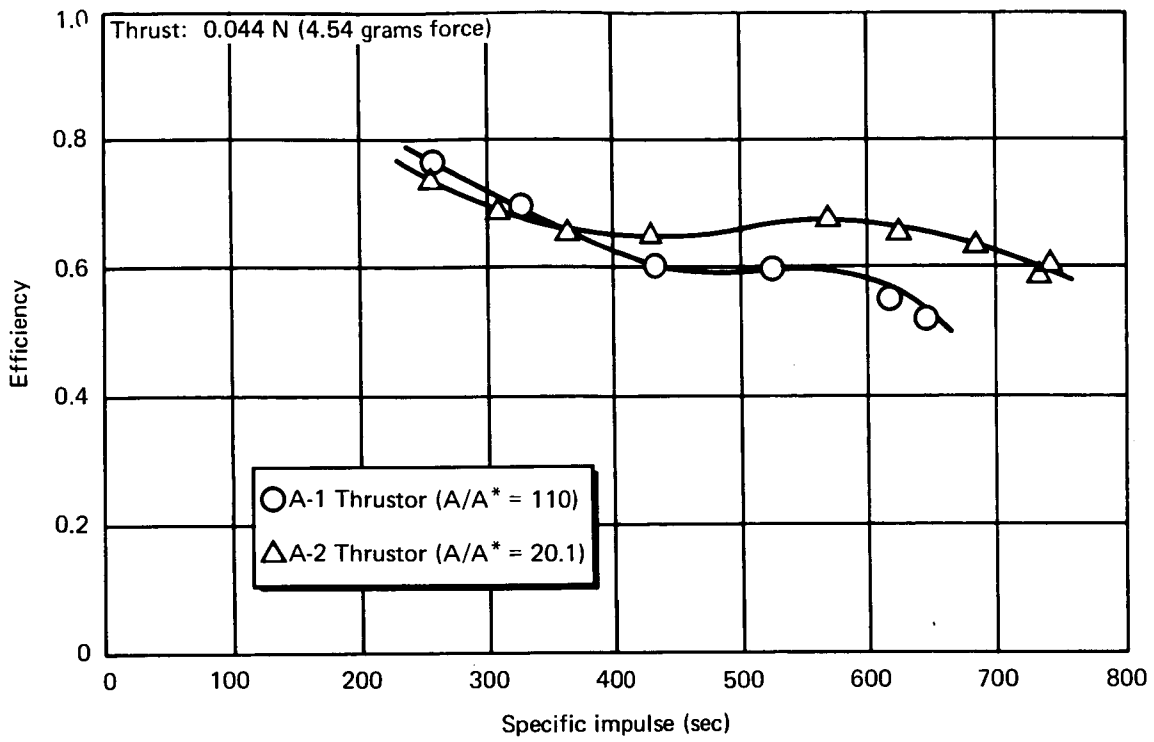
Figure 45. NH$_3$ Efficiencies
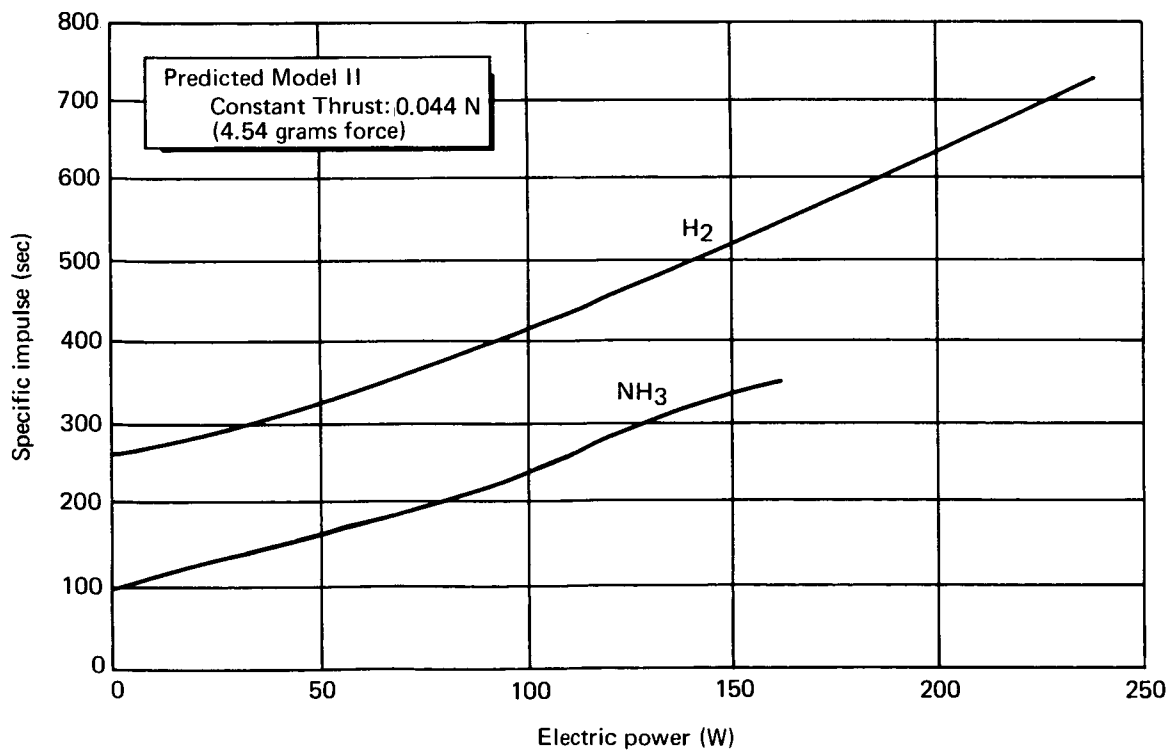
Figure 46. Overall Efficiency, H₂

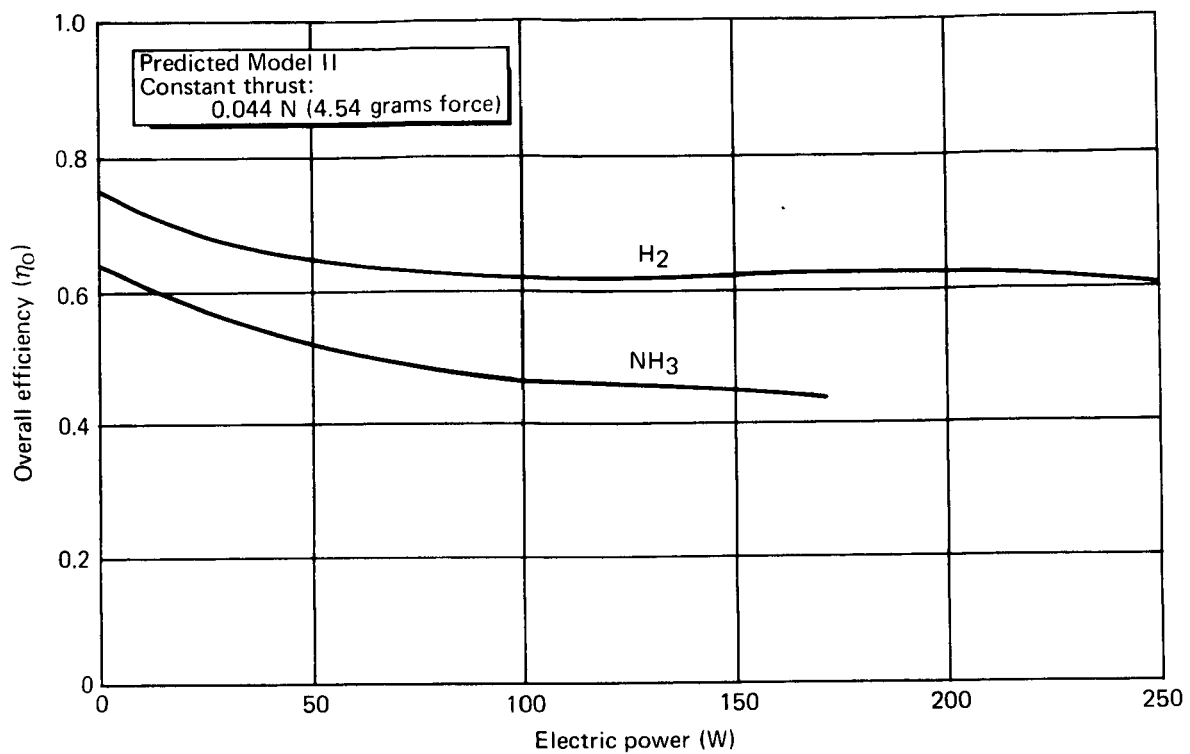**Figure 47. Specific Impulse vs. Electric Power**

Figure 48. Overall Total Power Efficiency vs. Electric Power

MODEL II DESIGN AND FABRICATION

Design

In the interest of improved performance with respect to long-duration tests, several improvements in the original Model I design were required. In addition, some changes were made for reasons of economy and ease of assembly. These changes resulted in the Model II configuration used in the 100-hour test. This is shown in fig. 49. The Model II thermal-expansion compensator was found to be inadequate. A force unbalance caused the inner element to elongate unnecessarily, as is described later. The compensator was redesigned. The resultant final Model II is shown in fig. 50, and its differences and improvements over Model I are described below.

Structure. — The inner and outer pressure cases of Model I required long fabrication times because of their geometry; therefore, cost was high. The change was made to straight-rolled and welded sheet tubes. Originally, 50% molybdenum/50% rhenium was selected because of its availability and low cost. Later, because the alloy exhibited joint cracking and because it was discovered that walled rhenium tubes could be made, pure rhenium was used. The inner case is made in two parts and brazed.

The inner-case stem--one of the parts subjected to lower temperatures-- is made of annealed 1/2% titanium-molybdenum, rather than rhenium, because this alloy offers better electrical conductivity and machinability compared to rhenium. This permitted the drilling of a 1.4-mm-diam central hole approximately 5 cm (for the vacuum-jacket vent).

The inner heater retains its former configuration; however, it is made from three simple parts instead of one because of difficulty in fabrication. These are electron-beam welded.

The case cover, previously cut from bar stock, is quickly stamped from sheet rhenium.

The outer heating element is tapered to allow greater clearance near the nozzle.

The housing mount has been changed in several ways. It is now drilled and tapped for rigid mounting (previously the thrustor mount was attached to the cover of the insulation housing). One end of the insulation housing is now integral with the housing mount. Also, the propellant line, previously connected with a threaded fitting, is now attached by brazing directly to the housing mount.
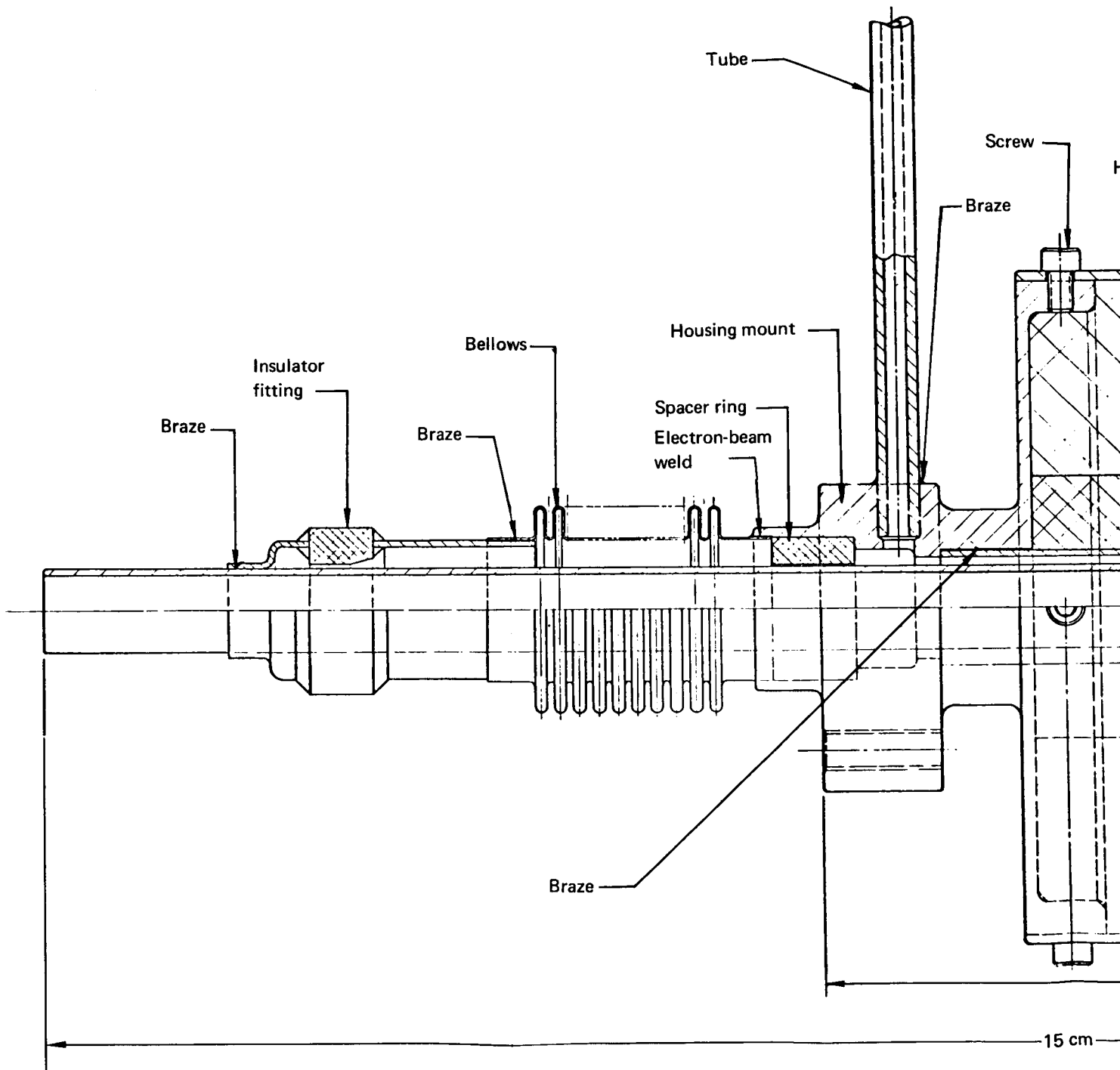
Figure 49. 10 mlb Resistojet Model II (Early Configuration)

Inner case

Radiation shield-inner

Electrical insulator

Outer case

Heater outer

Radiation shield-outer

Heater inner

Thermal insulation

Spacer pin

Strut connector

Nozzle

Thermal insulation

Case cover

Snap tube

Housing

Spot welding

Exit shield

5.23 cm

9 cm

Braze

28

29

26

20

24

21

23

Electron-beam weld

Electron-beam weld

Braze

10

11

19

18

TIG weld

Braze

22

27

13

8

1

15

7

4

25

9 c

15 cm

Spot
Weld

5.23 cm
Diam.

1 mm

Nozzle area rates
32:1
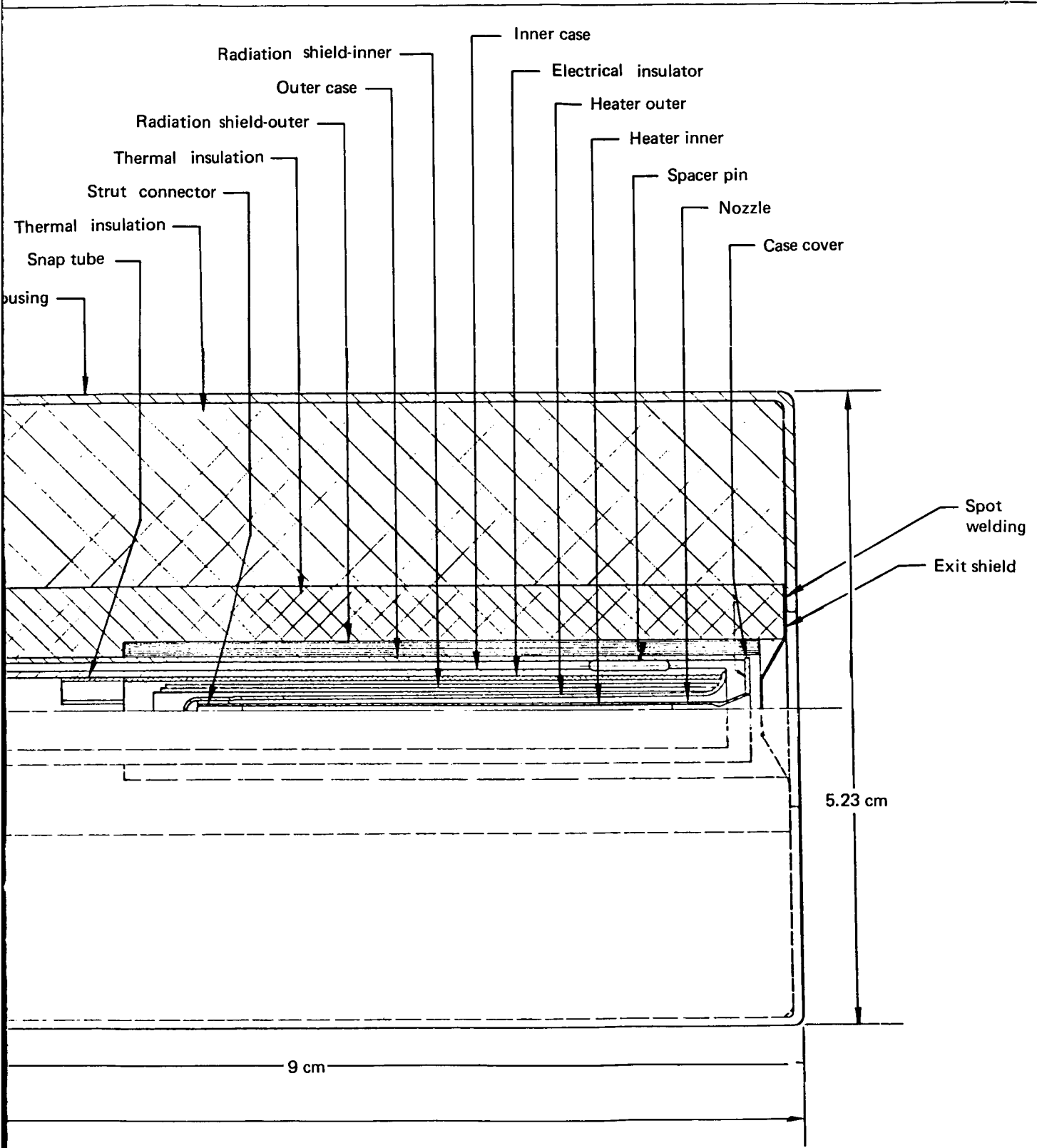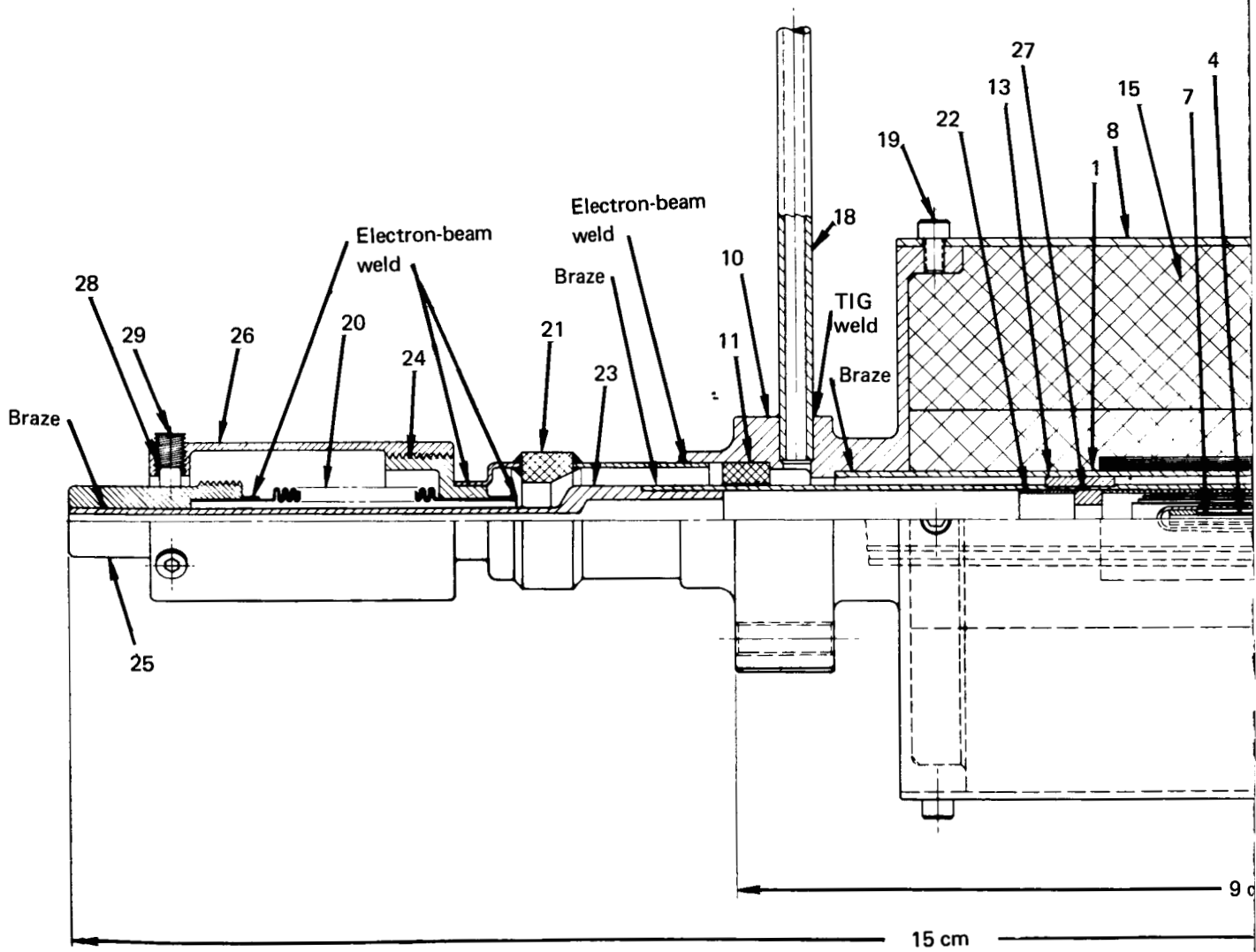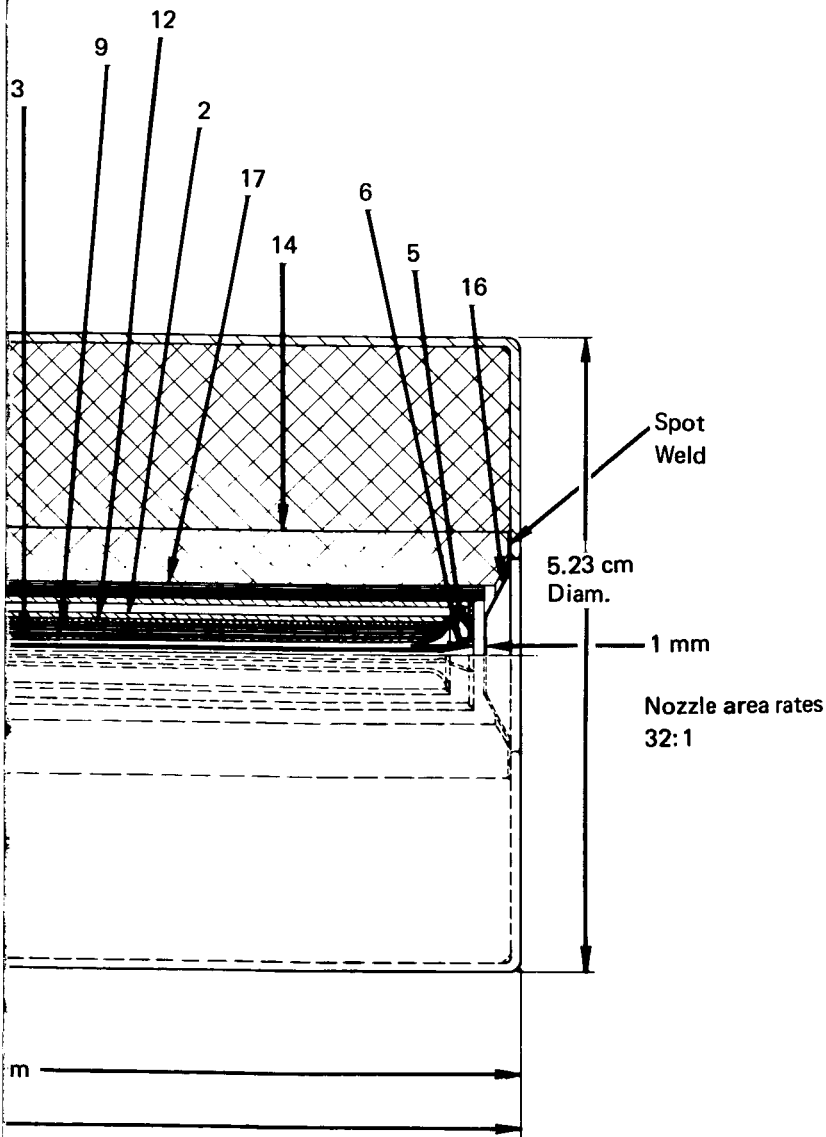
1	Outer case
2	Inner case
3	Heater outer
4	Heater inner
5	Case cover
6	Nozzle
7	Strut connector
8	Housing
9	Radiation shield inner
10	Housing mount
11	Spacer ring
12	Electrical insulator
13	Spacer
14	Thermal insulation
15	Thermal insulation
16	Exit shield
17	Radiation shield outer
18	Tube
19	Screw
20	Bellows
21	Insulator fitting
22	Snap tube
23	Inner case stem
24	Fitting
25	Fitting
26	Guard
27	Electrical insulator
28	Guide pin
29	Set screw

Figure 50. 10 mlb Resistojet Model II

The joints now all offer high-temperature capability, with the insulator-fitting braze (0.72 Ag-28 Cu) showing the lowest, at a melting point of 1053°K. Fig. 50 summarizes the joint types. The final joint is done by electron-beam welding so as not to lock in initial stresses between the inner and outer assemblies.

The guard is now made a radial guide, as shown. This was introduced because of the change in axial location of the electrical insulating pins described below.

Nozzle. — A conical nozzle was chosen of area ratio 32:1 with a 22° half angle. The geometric throat diameter was 0.465 mm with a meridianal wall curvature of 0.66 mm.

Electrical insulators. — A larger ceramic-metal insulator was used.

The spacer pins have been changed in geometry from a cylinder to a more substantial "bar." The spacer was moved 4.8 cm toward the propellant inlet to a cooler (500°K reduction) location.

A new part, a boron nitride washer, has been introduced between the snap tube and insulator to prevent the thermal shield from inadvertently shorting the outer heating element to the snap tube in the event of axial movement.

Thermal insulators. — The inner radiation shield was changed from tantalum to rhenium foil to avoid the long-term hydriding problem. The thickness desired, 0.013 mm (0.0005 in.) is less than that presently known to be available, 0.030 mm (0.0012 in.) in sheet rhenium. The number of turns of the shield was reduced to four to accommodate the available thickness. Only minor thermal losses (0.5%) are involved with this change but with a significant improvement in shield life.

During tests of the Model I thrustor, some destruction of the Min-K insulation occurred. A layer of higher-temperature insulation (Dyna-Quartz), which will withstand continuous temperatures of 1780°K has been added to protect the Min-K (table 28).

TABLE 28

HIGH-TEMPERATURE THERMAL INSULATION COMPARISON

Trade name*	Density g/cm^3	Thermal conductivity at 1273°K watts/cm$^{\circ}$K	Maximum continuous service temperature $^{\circ}$K ($^{\circ}$R)
Dyna-Quartz	0.16	1.60×10^{-3}	1780 (3210)
Min K-2000	0.26	0.46×10^{-3}	1255 (2260)
*John-Mansville			

In addition, several layers of radiation shielding have been added between the outer case and the Dyna-Quartz, to reduce thermal losses and protect the insulation. The insulation housing was enlarged from 3.5-cm to 5.0-cm diam to accommodate the extra insulation.

Thermal Expansion Compensator. — The purpose of the compensator is to allow the inner heating element to expand thermally in the axial direction relative to its external parts, with only minor stresses induced.

The axial growth of the inner assembly relative to the outer is permitted by the bellows. The physical characteristics (that is, spring constant, k, and effective area, A) of the bellows are selected so that the spring force term, (k · δ), acting against the net thermal expansion, δ, is compensated by the integrated pressure-area, $\int pda$, or "piston" term at the design condition. The latter term in this case can be closely represented by P_{supply} · A. Hence, eq. (35).

$$k \cdot \delta \simeq P_{supply} \cdot A \qquad (35)$$

Table 29 shows the approximate level of the forces and thermal expansions in the earlier two models as compared with the final design. Note that the level of forces has been greatly reduced. The net load is thus relatively insensitive to part tolerances.

The force levels of Model II (fig. 51) have been reduced one order of magnitude (by the significant reduction in bellows effective area) and are but one-half of those for Model I. The thermally induced compression load without any compensating pressure balancing (for example, a high-temperature no-flow case) is now less than one-fifth of the load computed to buckle the inner column at design temperature.

The exact value of the net force is unimportant because its magnitude is small. A minor thermal creep of the inner element would ultimately remove all loads at design. For the tabulated value of imbalance of 0.8 N this creep calculates to be approximately 0.04 mm.

In its final configuration, the bellows has an ID of 3.7 mm (nominal). Adequate clearance is thus provided as compared to the OD of the stem of 2.5 mm, and any possibility of binding is remote.

Fabrication

The first thrustor (Serial No. B-1) was assembled using the molybdenum-rhenium alloy tubes. This required two dissimilar metal weld joints to rhenium. Sample pieces of this alloy tubing were purchased and welded to pure rhenium to test the proposed design. The sample welding was successful (leak tight), and parts were purchased. During assembly of the actual engines,

TABLE 29

EXPANSION COMPENSATOR COMPARISONS

| Item	Thrustor		
	Model I	Model II	Model II
Bellows spring constant, N/cm (lbf/in.)	290 (164)	403 (228)	212 (120)
Bellows effective area, cm^2 ($in.^2$)	0.504 (0.078)	1.36 (0.210)	0.194 (0.030)
Net thermal expansion, mm (in.)	0.407 (0.016)	0.305 (0.012)	0.28 (0.011)
Thrustor supply pressure, N/m^2 (psia)	3.03×10^5 (44)	3.44×10^5 (50)	3.44×10^5 (50)
Bellows spring force at design, N (lbf)	11.7 (2.62)	12.3 (2.74)	5.92 (1.32)
Bellows pressure force at design, N (lbf)	15.4 (3.43)	47.1 (10.50)	6.7 (1.50)
Net tension on heating element at design, N (lbf)	3.63 (0.81)	34.8 (7.76)	0.81 (0.18)
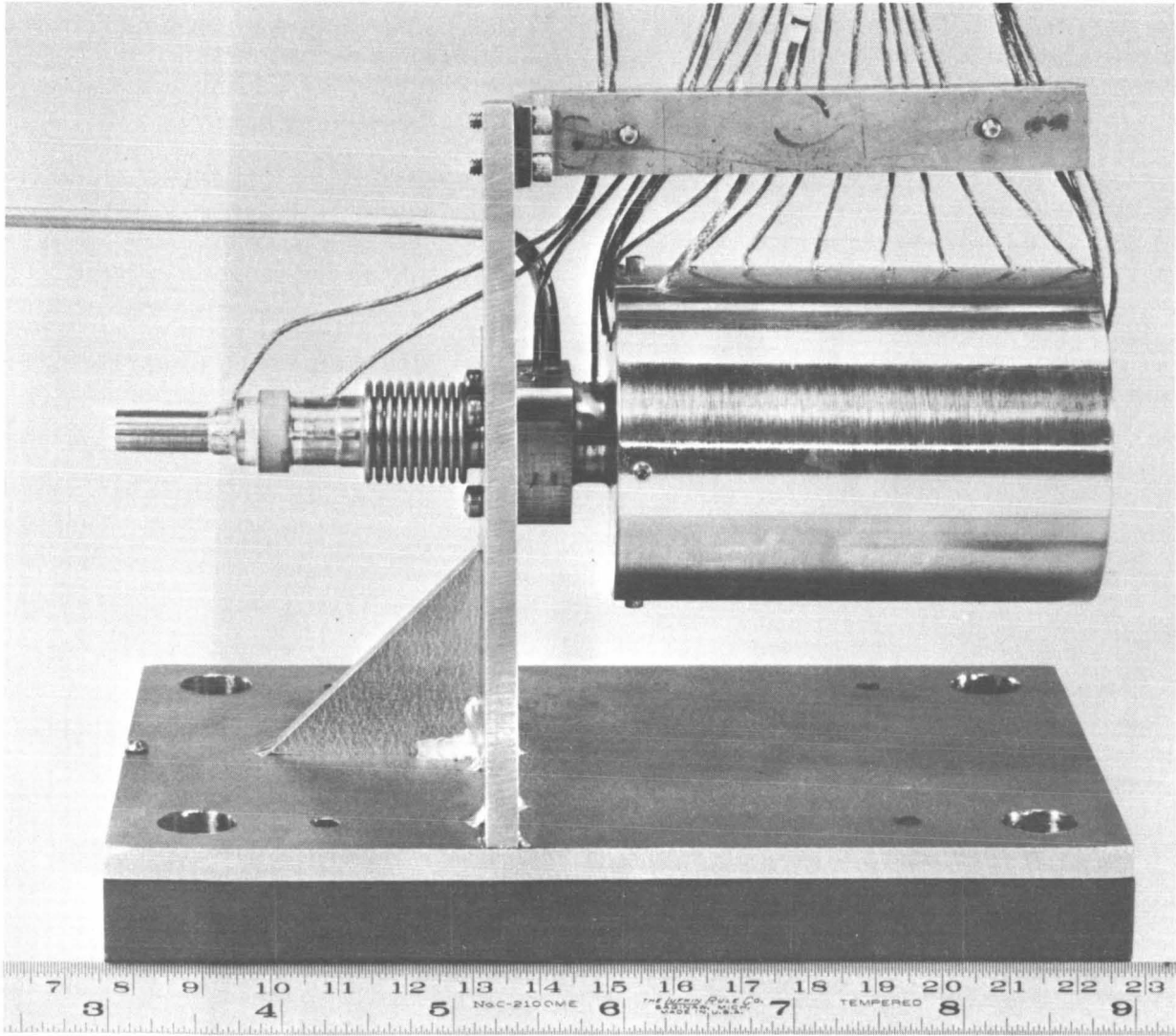
Figure 51. Model II-B2 Resistojet Instrumented for 100 Hour Test

however, the weld joints exhibited slight cracking. Later, this was found to have been caused by the formation of brittle intermetallics, compounds Mo_2Re_3 and Re_4Mo, (σ and X phase, respectively) in the weld joints.

When the change to molybdenum-rhenium tubes was originally made, pure rhenium tubes were not readily available. However, when the welding problem was encountered, it was discovered that the same tubes made of pure rhenium could be supplied and that this was clearly a superior technical choice. This change was made and the new material quickly supplied by Cleveland Refractory Metals (a division of Chase Brass and Copper Company).

When the rhenium tubes arrived, the B-2 thrustor was quickly assembled and made ready for test (fig. 51). Some changes were made in assembly procedure as compared to the Model I. The bellows is electron-beam welded to the housing mount, and the outer case is gold brazed to housing mount. The gold-braze has a temperature capability of $2010^{\circ}K$.

The B-2 thrustor is shown instrumented and attached to its dynamometer mounting stand in fig. 51.

MODEL II TESTS

Testing of the Model II thrustor was begun on August 31, 1967. Power was applied in approximately 1-hour intervals, reaching design conditions after 5 hours. The partial power-performance data gathered during startup are shown in figs. 52 through 54.

100-Hour Test

The engine operated continuously for 100 hours at specific impulses well above 700 sec. Test data are shown in figs. 55 and 56 and in table 30.

After the 100-hour test, a 20-hour test on NH_3 was attempted. Abnormal electrical characteristics, indicating a short, forced the NH_3 tests to be terminated. The instrumentation was checked and calibrated, the data were partially reduced, and the unit was partially disassembled. This examination has resulted in the following conclusions:

(1) The unit had been operated at an estimated gas temperature of $2600^\circ K$ (as compared to the design of $2350^\circ K$) for approximately half the test duration. Post-test calibrations showed that a supposed dynamometer zero shift had not occurred.

(2) A severe misbalance in the thermal-expansion compensator caused the inner element to creep thermally (to elongate).

(3) The permanently elongated 0.863-cm (~0.34-in.) inner element caused locked-in high compressive loads because the bellows were not allowed to return to the normal position. These loads, coupled with a fast shutdown from a greater-than-design specific-impulse condition, caused the inner element to buckle.

No such failures were experienced with the Model I design after many hours at a comparable temperature and many shutdowns. A comparative analysis was made of the Model I and Model II (100-hour unit). See table 29. The final thermal-expansion compensator configuration for the Model II shown in fig. 50. This configuration of the Model II was used for all subsequent testing.
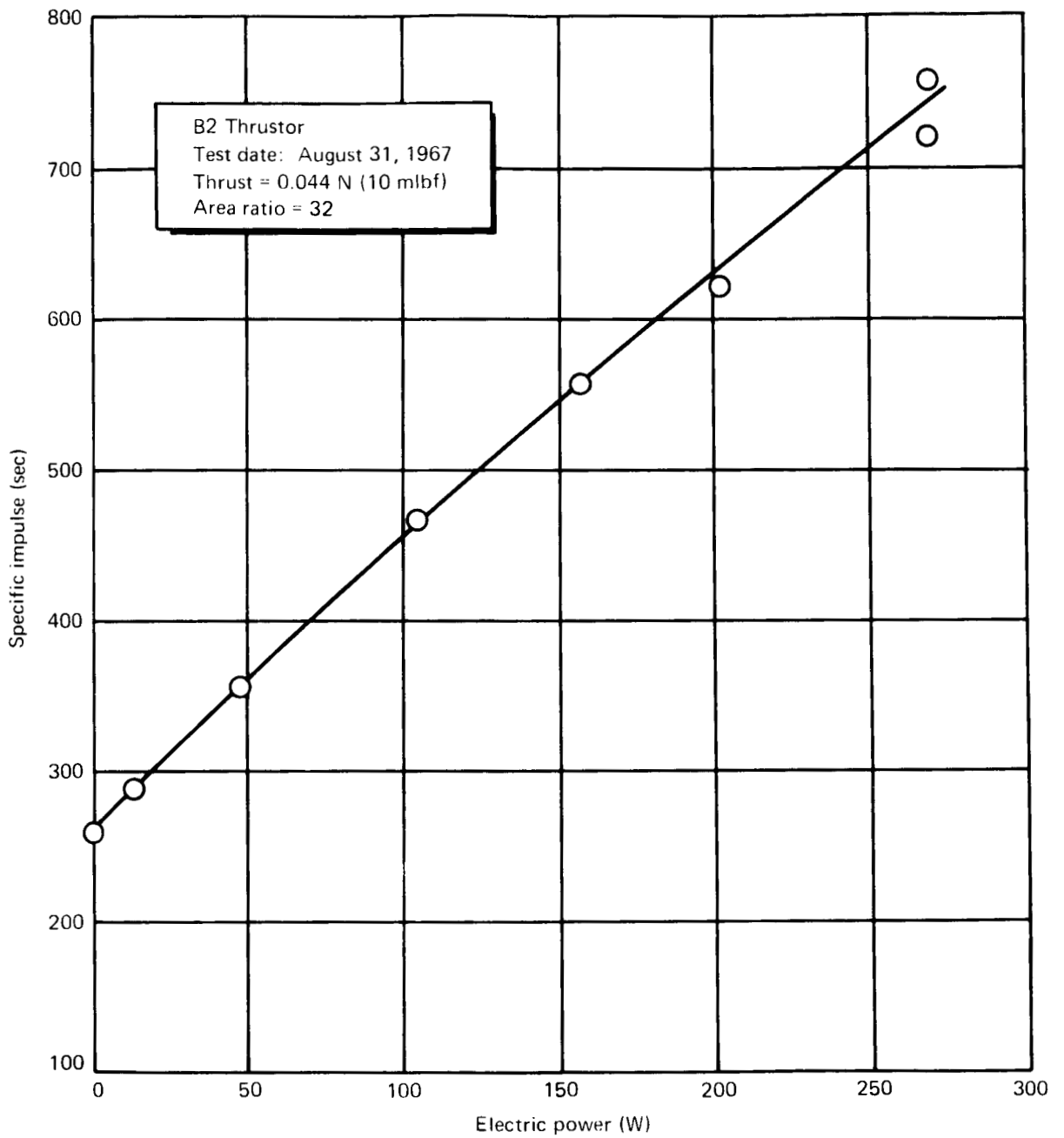
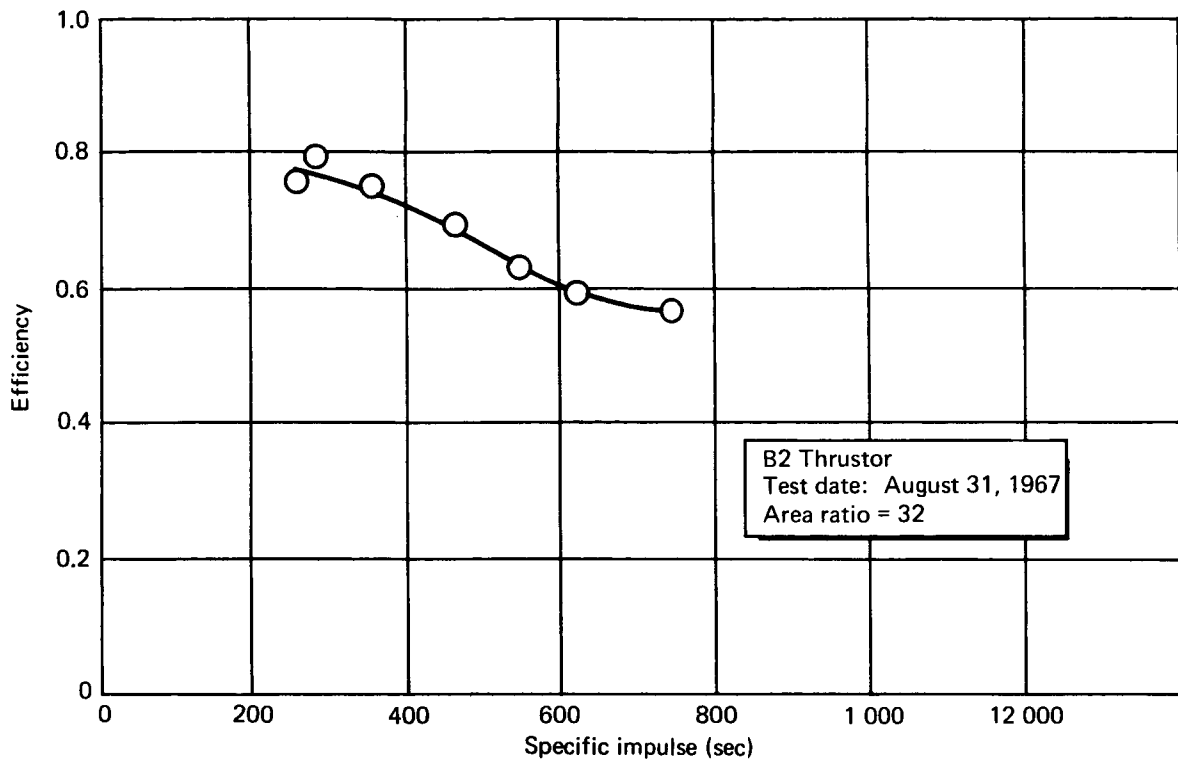Figure 52. Model II H_2 Resistojet Specific Impulse vs. Electric Power

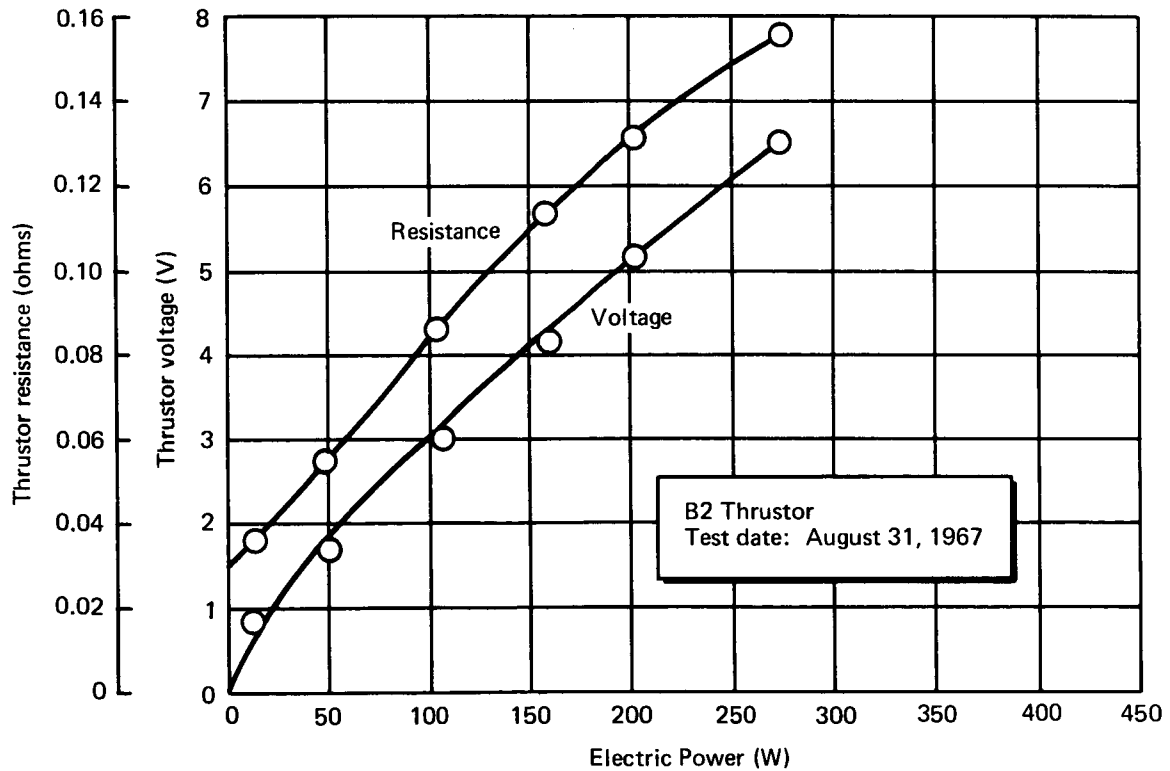Figure 53. Model II H$_2$ Resistojet Overall Total Power Efficiency

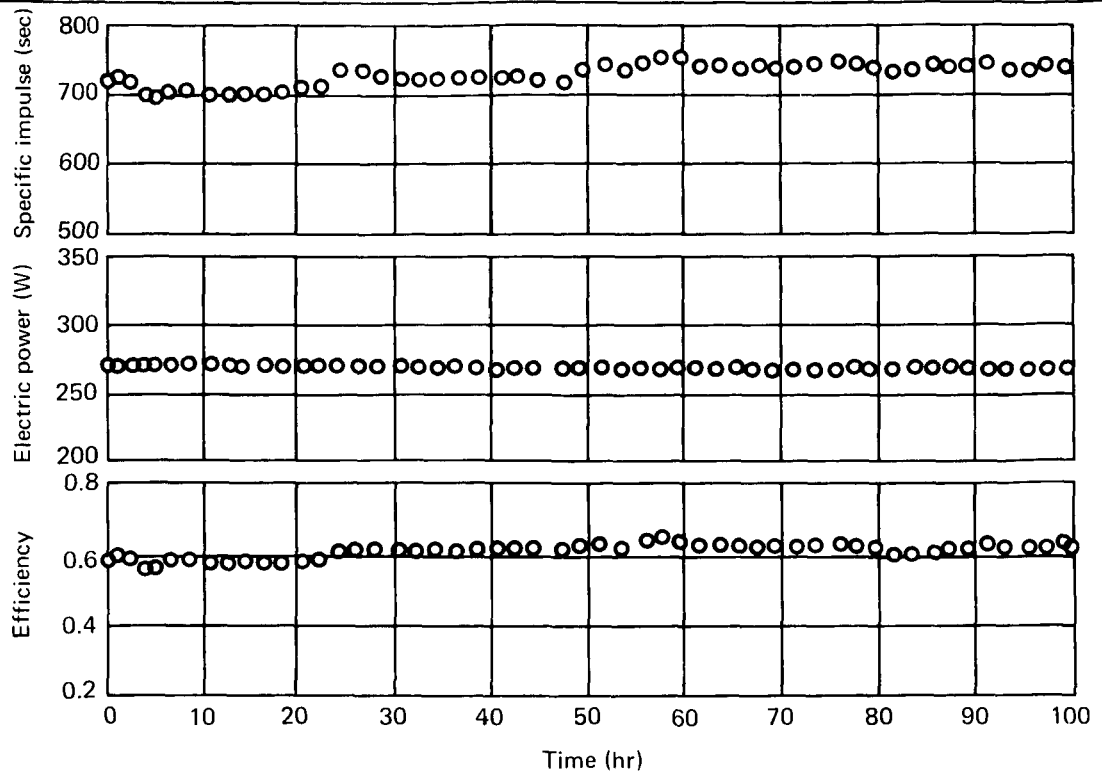Figure 54. Model II H$_2$ Resistojet Electrical Characteristics

Figure 55. Thrustor Performance --Model II-B2 Resistojet 100-Hour Test (H_2)
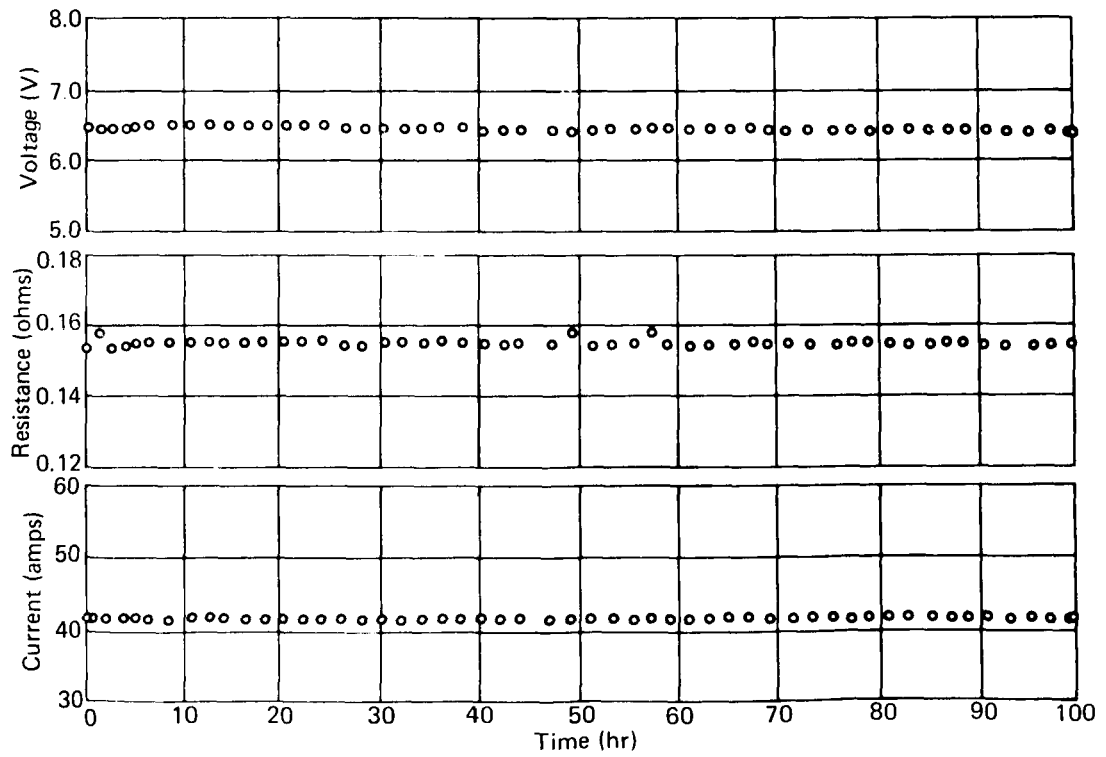
Figure 56. Electrical Performance -- Model II-B2 Resistojet 100-Hour Test (H_2)

TABLE 30

B-2 THRUSTOR PERFORMANCE SUMMARY

Item	Value
Data point no.	208
Test date	September 2, 1967
Propellant	H_2
Electric power, watts[*]	270.3
Voltage, volts	6.450
Current, A	41.9
Thrust, grams force	4.75
Mass flow, g/sec	0.0063
Specific impulse, sec[*]	754
Metering pressure, kN/m^2 (psia)	354 (51.4)
Metering temperature, $^\circ C$	31.75
Inlet pressure, kN/m^2 (psia)	347 (50.4)
Inlet gas temperature, $^\circ C$	30.24
Test cell pressure, μmHg	10
Maximum temperature, outer shell, $^\circ C$	396
Thrustor resistance, ohms[*]	0.1577
Estimated gas temperature, $^\circ K$[*]	2580
Thrustor chamber pressure, kN/m^2 (psia)[*]	207 (30.0)
Electric power efficiency, η_o[*]	0.637
Overall efficiency, η_o[*]	0.579

[*]Calculated.

Steady-State Performance with Varying Electric Power

The thrustors have been calibrated over the range of electric power from zero-to-design in two modes of operation: constant thrust and constant-supply pressure. Both types of data are valuable. The constant (design) thrust data are useful for selecting the design point. The control mode for MORL employs a constant-supply pressure. The constant-supply pressure data are useful primarily for determining the operational thrust variation between cold flow and design conditions. The design-point data for both sets are the same.

It was originally believed that these two modes were essentially the same. On a perfect gas basis, constant chamber pressure implies constant thrust independent of chamber temperature. However, a real-gas effect, the pressure drop from inlet (supply) to nozzle chamber, varies substantially from cold flow to design conditions, because of a transition from turbulent to laminar conditions, respectively.

Constant-thrust characteristics. — Figs. 57 and 58 show the constant-thrust mode characteristics for H_2 and NH_3, respectively. The associated supply pressure varied from (34.4 to 51 psia) and (27.7 to 42.8 psia), respectively, from zero-to-design electric power. Note that the efficiencies cited are total power ones. That is, the thrustor is charged with both the initial power in the gas and the electric power. On the basis of overall electric power efficiency, η^* (electric power only charged) at the maximum points these were 0.62 and 0.45 for H_2 and NH_3, respectively.

The throat size for the Model II thrustor used was 0.472 mm. The cell pressure at the maximum specific impulse conditions were 12.5 and 9 μm Hg, respectively.

Constant-pressure characteristics. — Fig. 59 shows the steady-state performance at a constant-supply pressure of 3.44 x 10^5 N/m^2 (50 psia) for H_2. The useful information over that of fig. 57 is that the cold-flow thrust in this mode is 0.072 N compared to 0.044 N at design or 55% higher.

The corresponding thrusts for NH_3 at 2.82 x 10^5 N/m^2 (41 psia) supply pressure again gives a cold-flow thrust of 0.072 N compared to 0.044 N at design.

Model II Design Verification Tests (DVT)

The Model II resistojet, S/N B-2, (shown in fig. 60) was assembled as defined by fig. 50. This thrustor met all the objectives of the Design Verification Tests (DVT). The unit was fired to a thrust of 0.044 N (10 mlbf) and specific impulse of >680 sec on H_2 and >320 sec on NH_3 propellant for 20 hours each. It was subsequently cycled on and off from the >680 sec condition on a 67% duty cycle for 24 hours.
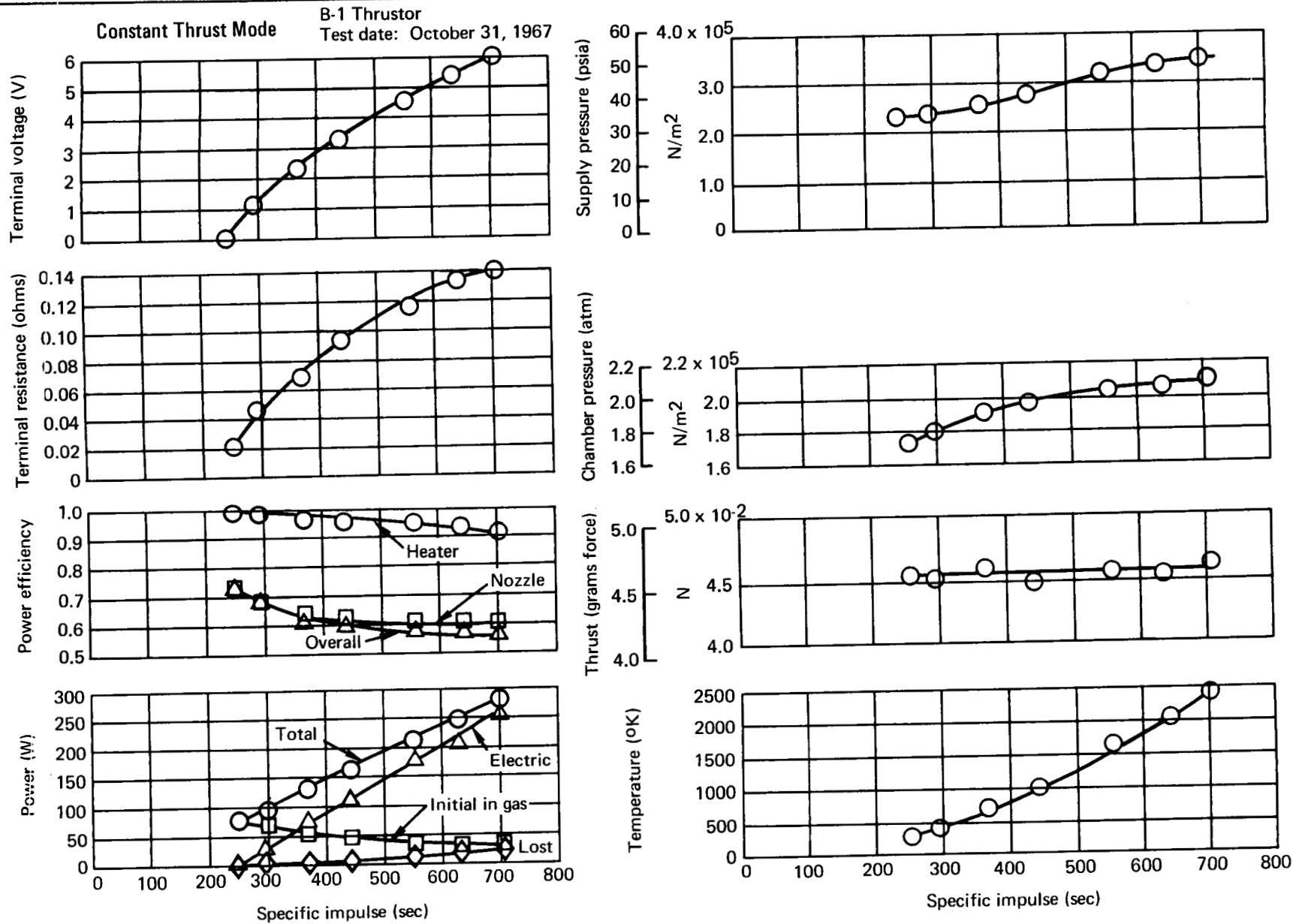
Figure 57. Model II Steady-State Performance Characteristics (H$_2$)

Figure 58. Model II Steady-State Performance Characteristics (NH3)

Constant Supply Pressure Mode

$P_s = 3.44 \times 10^5$ N/m^2 (50 psia)

B-2 Thrustor
Test date: November 22, 1967
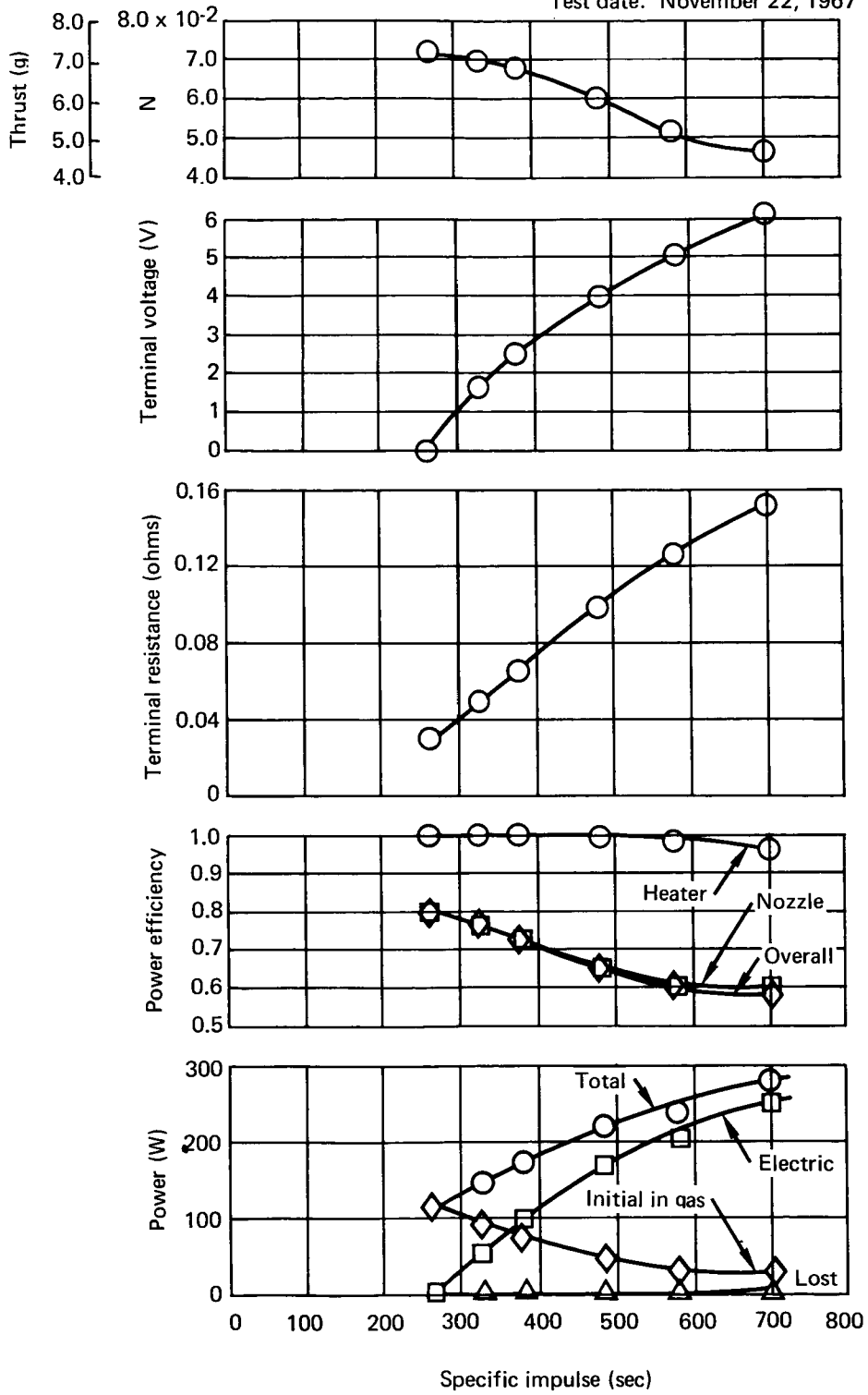
Figure 59. Model II Steady-State Performance Characteristics (H_2)

113
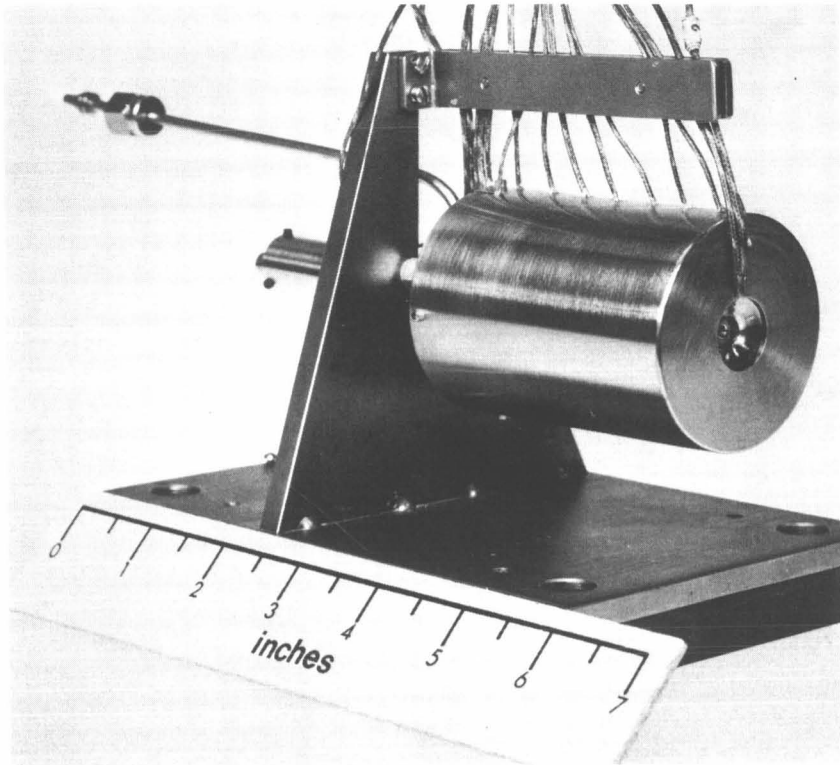
Figure 60. Model II - B2 Resistojet After Design Verification Tests

Steady design operation. — The steady-state performance data gathered during each of the phases of DVT are summarized in table 31 for H_2 and table 32 for NH_3. Data were taken at least every 2 hours.

The thrust data presented are conservative. These tests revealed that cell pressure, while 100 times lower than that required for inviscid full expansion of the nozzle, nevertheless had a pronounced effect on thrust performance.

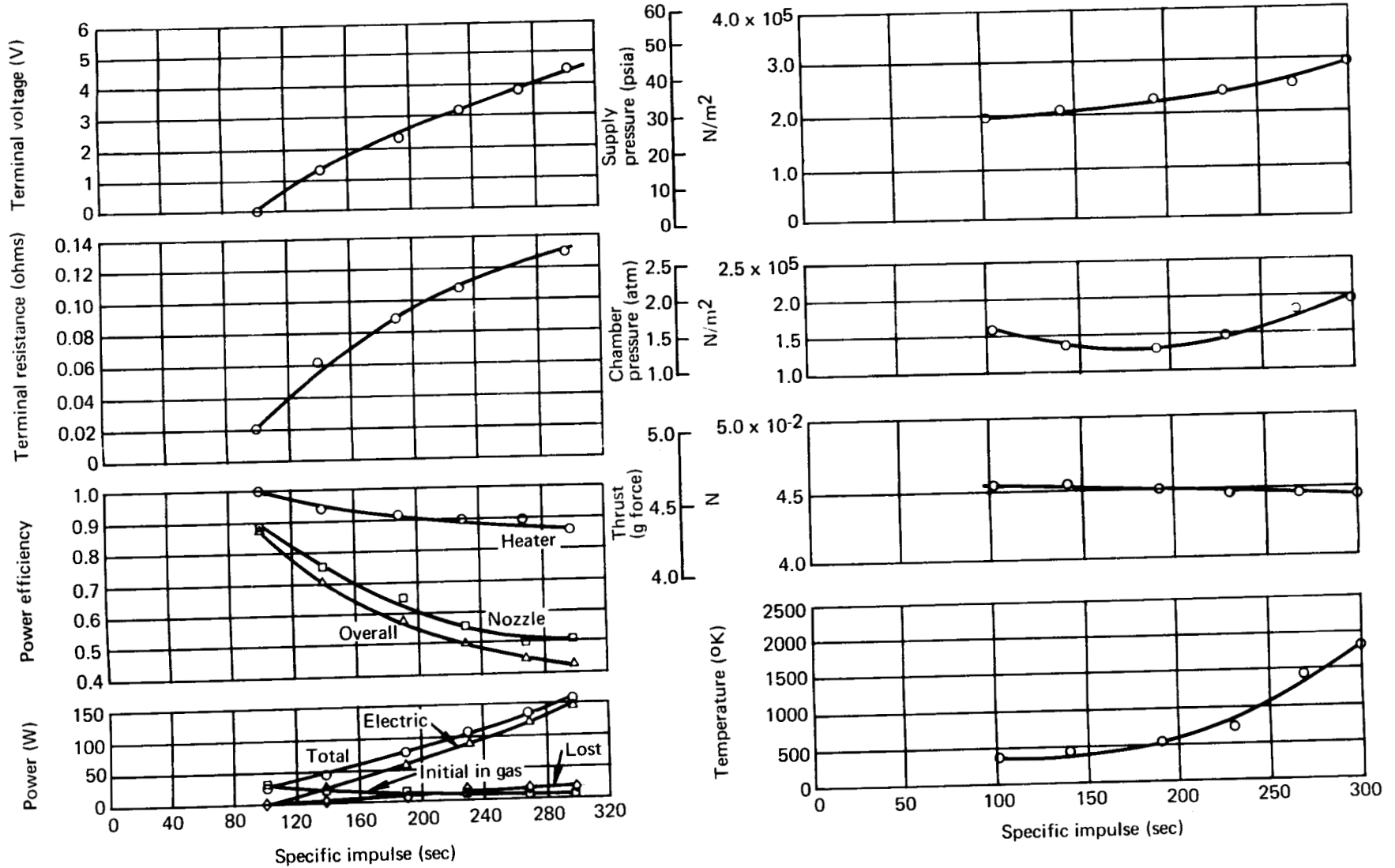Cyclic performance. — The objective of the cyclic test was to demonstrate the ability of the thrustors to withstand sudden starting and stopping. In these initial tests, no special effort was made for high-response valves or automatic timing. All controlling was done manually. The propellant solenoid was energized approximately 0.7 sec prior to application of electric power. As the heater glow extinguished following power shutoff, the propellant solenoid was de-energized. Extinction was observed by a radiation pyrometer focused upon the rear dome of the outer heating element.

Hydrogen cycling: The DVT requirement was 21 hours of cycling on H_2. This consisted of 14 cycles of 1 hour on and 1/2 hour off. Three additional cycles were later performed. (Total hours--steady-state and cycling on H_2 for the DVT thrustor prior to life test--are 49.)

Item					
Elapsed time, hours	1	3	4	5	7
Data point number	260	261	262	263	264
Thrust, N	0.0422	0.0475	0.0472	0.0467	0
Thrust, grams	4.31	4.85	4.82	4.77	4
Mass flow, grams/sec	0.00621	0.00691	0.00681	0.00678	0
Electric power, watts	237	264	264	264	246
Electric power, kN/m^2	345	345	346	346	346
Inlet pressure, psia	(50.1)	(50.1)	(50.2)	(50.2)	(50
Specific impulse, sec	694	701	708	703	695
Voltage, volts	5.949	6.304	6.300	6.307	6
Current, amperes	39.9	41.9	41.9	41.9	40
Inlet gas temperature, $^\circ C$	23.7	24.0	23.8	23.8	23
Initial gas power, watts	26.0	29.2	28.5	28.4	28
Total power, watts	263	293	293	292	275
Overall power efficiency, η_o	0.606	0.531	0.535	0.552	0
Overall electric efficiency, η_o^*	0.672	0.589	0.592	0.610	0

*B-2 Thrustor; November 23-24, 1967

ION TESTS (H_2, 20 HOURS STEADY-STATE)[*]

	Value						
	9	11	13	15	17	19	20
	265	266	267	268	269	270	271
.0472	0.0470	0.0472	0.0467	0.0467	0.0466	0.0465	0.0465
.81	4.80	4.81	4.77	4.77	4.76	4.75	4.75
.00691	0.00691	0.00691	0.00683	0.00683	0.0068	0.0068	0.0068
	246	247	246	246	247	246	245
	346	346	346	346	346	346	346
.3)	(50.3)	(50.3)	(50.2)	(50.2)	(50.2)	(50.3)	(50.3)
	695	695	698	698	700	699	699
.069	6.069	6.072	6.071	6.070	6.079	6.071	6.072
.5	40.5	40.7	40.5	40.5	40.5	40.4	40.4
.9	23.7	23.5	23.4	23.6	23.8	23.9	23.6
.9	28.9	28.9	28.6	28.6	28.6	28.7	28.4
	275	276	275	275	276	275	274
.584	0.585	0.583	0.592	0.582	0.580	0.582	0.606
.652	0.653	0.651	0.650	0.650	0.648	0.650	0.650

FOLDOUT FRAME

Item				
Elapsed time, hours	1	3	5	7
Data point number	279	280	281	282
Thrust, grams	4.60	4.58	4.58	4.58
Mass flow, grams/sec	0.0141	0.0142	0.0143	0.0143
Electric power, watts	160	159	158	157
Electric power, kN/m^2	296	296	296	296
Inlet pressure, psia	(43)	(43)	(43)	(43)
Specific impulse, sec	327	322	320	320
Voltage, volts	4.860	4.818	4.810	4.790
Current, amperes	32.9	32.9	32.9	32.9
Inlet gas temperature, $^{\circ}C$	24.1	23.6	23.4	23.7
Initial gas power, watts	8.1	8.1	8.2	8.2
Total power, watts	168	167	166	165
Overall power efficiency, η_o	0.431	0.424	0.425	0.427
Overall electric efficiency, η_o^*	0.452	0.445	0.446	0.448

[*]B-2 Thrustor; November 25-26, 1967

FOLDOUT FRAME 1

Value						
9	11	13	15	17	19	20
83	284	285	286	287	288	289
4. 60	4. 60	4. 56	4. 54	4. 57	4. 55	4. 54
0. 0142	0. 0142	0. 0142	0. 0142	0. 0142	0. 0141	0. 0141
58	158	157	157	159	159	159
95	295	295	294	296	296	295
(42. 8)	(42. 8)	(42. 8)	(42. 7)	(43)	(43)	(42. 9)
24	324	321	320	322	322	322
4. 790	4. 800	4. 784	4. 779	4. 819	4. 839	4. 844
32. 9	32. 9	32. 9	32. 9	32. 9	32. 9	32. 9
24. 0	23. 9	23. 9	23. 3	23. 4	23. 5	23. 6
8. 2	8. 2	8. 2	8. 2	8. 2	8. 1	8. 1
66	166	165	165	167	167	167
0. 433	0. 433	0. 427	0. 424	0. 424	0. 423	0. 421
0. 453	0. 453	0. 448	0. 445	0. 445	0. 443	0. 442

Table 33 summarizes the performance for each cycle approximately 10 min. before shutdown. Figs. 61 through 63 show the transient characteristics during a typical cycle. Note, in fig. 59, that the time between power off and propellant off on shutdown for this cycle is about 2 sec. The relatively long time constant for pressure decay is primarily a result of the large volume of the laboratory system rather than the volume of the thrustor itself.

Thrust response, primarily a function of the system volume, was approximately 2 sec. The time to reach design temperature, as evidenced by resistance, is approximately 400 sec. Note that, in this case, no holding power was supplied during the "off" condition.

Ammonia cycling: The cycling capabilities of the thrustor were demonstrated, as required, during DVT using H_2 as a propellant. However, to plan the duty cycle requirements for the life test, it was also necessary to obtain cycling data on NH_3. To obtain these transient characteristics, three cycles were made. The "on" condition during cycling corresponded to those already noted in table 32. Figs. 64 and 65 show the transient performance, off and on. The total hours, steady-state and cycling on NH_3, were 28.

The time to reach thermal equilibrium, as evidenced by reaching design thrust and resistance, was approximately the same for both propellants, ~400 sec.

The cyclic control used here is adequate to demonstrate life as influenced by thermal cycling and sublimation on the forthcoming life tests. Thrustor data of the type here are needed in the future for system design where the Model II resistojet has (1) close-coupled high response valves, (2) automatic controls, and (3) thermal holding power supplied during nonthrusting period.

Influence of Cell Pressure on Observed Thrust

Phenomenon. — One of the established facts of continuum gas flow through a nozzle at high Reynolds number is that, when the expansion from the stagnation conditions results in a sonic velocity at the throat, no additional increase in mass flow rate can be established by decreasing the back pressure. Similarly, there can be no increase in thrust except for a relatively small pressure-exit area effect term. In effect, no signal can be transmitted upstream to influence the flow.

Recent investigations (refs. 11, 12, and 13) have shown that at low Reynolds numbers (high Knudsen numbers) the above facts are no longer true. The threshold of this effect and the effect itself are not clearly understood.

It was known that jets with thrusts in the micropound class are strongly influenced by back pressure in the test chamber, but little or none were expected at the (10-mlbf) level. The early single thrustor data came close to that predicted with cell pressures of ~5 μmHg.

117

Item						
Cycle	1	2	3	4	5	6
Data point number	296	297	298	299	300	301
Thrust, grams	4.54	4.57	4.53	4.53	4.53	4.52
Mass flow, grams/sec	0.00654	0.00660	0.00660	0.00660	0.00650	0.00650
Electric power, watts	237	236	237	236	236	239
Electric power, kN/m^2	230	340	340	340	340	340
Inlet pressure, psia	(49.3)	(49.3)	(49.3)	(49.4)	(49.3)	(49.4)
Specific impulse, sec	695	693	686	686	697	696
Voltage, volts	5.939	5.919	5.929	5.920	5.919	5.990
Current, amperes	39.9	39.9	39.9	39.9	39.9	39.9
Inlet gas temperature, $^{\circ}C$	24.1	24.1	23.3	23.3	23.0	23.4
Initial gas power, watts	27.4	27.6	27.6	27.6	27.1	27.2
Total power, watts	264	264	264	264	263	266
Overall power efficiency, η_o	0.574	0.577	0.565	0.566	0.577	0.568
Overall electric efficiency, $\eta_o{}^*$	0.640	0.645	0.631	0.631	0.643	0.633

NOTES:

(1)   B-2 Thrustor; November 27-29, 1967.

(2)   Cycle: 1 hr power on; 1/2 hr power off alternately.

(3)   Data point takes 10 min (approx) before shutdown.

(4)   Test cell pressure 12 μmHg thrustor on; 4 μmHg thrustor off.

TESTS (H$_2$, 21 HOURS, 66.7% DUTY CYCLE)

| Value							
7	8	9	10	11	12	13	14
302	303	306	307	308	309	310	311
4.51	4.52	4.52	4.53	4.50	4.50	4.50	4.50
0.00650	0.00650	0.00654	0.00654	0.00650	0.00651	0.0066	0.0065
237	236	237	238	237	236	237	239
340	340	340	340	340	340	340	340
(49.4)	(49.3)	(49.3)	(49.3)	(49.3)	(49.3)	(49.4)	(49.4)
694	696	691	692	692	691	682	687
5.936	5.910	5.929	5.955	5.930	5.916	5.949	5.990
39.9	39.9	39.9	39.9	39.9	39.9	39.9	39.9
23.2	23.2	23.6	23.4	23.5	23.6	23.6	23.4
27.1	27.1	27.3	27.3	27.2	27.3	27.2	27.3
264	263	264	265	264	263	265	266
0.570	0.575	0.569	0.569	0.571	0.568	0.557	0.562
0.635	0.641	0.635	0.634	0.633	0.631	0.621	0.622
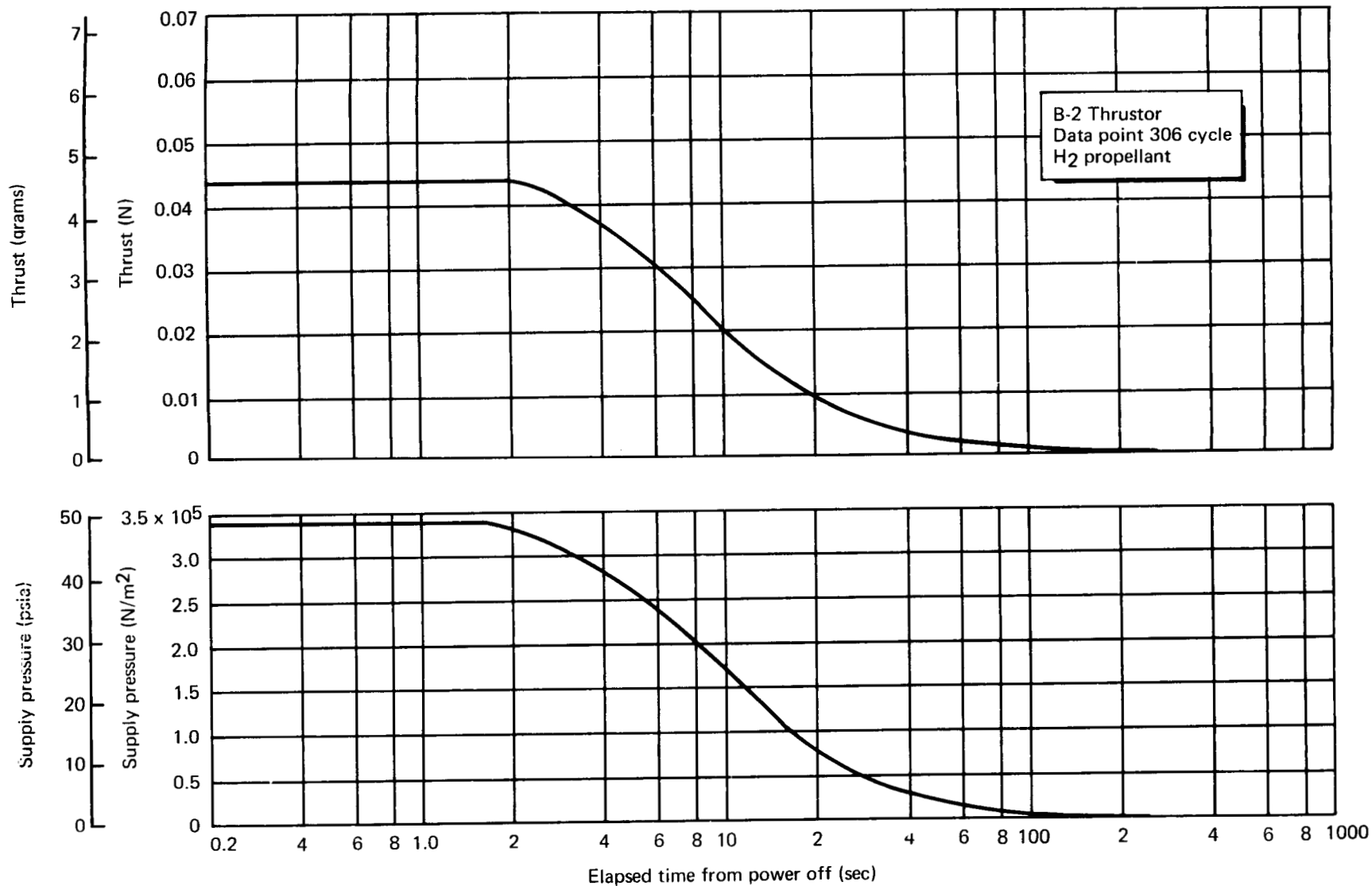
Figure 61. Transient Performance -- Model II Resistojet
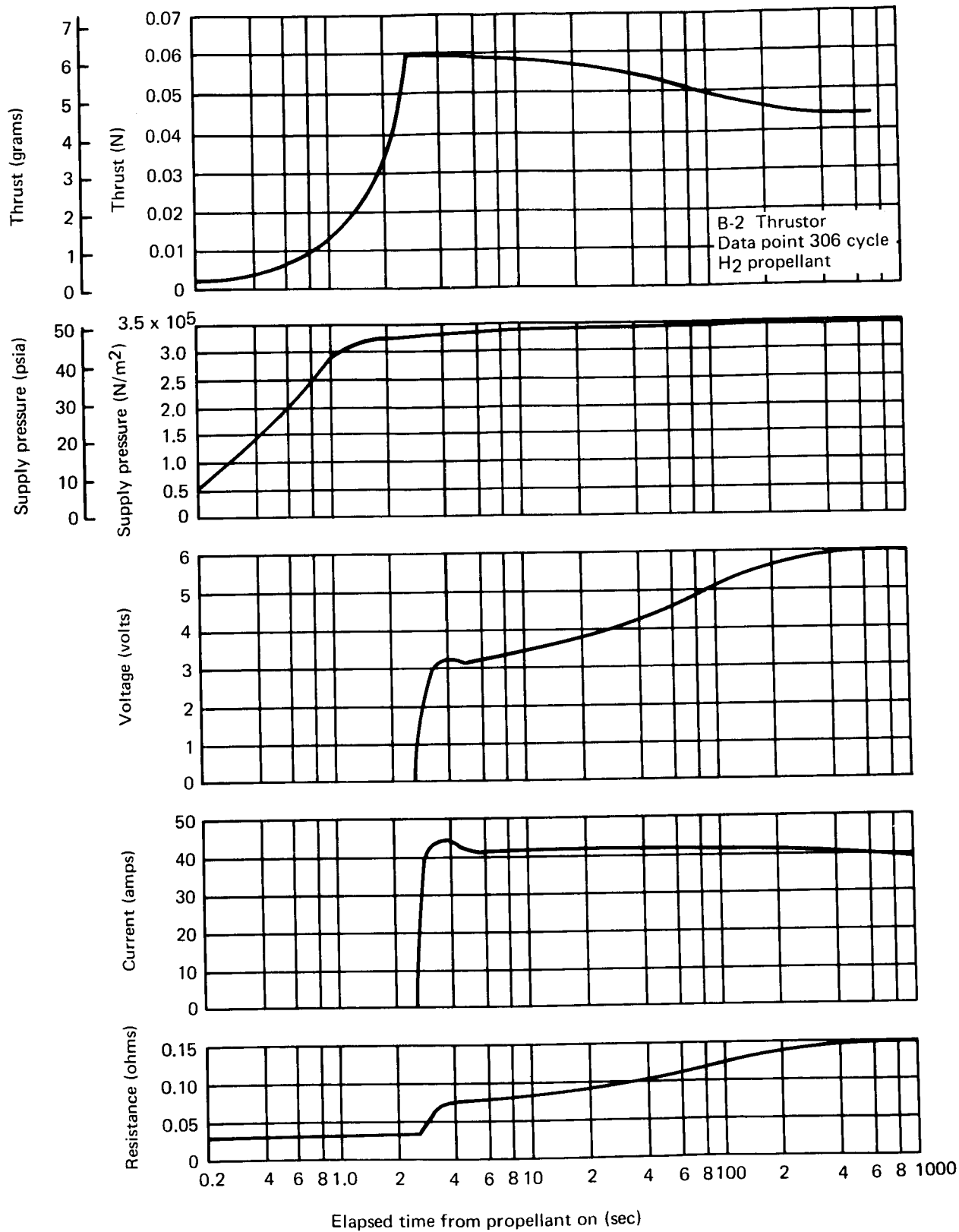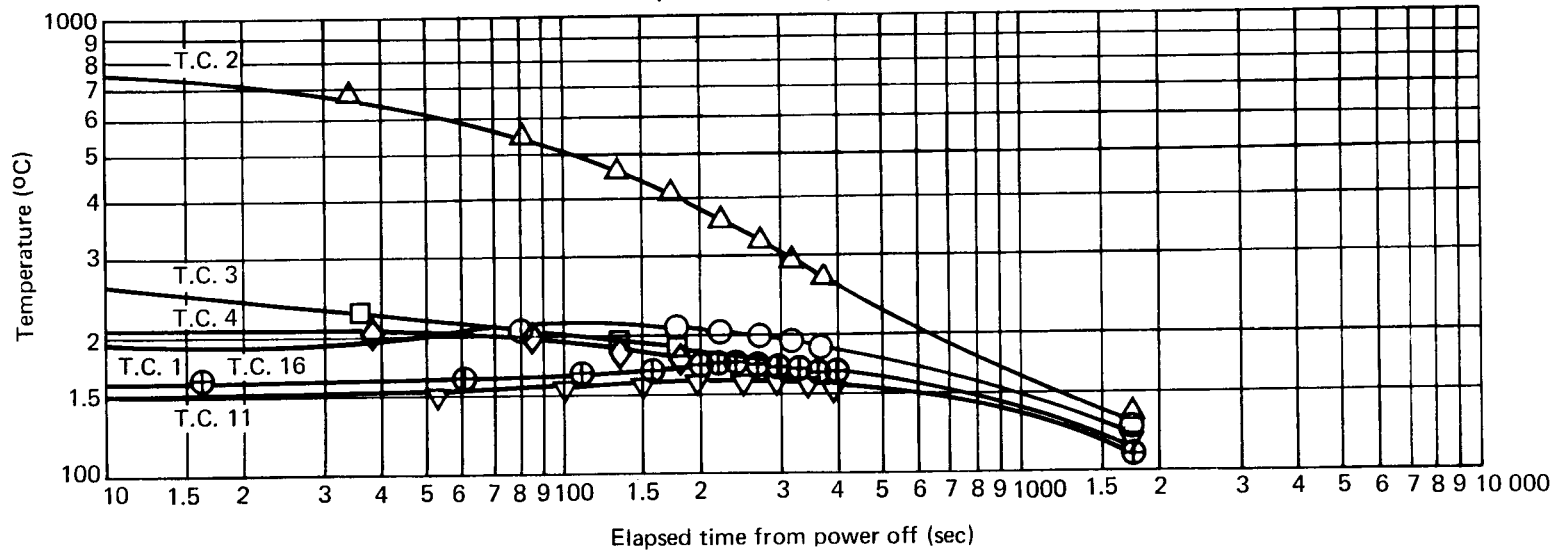
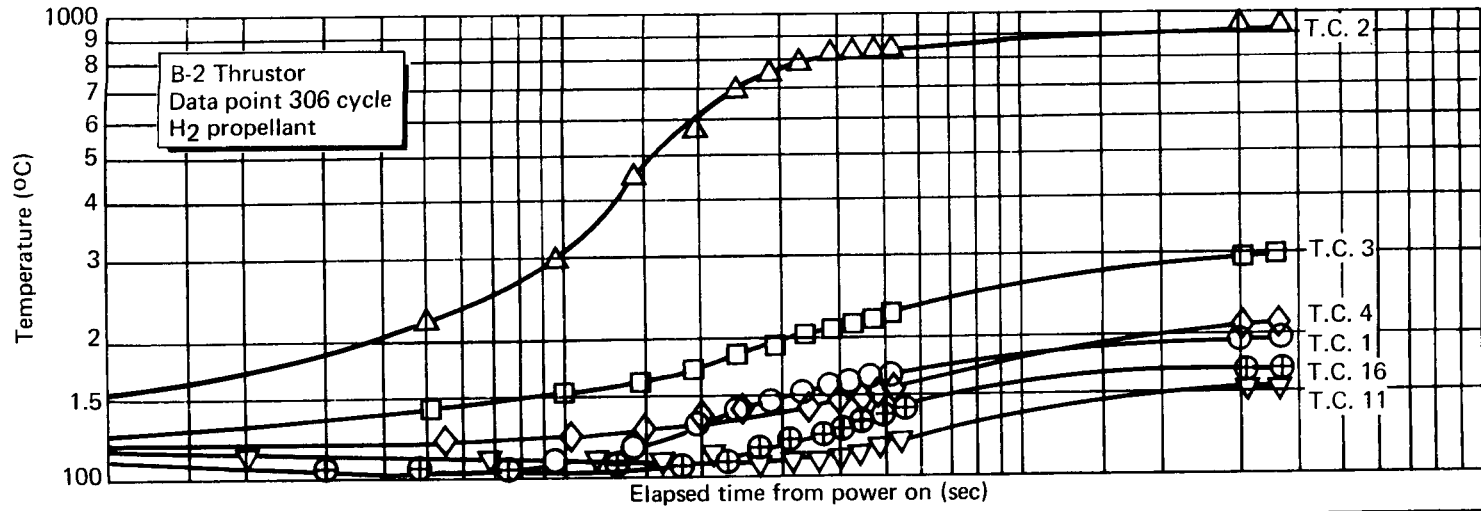Figure 62. Transient Performance -- Model II Resistojet

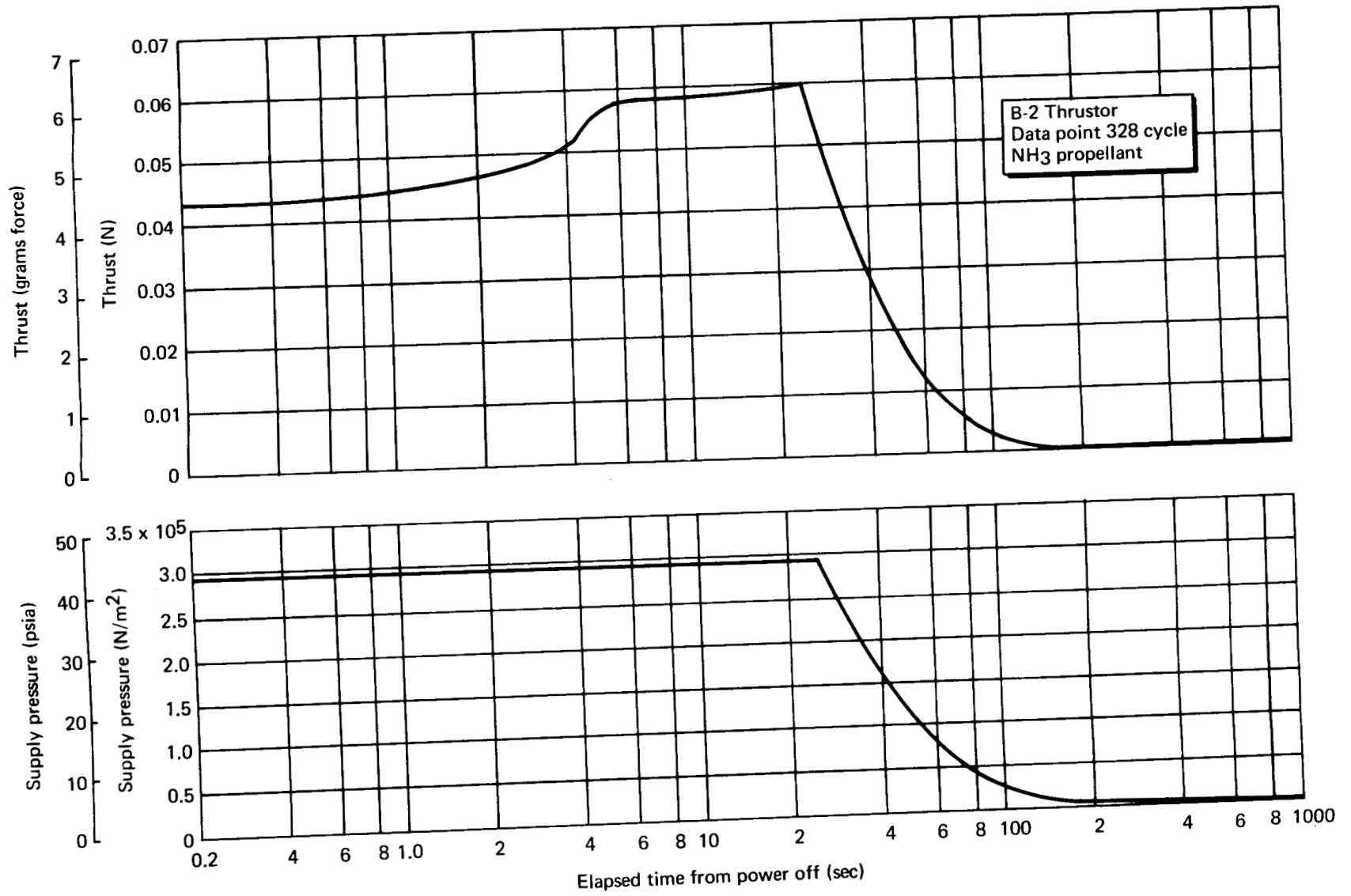Figure 63. Thrustor Exterior Temperatures

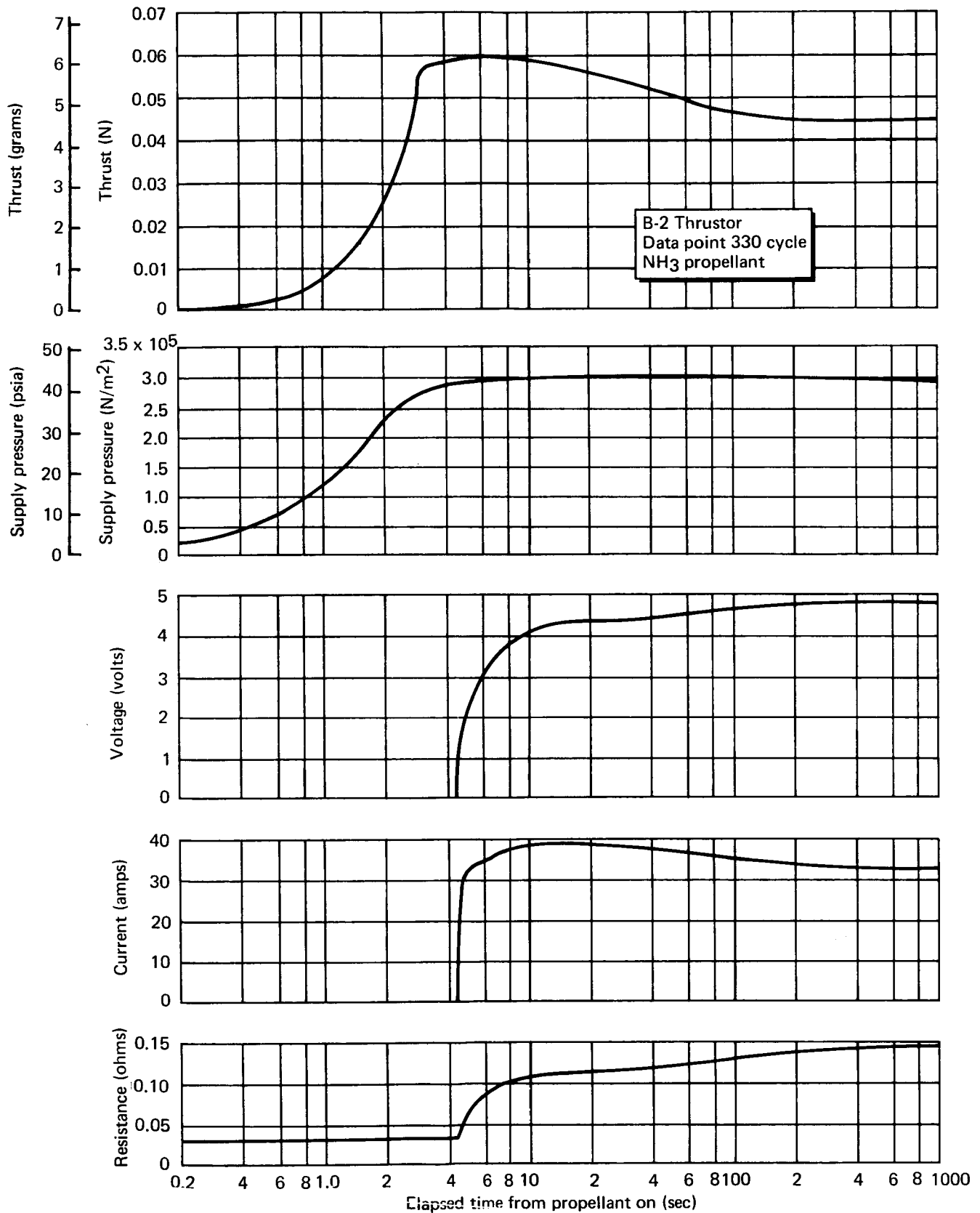Figure 64. Transient Performance -- Model II Resistojet

Figure 65. Transient Performance -- Model II Resistojet

Cell Pressure Tests. — In August 1967, performance of the vacuum station degenerated during tests of the Model I thrustor. A lower thrust and, simultaneously, higher cell pressure were observed at that time.

Because of the multi-thrustor operation planned for the life tests and the resulting increase caused in cell pressure, it was decided to investigate the effect of cell pressure. Tests were run on both H_2 and NH_3 at operating conditions ranging from cold flow to design performance over the full range of cell pressures possible. These results show (fig. 66) that a definite cell back-pressure effect exists in the range in which tests have been run.

The effect is such that the measured thrust is less than the same unit would produce in space. Depending on cell pressure, the measured values were from 4 to 12% lower than predicted. The effect is manifested on semi-log paper as the lower portion of an "S" curve (reversed). However, the upper portion of the curve has not been located because of vacuum system limitations. Fig. 66 shows the decrease in specific impulse while operating on H_2 that is caused by the cell pressure lowering the thrust (for the same mass flow and electric power). At increasing cell pressure, the curve approaches the performance of an inviscid nozzle with $A/A^* = 1$. In like manner, the upper part of the curve is expected to approach the theoretical performance line (for optimum A/A^*) shown. To verify the shape of the upper part of the curve, a harder vacuum will be required.

This transition regime flow is not fully understood. The current planning for life testing is to calibrate thrustors singly, periodically, using the same input conditions as during multiple-thrustor operation. The thrust values during multiple operation will be used as a guide only.
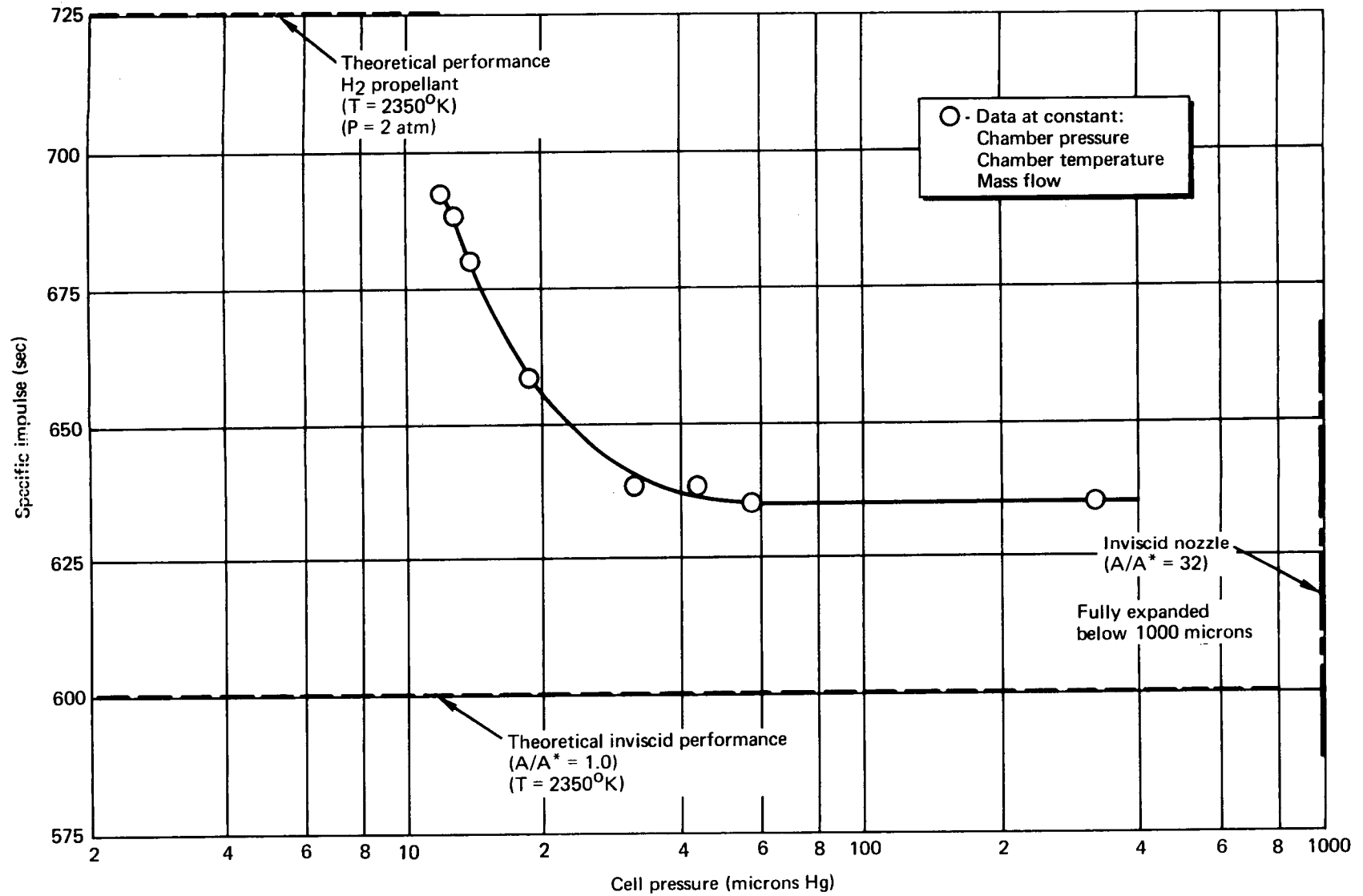
Figure 66. Cell Pressure Effect On Specific Impulse

CONCLUSIONS

1. The specific-impulse objectives of the 0.044-N (10-mlb) resistojet design were met on both H_2 and NH_3 during hours of testing. Specific impulses of up to 750 sec for H_2 and 340 sec for NH_3 were measured. Life tests of progressive increases in specific impulse are required to establish the thrustor rating for long life on each propellant.

2. The method for predicting resistojet performance is confirmed within the accuracy of the presented experimental data using H_2 and NH_3 propellants. The parameterized performance curves may be used for preliminary design studies.

3. The review of materials for resistojet components using H_2 or NH_3 shows that a number of materials are suitable. Rhenium and 26% rhenium/ 74% tungsten are the prime candidates for the high-temperature elements. Which of these materials is ultimately superior for each use can only be demonstrated by extended tests to properly evaluate the combined deteriorating actions on them.

4. Critical loading on the inner element (both steady-state and transient) requires the smallest bellows diameter to compensate for thermal expansion. The bellows spring constant must be chosen so that the thermally enduced force through the bellows expansion is balanced at design by the pressure force axially.

5. The thermal-insulation package designed for a single (10-mlb) thrustor has successfully passed a 100-hour test operating on H_2 at up to 750-sec specific impulse. No deterioration was noted.

6. No changes in throat dimension occurred as a result of the 100-hour testing. Life predictions indicate a life of thousands of hours.

APPENDIX

DEFINITIONS OF PERFORMANCE PARAMETERS[*]

Specific impulse, I_{sp}, sec

$$I_{sp} \triangleq \frac{F}{\dot{m}} \tag{1}$$

where

$$F = \text{measured thrust by dynamometer, g} \tag{a}$$

$$\dot{m} = \text{propellant mass flow, g-sec}^{-1} \tag{b}$$

Electric power to terminals, P_e, watts

$$P_e = E_t \times I_t \tag{2}$$

$$E_t = \text{electric voltage difference between thrustor} \\ \text{terminals, V} \tag{c}$$

$$I_t = \text{electric current passing between terminals, amp} \tag{d}$$

Supply pressure, p_s, atm

$$p_s = \text{propellant pressure measured at a tee fitting} \\ \text{at entrance to thrustor.} \tag{e}$$

Note chamber pressure is not directly measured but is inferred from nozzle throat continuity calculations.

---

[*] $\triangle$ means "definition."

Efficiency--electric power overall, η_o*

$$\eta_o* \triangleq \frac{F \times I_{sp}}{20.8\ P_e} \tag{3}$$

Efficiency--total power overall, η_o

$$\eta_o \triangleq \frac{F \times I_{sp}}{20.8\ (P_e + P_i)} \tag{4}$$

Initial power in gas, P_i, watts

$$P_i = \dot{m}\ h\ 4.186 \tag{5}$$

$$h = \text{enthalpy of an ideal gas above absolute zero,} \atop {}^oK,\ cal/gm\ (ref.\ 10) \tag{f}$$

Power in the jet, P_j, watts

$$P_j = P_e + P_i - P_1 \tag{6}$$

$$P_1 = \text{heat lost from the thrustor prior to the} \atop \text{exhaust jet, watts} \tag{g}$$

Heater efficiency, η_H

$$\eta_H \triangleq \frac{P_j}{P_e + P_i} \tag{7}$$

Nozzle efficiency, η_N

$$\eta_N \triangleq \frac{F \times I_{sp}}{20.8\ P_j} \tag{8}$$

or

$$\eta_N = \frac{\eta_o}{\eta_H} \tag{9}$$

---

*$\triangleq$ means "definition."

BIBLIOGRAPHY

1. High-Temperature Materials and Reactor Component Development Programs, Vol. I--Materials. General Electric Corporation, Cincinnati, Ohio, Feb. 26, 1965.

2. Hokanson, H. A.: High-Voltage Electron Beam Welding of Aerospace Components. Hamilton Standard Division, United Aircraft Corporation; presented to Society of Automotive Engineers, Inc., National Aerospace Meeting, New York, New York, Apr. 3-6, 1962.

3. Hokanson, H. A. and Kern, W. I.: Electron Beam Welding of Tungsten and Molybdenum. Hamilton Standard Division, United Aircraft Corporation, Aug. 1961.

4. Jaffee, R. I.: Refractory Materials. Defense Metals Information Center Memorandum No. 44, Feb. 1960.

5. Kerns, W. H.: Electron Beam Welding of Tungsten, Applied Research Operation, Flight Propulsion Laboratory Department, General Electric Corporation.

6. Monroe, R. E.: Joining of Tungsten. Metals Joining Division, Battelle Memorial Institute, Columbus, Ohio, Nov. 24, 1960.

7. Monroe, R. E. and Evans, R. M.: Electron Beam Welding of Tungsten. Metals Joining Division, Battelle Memorial Institute, Columbus, Ohio, May 21, 1962.

8. Propellant, Ammonia. Military Specification No. MIL-P-27406 (OASF), May 9, 1966.

9. Rhenium, etc., Chase Brass and Copper Company Publication No. RE-3, May 1964.

10. Zima, G. E.: Vaporization of Advanced Powerplant Metals Under Vacuum and Forced Convection Conditions. Lawrence Radiation Laboratory, University of California Publication No. UCRL-14274, June 24, 1965.

REFERENCES

1. Page, R. J.; Halback, C. R.; and Short, R. A.: 3-Kw Concentric Tubular Resistojet Performance. AIAA J Spacecraft, pp. 1667-1674, 1966.

2. Hampel, Clifford A.; ed: Rare Metals Handbook. Second ed., Reinhold Publishing Corp. (London), 1961. Ch. 16--Molybdenum, R. S. Archer; Ch. 20--Rhenium, A. D. Melaven; Ch. 30--Tungsten, K. C. Li.

3. Jonsen, B. W. ed.: Rhenium. Elsevier Publishing Co., N. Y., 1962.

4. Anon.: Rhenium-Molybdenum Alloys. Bulletin No. 2 Chase Brass and Copper Co. Rhenium Div., Salon, Ohio, Dec. 1963.

5. Zima, G. E.: Vaporization of Advanced Powerplant Metals Under Vacuum and Forced Convection Conditions. UCRL-14274, Lawrence Radiation Laboratory, Livermore, California.

6. Anon.: High Temperature Materials and Reactor Component Development Programs. Vol. I - Materials. Fourth Annual Report. General Electric Corporation, Feb. 1965.

7. King, C. R.: Compilation of Thermodynamic Properties, Transport Properties and Theoretical Rocket Performance of Gaseous Hydrogen. NASA TN D-275, April 1960.

8. Dushman, S.: Scientific Foundations of Vacuum Technique. John Wiley & Sons, Inc., Second ed., 1962, pp. 25-53.

9. Grier, N. T.: Calculation of Transport Properties and Heat Transfer Parameters of Dissociating Hydrogen. NASA TN D-1406, October 1962.

10. Anon: JANAF Thermochemical Tables, The Dow Chemical Company, Midland, Michigan.

11. Milligan, M. W.: Nozzle Characteristics in the Transition Regime between Continuum and Free Molecular Flow. AIAA J., 1964, pp. 1088-1092.

12. Kanning, Gerd: Measured Performance of Water Vapor Jets for Space Vehicle Attitude Control Systems. NASA TN D-3561, Aug. 1966.

13. John, R. R.: Resistojet Research and Development. NASA CR-54688, Dec. 1966, p. 84.